



NTNU – Trondheim
Norwegian University of
Science and Technology

Evaluation and Design of Large Precast Concrete Panels as Modules of Tanks for Smolt Breeding

Thomas Hasvåg

Marine Technology

Submission date: June 2015

Supervisor: Bernt Johan Leira, IMT

Norwegian University of Science and Technology
Department of Marine Technology



NTNU
Norwegian University of Science and Technology
Department of Marine Technology



Master thesis, Spring 2015
for
Master Student Thomas Hasvåg

Evaluation and Design of Large Precast Concrete Panels as Modules of Tanks for Smolt Breeding

Evaluering og Dimensjonering av Store Prefabrikerte Betongpaneler som Moduler i Tanker for Smolt-oppdrett

Traditional concrete tanks for breeding of smolt typically have a circular shape. However, a novel design based on tanks with a polygon shape may offer benefits with respect to production, transport and installation. This issue is to be addressed by the present project work.

It is proposed that the work is performed according to the following plan:

1. A description of traditional concepts regarding liquid-retaining concrete tanks is to be given. A particular novel concept is subsequently to be described. The tank walls of this novel concept should be constructed from plane rectangular elements by means of precasting. As part of the study to follow, the benefit from prestressing the structure should be highlighted.
2. A review of present design rules, design procedures and capacity checks which are relevant for this type of structure is to be performed. Relevant loading conditions are also to be described. Applied serviceability criteria (e.g. related to water tightness) are also to be outlined.
3. A buckling analysis of a homogenous rectangular plate subjected to a combination of compressive and lateral loads is to be performed. The plate model should correspond to a representative planar component of the novel tank concept. The performance of the plate should be evaluated as a function of relevant slenderness parameters. The effect of reinforcement can be included by means of simplified methods.
4. Serviceability criteria regarding water tightness should be evaluated as the tank dimensions increase. The effect of both slack-reinforcement and pre-stressed reinforcement is to be considered.
5. A large concrete panel is to be modeled by means of a relevant Finite Element computer program such as SAP2000/Etabs. By application of this computer program, the corresponding force/moment distribution should be used as basis for the following prestressing design.

The work-scope may prove to be larger than initially anticipated. Subject to approval from the supervisor, topics may be deleted from the list above or reduced in extent.

In the thesis the candidate shall present his personal contribution to the resolution of problems within the scope of the thesis work. Theories and conclusions should be based on mathematical derivations and/or



logic reasoning identifying the various steps in the deduction. The candidate should utilise the existing possibilities for obtaining relevant literature.

The thesis should be organised in a rational manner to give a clear exposition of results, assessments, and conclusions. The text should be brief and to the point, with a clear language. Telegraphic language should be avoided.

The thesis shall contain the following elements: A text defining the scope, preface, list of contents, summary, main body of thesis, conclusions with recommendations for further work, list of symbols and acronyms, references and (optional) appendices. All figures, tables and equations shall be numerated.

The supervisor may require that the candidate, at an early stage of the work, presents a written plan for the completion of the work. The plan should include a budget for the use of computer and laboratory resources which will be charged to the department. Overruns shall be reported to the supervisor.

The original contribution of the candidate and material taken from other sources shall be clearly defined. Work from other sources shall be properly referenced using an acknowledged referencing system.

The thesis shall be submitted in electronic form:

- Signed by the candidate
- The text defining the scope included
- Drawings and/or computer prints can be organised in a separate folder.

Supervisor: Professor Bernt J. Leira

Contact person at Overhalla BB: Inger Hilde Solstad

Start: January 16th, 2015

Deadline: June 10th, 2015

Trondheim, 16th January 2015

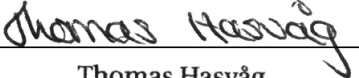
Bernt J. Leira

Preface

This report presents a master thesis within the Department of Marine Technology at the Norwegian University of Science and Technology, NTNU. It has been carried out during the spring semester of 2015.

The thesis is formulated on behalf of some interest from the industry. After making contact with a firm appealing to my foreseeing career as a structural engineer, Overhalla Betongbygg proposed some fields for investigation. As the firm recently entered the onshore aquaculture industry, this became a natural field for further investigation. A proposal for the master thesis was then formulated as a result from meetings. The explicit formulation is made by my supervisor at NTNU, Bernt J.Leira.

Trondheim, June 10, 2015


Thomas Hasvåg

Acknowledgment

During this period I have received valuable information from various people. My NTNU supervisor, Bernt Johan Leira, has with his knowledge preserved progress and continuity in my work. I am grateful for his availability throughout the period of writing.

The master thesis has been formulated and completed in cooperation with Overhalla Betongbygg. I appreciate the opportunity this final assignment has given me. On behalf of Overhalla Betongbygg, Inger Hilde Solstad has served as my secondary supervisor. Through meetings and e-mails I have received valuable information. The inputs and corrections given from M.Sc Mari Bergin at Overhalla Betongbygg have been of great value to my work. I would like to thank the company for acting professional parallel with their projects of economic value.

Last but not least, I want to thank my family for the encouragement during my years as a student. My girlfriend has really inspired me in making a solid educational foundation for our future.

T.H

Abstract

With increasing permissions for onshore smolt breeding, the industry may long for solutions that are competitive and robust. A part of this demand relates to breeding tanks that should be able to handle the given quantity of smolt, while holding the costs of construction within reasonable limits. Concrete is a high-strength material well suited for increasing structural requirements. Reinforced by steel, the composite may be given characteristics beneficial for a tank in this environment.

Precast concrete states a production method creating the structural elements prior to the mounting. A part of the work is then performed at fabrication halls within a stable environment, which may reduce the overall time of deliverance. Although the use raises additional issues related to transportation and installation, reinforced concrete panels is potentially a competitive solution as modules in a tank used for smolt breeding.

The demand for an optimized smolt breeding plant may encourage the use of larger concrete panels. In order to still remain functional, the tank could be strengthened by application of prestressed steel within each panel. As concrete possess low tensile strength leading to crack formulations, prestressing is an efficient tool in providing a watertight structure.

The thesis investigates buckling limits with respect to the application of prestress. With increasing span-ratio and decreasing panel thickness, this may become an upper bound for its use. Buckling analyses are performed within the three following stages in the construction.

- Vertical prestressing in fabric \Rightarrow panel subjected to compressive stress at short edges
- Further prestressing at site along the perimeter \Rightarrow panel subjected to biaxial compression
- Design condition \Rightarrow biaxially compressed panel subjected to a hydrostatic pressure

A design of the largest panel followed throughout the study is then proposed. The procedure governs the utilization of prestressed steel within a slab in two-way flexural action so to limit formulation of cracks. According to NS-EN-1992-3 (2009) for a completely watertight structure, this is fulfilled by maintaining a certain zone of compression within the panel.

For the proposed design, the equivalent compressive forces from prestressing do not violate the corresponding buckling limits. However, as a panel within the first stage of construction shows a considerable low buckling capacity, this may become a design issue for slender panels.

The design is further approved by a finite element analysis in Etabs. While the appearing stresses are reasonable regarding concrete compressive capacity, the maximum deflection of the panel turns out as a governing issue. An improved solution should then really iterate on the prestressed design in order to fulfill this requirement.

Sammendrag

I takt med den økende aktiviteten innenfor landbasert oppdrett stilles det krav til mer kostnadseffektive og solide løsninger. En del av dette kravet er rettet mot selve tankene. De må kunne håndtere økende mengde fisk men samtidig vise til et konkurransedyktig design. Betong er et sterkt materiale som egner seg for bruk når det stilles høye krav til styrke. Ved å armere betong kan man oppnå en kompositt tilpasset for en tank i disse omgivelsene.

Prefabrikkert betong betegner en produksjonsmetode som utformer elementer før selve monteringen på byggeplass. En del av produksjonen er da forbeholdt fabrikk i kontrollerte omgivelser, noe som senker den totale leveransetiden. Selv om denne produksjonsmetoden stiller andre krav til transport og montering, virker prefabrikerte paneler i betong å være en potensielt lønnsom løsning som moduler i tanker for oppdrett av smolt.

Etterspørselen for optimaliserte løsninger kan fremme behov for store paneler. For at tanken fremdeles skal kunne oppfylle sine funksjonelle krav kan det være nødvendig å benytte seg av forspent armering. Siden betong viser lav styrke ved strekkbelastninger, kan forspenning benyttes for å fremdeles opprettholde krav rettet mot vanngjennomtrengning.

Avhandlingen tar for seg begrensninger i påsatt forspenning med tanke på knekkkapasiteten av panelet. Med økende spennvidde og avtagende tykkelse kan knekking vise seg å bli dimensjonerende. Knekkanalyser er gjennomført for de følgende faser i produksjonen, representert som caser i undersøkelsen.

- Forspenning i vertikal retning på fabrikk \Rightarrow panel utsatt for trykklast på de korteste endene
- Videre horisontal forspenning på byggeplass \Rightarrow panel utsatt for trykklast i begge retninger
- Design tilstand \Rightarrow biaksialt trykksatt panel utsatt for vanntrykk

Videre fremlegges et design av det største panelet fulgt gjennom oppgaven. Prosedyren omhandler mengde og beliggenhet av forspent armering for to-veis platebøyning i den hensikt å begrense opprissing. I følge NS-EN-1992-3 (2009) for en helt vanntett konstruksjon, kan dette sies å være oppfylt om man opprettholder en bestemt trykksonehøyde i panelet.

For det foreslåtte designet vil ikke trykkreftene, gjenspeilende effekten av forspenning, overgå de korresponderende knekkkapasiteter. Panelet viser allikevel lav knekkstyrke i første fase av produksjonen, noe som kan bli dimensjonerende for lange og slanke elementer.

Løsningsforslaget er videre satt på prøve gjennom en elementanalyse i Etabs. Selv om de opp tredende spenninger virker å være lavere enn kapasiteten tilsvarende knusing av betong, viser deformasjonen av panelet seg å bli et relevant problem. En forbedret løsning vil kunne oppnås ved å iterere på mengde og beliggenhet av forspenning for å tilfredstille krav rettet mot utbøyning.

Contents

Problem definition	i
Preface	iii
Acknowledgment	v
Abstract	vii
Sammendrag	ix
1 Introduction	1
1.1 Background	1
1.1.1 Literature review	3
1.2 Approach	3
1.3 Structure of the Report	4
I Concrete for load-carrying purposes	5
2 The structural materials	6
2.1 Concrete	6
2.2 Reinforcement steel	8
2.2.1 Reinforced concrete	8
2.3 Prestressing steel	9
2.3.1 Prestressed concrete	10
3 Precast concrete tanks for smolt breeding	13
3.1 Polygonal shaped tanks	14
3.2 Load conditions	15
3.2.1 Self-weights	15
3.2.2 Prestress as external edge loads	16
3.2.3 Hydrostatic pressure	17
3.3 Static model	17
3.4 Design checks	18

3.4.1	Ultimate limit state	19
3.4.2	Serviceability limit state	23
3.5	Prestressed concrete tanks	27
3.5.1	Abetong	27
3.5.2	XPRES tank	29
II	Investigation of large concrete panels	31
4	Buckling of large prestressed concrete panels	32
4.1	Problem description	33
4.1.1	Simplification of reinforced concrete properties	34
4.2	Case study	38
4.2.1	Concrete panel subjected to monoaxial compressive stress	39
4.2.2	Concrete panel subjected to biaxial compressive stress	44
4.2.3	Biaxially loaded concrete panel subjected to a triangular lateral pressure	47
5	Flexural cracking of concrete	50
5.1	Design philosophies	51
5.2	Parameter study regarding the zone of compression, x	53
5.2.1	Degree of partial prestress	58
5.2.2	Eccentricity of prestressed reinforcement	60
III	Design for a watertight concrete panel	63
6	Non-prestressed concrete panel	64
6.1	Design condition	64
6.1.1	Moment distribution	65
6.1.2	Assessment of the compressive zone as design basis	67
6.2	Controlling the compressive zone by application of prestress	69
6.2.1	Prestressing y-directional strips of the panel	69
6.2.2	Prestressing x-directional strips of the panel	72
7	Two-way prestressed concrete panel	77
7.1	The design proposition	77
7.1.1	Y-directional prestressed steel	77
7.1.2	X-directional prestressed steel	79
7.2	Finite element analysis in Etabs	80
7.2.1	Shell element modeling	80

7.2.2	Modeling prestress as compressive point loads	83
7.2.3	Response of the prestressed solution	85
8	Summary	90
8.1	Conclusions	90
8.2	Strength and limitations	92
8.2.1	Non-linear effects	93
8.3	Recommendations for Further Work	95
	Bibliography	96
	Appendices	99
A	Results from buckling analysis	I
A.1	Concrete panel subjected to monoaxial compressive stress	I
A.2	Concrete panel subjected to biaxial compressive stress	IV
A.3	Biaxially loaded concrete panel subjected to a triangular lateral pressure	VII
B	Finite element analysis of concrete panel	X
B.1	Response of non-prestressed panel	X
B.1.1	Stress	X
B.1.2	Deflection	XII
B.2	Response of prestressed panel	XIII
B.2.1	Stress	XIII
C	Matlab scripts	XV
C.1	Design for cracking limit state	XV

List of Figures

1.1	A concrete tank established from precast elements, Abetong (2015).	2
2.1	Compressive stress-strain curve for concrete, (adapted from Sørensen, 2013, p. 9).	6
2.2	Typical stress-strain curve for reinforcement steel, (adapted from Sørensen, 2013, p. 18).	8
2.3	Ductile design of a reinforced concrete beam loaded in bending.	9
2.4	Typical stress-strain curve for prestressed steel, (NS-EN-1992-1, 2008, Chapter 3). .	9
2.5	Behavior of a reinforced concrete beam versus a prestressed concrete beam.	10
2.6	Eccentric prestressed beam loaded in bending.	11
2.7	Beam prestressed with varying eccentricity loaded in bending, (adapted from Sørensen, 2013, p. 201).	12
3.1	Modern smolt breeding plant currently under construction, OverhallaBetongbygg (2015)	13
3.2	Polygonal shape of a tank as a function of the number of equal panels, n	14
3.3	Comparison of stress along the perimeter within tanks constructed of n equal concrete panels.	14
3.4	Definition of the span-directions within a concrete panel.	15
3.5	Self-weight distribution for different orientations of a concrete panel.	16
3.6	Prestress captured as external compressive loads acting at the edge of the concrete panel.	17
3.7	A concrete panel on a base foundation subjected to in-plane compressive loads and a triangular distributed pressure.	18
3.8	A strip of a concrete panel acting as reference for the ultimate strength considerations.	20
3.9	Strains and corresponding internal forces within the reference strip section at flexural failure.	20
3.10	Illustration of an M-N diagram specifying the design capacity for a combination of axial forces and moments.	21

3.11 Recommended values for maximum crack-width, w_{max} (mm), sorted for exposure classes, (NS-EN-1992-1, 2008, p. 119).	24
3.12 A section of the reference strip loaded in bending developing a flexural crack.	25
3.13 A section of the reference strip loaded in tension developing a through-thickness crack.	25
3.14 Classification of tightness in accordance to requirements for leakage, (NS-EN-1992-3, 2009, p. 10).	26
3.15 The structural effects arising when prestressing a precast concrete tank in both directions, Abetong (2015).	27
3.16 Illustration of the pre-tensioning process during casting of a concrete panel at fabric, CivilEA (2015).	28
3.17 Illustration of post-tensioning along the perimeter covering all precast concrete panels in one operation, Abetong (2015).	28
3.18 Layout of post-tensioned steel inside a horizontal section of two adjacent concrete panels, Abetong (2015).	29
3.19 Steel tendons placed at the outside of a concrete tank prepared for tensioning, MooreConcrete (2015).	30
3.20 Sealing a vertical joint by post-tensioning the steel tendons placed at the outside of a concrete tank, ConsolisGroup (2015).	30
4.1 The geometry of the panel used as reference for the buckling analyses.	33
4.2 Internal forces for an uncracked section of a strip of the concrete panel loaded in bending.	34
4.3 Internal forces for a cracked concrete section of a strip of the concrete panel loaded in bending.	35
4.4 Concrete panel prestressed with a uniform distribution at the short edges.	39
4.5 First eigenmode for Panel 1 within the first case study.	40
4.6 Second eigenmode for Panel 1 within the first case study.	40
4.7 Third eigenmode for Panel 1 within the first case study.	41
4.8 Buckling stress as a function of panel slenderness within the first case study.	43
4.9 Concrete panel with a uniform prestress at short edges and a linearly distributed prestress at long edges.	44
4.10 Buckling stress for concrete panels within the second case study.	45
4.11 Lowest eigenmode for Panel 1 within the second case study experiencing minor influence from the vertical prestress.	46
4.12 First eigenmode for Panel 1 within the second case study experiencing major influence from the vertical prestress.	46
4.13 Two-way prestressed concrete panel subjected to a hydrostatic pressure.	47

4.14	Buckling stress for concrete panels within the third case study.	48
4.15	Lowest buckled shape for Panel 1 within the third case study.	49
5.1	Cracking of concrete panel in a liquid-retaining concrete tank followed by a leakage, AlchemyPolymers (2015).	50
5.2	Controlling cracking by ordinary reinforcement, $\sigma_c^{tens} < f_{ctm}$	51
5.3	Controlling cracking by prestressed reinforcement, $x \rightarrow \infty$	52
5.4	Controlling cracking by combining the use of ordinary and prestressed reinforcement.	53
5.5	Cross-sectional calculation model as basis for the parameter study on the compressive zone, x	54
5.6	Graphic illustration of the iteration process utilized when solving for the compressive zone, x	56
5.7	Residual bending stress distribution within a strip section of a prestressed concrete panel loading in bending.	59
5.8	Effect on the compressive zone with increasing reinforcement ratio, $\frac{A_p}{A_s}$	59
5.9	Effect on the compressive zone with increasing eccentricity of the prestressed steel, d_p	60
5.10	Resulting stress distribution and height of compressive zone for prestressing with $d_{p1} < d_{p2}$	61
5.11	Resulting stress distribution and height of compressive zone for prestressing with $d_{p2} > d_{p1}$	62
6.1	Non-prestressed concrete panel subjected to a hydrostatic pressure as the design condition.	64
6.2	Distribution of moments throughout the concrete panel due to the hydrostatic pressure.	65
6.3	Moment distribution throughout the critical x-directional strip of the concrete panel.	66
6.4	Moment distribution throughout the critical y-directional strip of the concrete panel.	66
6.5	Internal forces within a section of the critical strip of the concrete panel as basis for the design.	67
6.6	Concrete stress distribution throughout the compressive zone in the critical strips.	69
6.7	Height of compressive zone at the most loaded location of the critical y-directional strip for increasing amount of prestress.	70
6.8	Resulting stress at concrete top due to y-directional prestress.	71
6.9	Resulting stress in ordinary reinforcement steel due to y-directional prestress.	71

6.10	Two approaches to obtain a linear force distribution from the process of post-tensioning along long edges.	73
6.11	Height of compressive zone at the most loaded location of the critical x-directional strip for increasing amount of prestress.	74
6.12	Resulting stress at concrete top due to x-directional prestress.	75
6.13	Resulting stress in ordinary reinforcement steel due to x-directional prestress. . . .	75
7.1	Resulting reinforcement design for load-transferring in y-direction.	78
7.2	Resulting reinforcement design for load-transferring in x-direction.	80
7.3	Forces acting within a plate element, Leira (2011)	81
7.4	Stresses acting within a plane stress element, Leira (2011)	82
7.5	The four-node quadrilateral shell element used in Etabs, CSi (2013).	83
7.6	Distribution of prestressed steel throughout the panel.	83
7.7	Stress distribution in x-direction for the prestressed concrete panel.	85
7.8	Stress distribution in y-direction for the prestressed concrete panel.	85
7.9	Out-of-plane deformations for the prestressed concrete panel.	87
7.10	Illustration of the scheme used to approximate the creep coefficient, (NS-EN-1992-1, 2008, Section 3)	88
8.1	Illustration of a non-linear stress-strain relationship.	93
8.2	Illustration of a non-linear load-deformation relationship. Moan (2003, p. 12.9) . .	94
A.1	Lowest eigenmode for Panel 2 within the first case study.	I
A.2	Lowest eigenmode for Panel 3 within the first case study.	II
A.3	Lowest eigenmode for Panel 4 within the first case study.	III
A.4	Lowest eigenmode for Panel 2 within the second case study for various degree of vertical prestress.	IV
A.5	Lowest eigenmode for Panel 3 within the second case study for various degree of vertical prestress.	V
A.6	Lowest eigenmode for Panel 4 within the second case study for various degree of vertical prestress.	VI
A.7	Lowest buckled shape of Panel 2 within the third case study.	VII
A.8	Lowest buckled shape of Panel 3 within the third case study.	VIII
A.9	Lowest buckled shape of Panel 4 within the third case study.	IX
B.1	Stress distribution in x-direction at the side of the non-prestressed panel experiencing tensile stress at the critical location.	X
B.2	Stress distribution in y-direction at the side of the non-prestressed panel experiencing tensile stress at the critical location.	XI

B.3 Stress distribution in x-direction at the side of the non-prestressed panel experiencing compressive stress at the critical location. XI

B.4 Stress distribution in y-direction at the side of the non-prestressed panel experiencing compressive stress at the critical location. XII

B.5 Out-of-plane deflection of non-prestressed concrete panel. XII

B.6 Stress distribution in x-direction at the side of the prestressed panel experiencing compressive stress at the critical location. XIII

B.7 Stress distribution in y-direction at the side of the prestressed panel experiencing compressive stress at the critical location. XIV

Nomenclature

Abbreviations

COG Center Of Gravity

In-situ Construction performed at the building site

NA Neutral Axis

RC Reinforced Concrete

SLS Serviceability Limit State

ULS Ultimate Limit State

FEA Finite Element Analysis

FEM Finite Element Modeling

Capital letters

A_s	Cross sectional area of the reinforcement steel	$[mm^2]$
A_p	Cross sectional area of the prestressed reinforcement	$[mm^2]$
A_{sc}	Cross sectional area of the compressive reinforcement steel	$[mm^2]$
$C_{Rd,c}$	Coefficient derived from concrete tests	[-]
E_c	Concrete modulus of elasticity	$[\frac{N}{mm^2}]$
E_s	Reinforcement steel modulus of elasticity	$[\frac{N}{mm^2}]$
E_{cl}	Concrete long-time modulus of elasticity	$[\frac{N}{mm^2}]$
E_t	Tangent modulus of elasticity	$[\frac{N}{mm^2}]$

I_c	Concrete moment of inertia	$[mm^4]$
I_s	Reinforcement steel moment of inertia	$[mm^4]$
I_{c-eq}	Moment of inertia for a reinforced concrete section	$[mm^4]$
K_0	Initial stiffness matrix	$[\frac{N}{m}]$
K_Δ	Additional stiffness matrix due to the loading	$[\frac{N}{m}]$
L_x	Panel span in x-direction	$[m]$
L_y	Panel span in y-direction	$[m]$
M_{Ed}	Design value of applied bending moment	$[Nm]$
M_{Rd}	Design moment capacity	$[Nm]$
N_{Ed}	Design value of applied axial force	$[N]$
Q	Base load in the buckling analysis	$[N]$
S	Force in reinforcement steel	$[N]$
S_c	Force in the compressive reinforcement steel	$[N]$
S_p	Force in the prestressed reinforcement steel	$[N]$
V_{Ed}	Design value of applied shear force	$[N]$
V_{Rd}	Design shear capacity for concrete	$[N]$

Small letters

a	Eccentricity relative to the COG for an equivalent compressive force	$[mm]$
b	Width of a concrete section, here as a unit strip	$[mm]$
c_{nom}	Required concrete cover for the reinforcement steel	$[mm]$
d_p	Largest distance from the centre of prestressed reinforcement to the section surface	$[mm]$
d_s	Largest distance from the centre of ordinary reinforcement to the section surface	$[mm]$
e	Eccentricity relative to the COG for a prestressing force	$[mm]$
f_{cd}	Design compressive strength of concrete	$[\frac{N}{mm^2}]$
f_{ck}	Characteristic compressive cylinder strength of concrete	$[\frac{N}{mm^2}]$

f_{ctm}	Mean value axial strength of concrete	$[\frac{N}{mm^2}]$
$f_{p0,1k}$	Characteristic 0.1% tensile strain limit for prestressed steel	$[\frac{N}{mm^2}]$
f_{pk}	Characteristic tensile strength of prestressed steel	$[\frac{N}{mm^2}]$
f_{yd}	Design yield strength of reinforcement steel	$[\frac{N}{mm^2}]$
f_{yk}	Characteristic yield strength of reinforcement steel	$[\frac{N}{mm^2}]$
g	Acceleration of gravity	$[\frac{kg \cdot m}{s^2}]$
g_c	Self-weight distribution of a concrete panel	$[\frac{N}{m}]$
p	Hydrostatic pressure	$[\frac{N}{m^2}]$
t	Thickness of panel	[mm]
x	Height of the compressive zone in a concrete section	[mm]
x_{min}	Minimum value of the compressive zone regarding watertightness	[mm]

Symbols

α	A factor regarding height of the compressive zone	[-]
$\Delta\epsilon_s$	Strain in reinforcement steel	[-]
$\Delta\epsilon_c$	Strain at concrete top	[-]
$\Delta\epsilon_p$	Strain in prestressed steel	[-]
$\Delta\epsilon_{sc}$	Strain in compressive reinforcement steel	[-]
ϵ_{ca}	Autogenous shrinkage strain of concrete	[-]
ϵ_{cd}	Drying shrinkage strain of concrete	[-]
ϵ_{cu}	Strain value at compressive crushing of concrete	[-]
η	Ratio of the material stiffness, E_s to E_c	[-]
γ_c	Concrete material factor	[-]
γ_s	Reinforcement steel material factor	[-]
λ_i	Eigenvalue corresponding to i'th eigenmode	[-]
v_i	Displacement vector corresponding to i'th eigenmode	[m]

$\phi(\infty, t_0)$	Creep coefficient	[-]
ϕ	Diameter of reinforcement bar	[mm]
ρ_L	Reinforcement ratio	[-]
ρ_w	Density of freshwater	$[\frac{kg}{m^3}]$
σ_c	Compressive stress in concrete	$[\frac{N}{mm^2}]$
σ_{cp}	Stress in concrete due to prestress or an axial force	$[\frac{N}{mm^2}]$
$\sigma_{p,max}$	Maximum stress in prestressed steel when jacking	$[\frac{N}{mm^2}]$
σ_c^{tens}	Tensile stress in concrete	$[\frac{N}{mm^2}]$

Chapter 1

Introduction

1.1 Background

For the purpose of onshore smolt breeding, concrete tanks seem to expand in use. Traditionally tanks used for this purpose have been small in size. A small tank implies rather small loads setting few restrictions to the material involved. This has led to a wide range of the governing material within liquid-retaining applications. A typical material used is fiber reinforced plastic acting as an economical solution.

The general restriction for onshore smolt breeding limits their weights up to 250g. A dispensation may however be given to extend the production up to 1000g. As Holm (2015) states, there is now an ongoing discussion whether or not this permission should also apply for onshore edible fish-farming. An effective production may then suggest the need for larger tanks, as these permissions trigger a competitive industry. Larger tanks may farm more fish within a given time interval, leading to a more economical way of running a business. As the tanks gets more heavily loaded, the material selection becomes a relevant issue. Although concrete is more expensive than plastic as the primary material, its structural properties may become necessary in providing sufficient capacity. Together with an inner coating, concrete becomes well suited for these heavier load-conditions.

The concrete tank could either be casted on-site, or produced prior to the assembly. Referring to the latter, we are entering the precast concrete industry. By precasting elements, the overall time of deliverance may be considerably reduced. In fabrication halls having stable environmental conditions, the concrete is also more likely to obtain the desired properties. A precast plane element is, as the name suggests, a non-curved element. Joining together multiple elements then results in a polygonal concrete tank as seen in Figure 1.1.

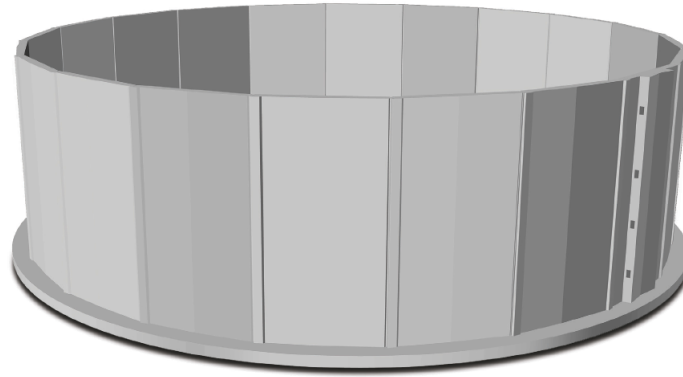


Figure 1.1: A concrete tank established from precast elements, Abetong (2015).

Increased tank dimensions really imply larger concrete panels. In order to remain sustainable, the panels must be able to resist the corresponding increase of acting loads. Cracking of concrete typically becomes the main design issue as this relates to watertightness. The structural characteristics introduced by prestressing the reinforcement may then become beneficial. As panel thickness also serves as a structural resistance, an optimized cross-section with respect to costs and structural capacity combines the use of prestressed and ordinary reinforcement steel within a certain panel thickness.

1.1.1 Literature review

NS-EN-1992-1 (2008), as well as Betongelementforeningen (2010), present general rules when applying concrete in structural applications. They also cover the use of ordinary reinforced and prestressed concrete. Most of these guidelines are served by Sørensen (2013), where they are presented in a more practical and compact manner. When operating in the field of aquaculture, there are some standards giving special design requirements mainly to resist evacuation of fish. While NS-9415 (2009) covers the floating fish-farms, NS-9416 (2013) presents precautions applying to onshore farming.

In order to meet the formal requirements given by NS-9416 (2013), the study makes use of a panel tightness classification stated in NS-EN-1992-3 (2009) covering liquid-retaining containers in general. With respect to the governing class of tightness, this standard encourage the use of prestressed reinforcement to resist cracking.

When it comes to previous work done within this field, a bachelor thesis by Bergin et al. (2011) is relevant. It presents an extension of agriculture tanks into fish-farming applications. The thesis was formulated on behalf of the same supervisor, namely Overhalla Betongbygg. In general, Bergin et al. (2011) covers aspects related to full design of a precast concrete tank. Since my study mainly considers the individual panels, the bachelor thesis will serve as background information.

1.2 Approach

Buckling analyses of the panels are performed by the use of Abaqus/CAE. In order to check for reasonability, some of these analyses are reproduced in Etabs, a software for structural analysis and design of buildings. Etabs is further used for some final considerations of the proposed design. As the evaluation version does not permit export of model files, I will not be able to provide this information within the thesis.

The prestressing design is performed manually by a calculation model attached as a Matlab routine. This routine aims to incorporate the complex behavior of reinforced concrete panels by a strip formulation, as this is not an easily accessed feature in the considered softwares.

Most of the graphical illustrations are drawn by the author using libraries for structural analysis within the tikz package. As graphical illustrations are an important part of my study, I have spent a considerable amount of time making these. Hopefully it will give the reader a clear understanding of the corresponding topics.

1.3 Structure of the Report

The rest of the report is sorted into parts. Part I provides some information of concrete and its use in the governing application. The second part investigates some special issues regarding large concrete panels with importance for the design proposal covering the last part.

A more specific description is given as follows:

Chapter 2 introduces the structural materials by presenting its characteristics and purpose. The chapter will then give the reader necessary information when planning to use reinforced concrete for load-carrying purposes.

Proceeding with some theory, Chapter 3 considers the use of reinforced concrete as tanks for smolt breeding. Relevant design checks under the governing load-conditions are also presented. As the application of prestress is an essential part of the study, the chapter highlights the advantage of prestressed concrete tanks by presenting the practices within some existing concepts.

Chapter 4 and 5 should prepare the reader for the design proposal of a large precast concrete panel. From buckling analyses investigating limits of prestress, as well as a parameter study covering cracking of concrete, the results provide limitations and general knowledge important for the following design procedure.

Chapter 6 considers a design of the largest concrete panel followed throughout the study. The method covers amount and placement of prestressed steel in order to control cracking in a two-way slab. Chapter 7 further presents the solution followed by some final considerations reported by a finite element analysis in Etabs.

The last chapter presents a summary of the work. Through a discussion, the strength and limitations of this thesis are presented to the reader. As an important part of the study, this chapter also gives recommendations for further work within this task.

Part I

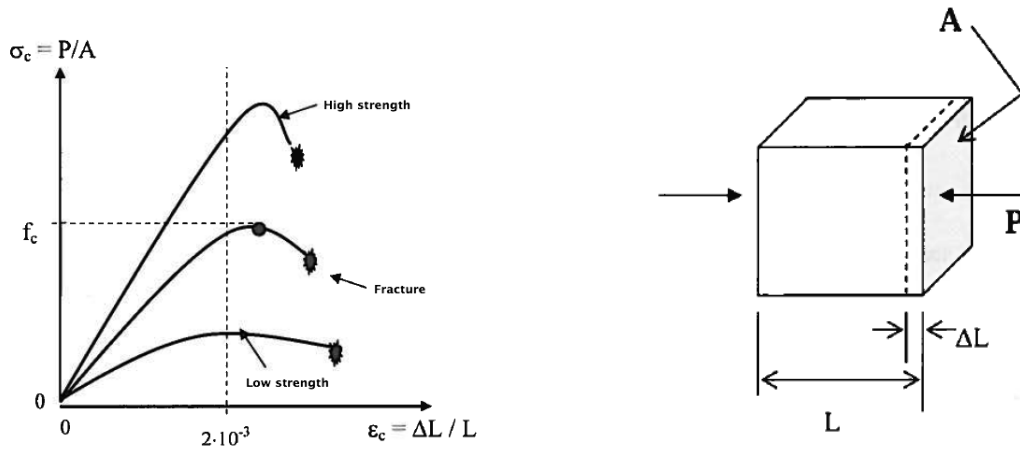
Concrete for load-carrying purposes

Chapter 2

The structural materials

2.1 Concrete

Concrete is a material made of cement, water and what is called aggregate. The aggregate is typically a mixture of sand and gravel. By applying a different composition of these components, the manufacturer may obtain a wide range of the structural property. This structural property is referred to as compressive strength, which is the desired attribute for the use of concrete as a load-carrying material.



(a) Stress-strain curve for various types of concrete.

(b) Illustration of measurement.

Figure 2.1: Compressive stress-strain curve for concrete, (adapted from Sørensen, 2013, p. 9).

Figure 2.1 shows the stress-strain relationship for concrete in compression. The high compressive strength makes concrete a useful material in applications governed by such loads. As one

may see, there is a clear difference in ductility for the various types of concrete. However, the ultimate stress takes place at approximately the same strain regardless of concrete type.

Long-term effects

The structural properties of concrete typically change over time. Creep is characterized by an additional time-dependent deformation beyond the statical solution. A concrete element subjected to compressive forces will thus experience a deformation magnitude increasing with time. The effect is typically represented in calculations as a long-time modulus of elasticity, E_{cl} .

$$E_{cl} = \frac{E_c}{1 + \phi(\infty, t_0)} \quad (2.1)$$

The issue is then captured by a softening effect of the initial structural characteristics. A decrease of the modulus of elasticity gives larger deformations for a given load-condition. Here $\phi(\infty, t_0)$ denotes the creep coefficient, which is a function of the time of applied loading and the following duration. The factor is found from a procedure considering the use of Figure 3.1 in NS-EN-1992-1 (2008).

Although shrinkage of concrete is time-dependent, this issue is independent of the governing loads. The effect is represented by additional strain components presented in Equation (2.2).

$$\epsilon_{cs} = \epsilon_{cd} + \epsilon_{ca} \quad (2.2)$$

ϵ_{cd} represents the drying shrinking strain for the passing of water through the hardened concrete, while ϵ_{ca} denotes the additional strain developing during hardening of concrete. (NS-EN-1992-1, 2008, Chapter 3) shows how to incorporate these effects into the calculation.

When loaded in tension, the concrete possess rather poor properties. The tensile strength, f_{ctm} , is low and typically referred to as negligible in calculations. A homogenous concrete structure loaded above the tensile strength is subjected to cracks. The result is a degradation of the cross section, such that the structure lose some of its initial structural properties. Cracks are also important when considering the serviceability limit state. The presence may affect the primary purpose of the construction, as well as the esthetics which often is essential.

2.2 Reinforcement steel

In most applications, the loading is governed by a combination of compression and tension forces. For concrete to still be a suited material, it has to be reinforced. This is typically obtained by adding bars of steel within the concrete. By means of the bond between concrete and the reinforcement, the tensile forces transfer from concrete to steel. A typical stress-strain curve for the ordinary reinforcement steel is given as Figure 2.2.

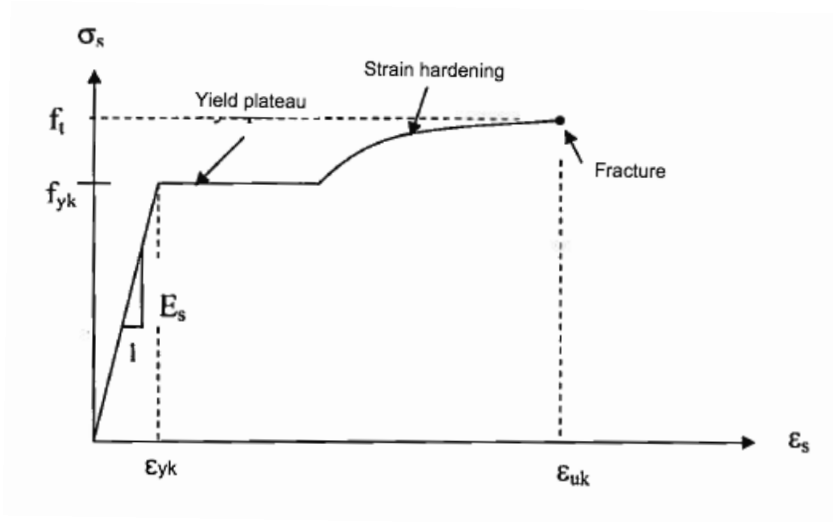


Figure 2.2: Typical stress-strain curve for reinforcement steel, (adapted from Sørensen, 2013, p. 18).

The characteristic strength is reported as the yield strength, f_{yk} , with a corresponding strain as ϵ_{yk} .

2.2.1 Reinforced concrete

Reinforced concrete states a composite material suited for more general applications. In addition to the increased ultimate capacity, the amount of reinforcement steel may be chosen to give the member a degree of ductility. According to (Sørensen, 2013, Chapter 4) there exists a practical way of designing reinforced concrete sections in Norway. By providing the member with an amount of reinforcement steel yielding prior to the state of ultimate capacity, the deflection may be used to keep track of the residual strength. This ductile behavior is achieved by choosing a steel quantity experiencing twice the yield strain when concrete crushing appears. An illustration of this concept is shown in Figure 2.3, considering the capacity of a beam loaded in bending.

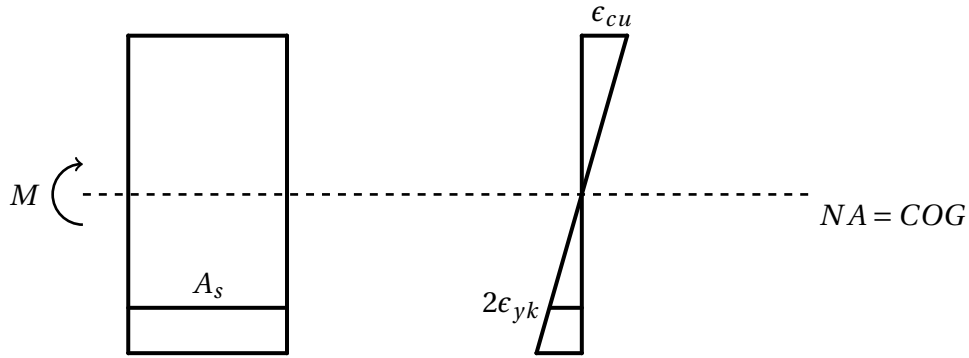


Figure 2.3: Ductile design of a reinforced concrete beam loaded in bending.

Here ϵ_{cu} denotes the strain value defining compressive crushing of concrete, while ϵ_{yk} gives the strain value for first yield of steel. The figure illustrates the concept by considering a section of a beam. The same approach may be utilized in ductile design of slabs, when defining the beam as a corresponding strip of the element.

2.3 Prestressing steel

In ordinary reinforced concrete, as described previously, tension forces transfer to the steel by the concrete-steel interaction. Although the cracking now gets limited, it will be present as long as a part of the section is loaded in tension. The only way to theoretically prohibit its presence is to fully counteract the tensile forces. A way of doing this is to make use of prestressed steel within the concrete.

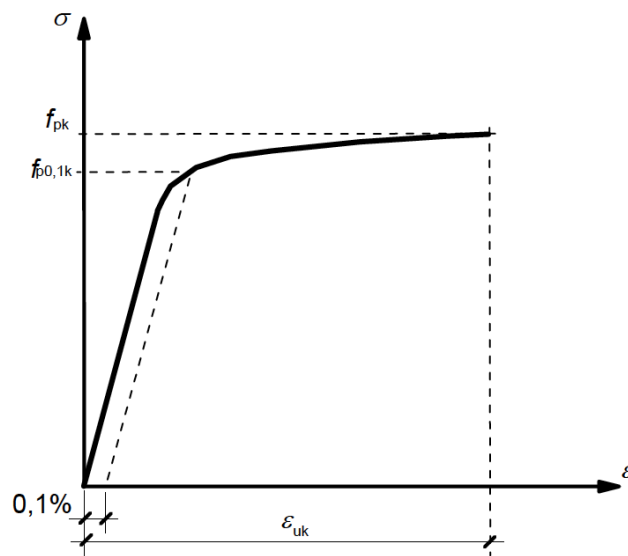


Figure 2.4: Typical stress-strain curve for prestressed steel, (NS-EN-1992-1, 2008, Chapter 3).

Figure 2.4 shows a typical stress-strain curve for prestressed steel. While ordinary reinforcement often are introduced as bars, the prestressed reinforcement may also consist of wires acting individually or wrapped together. Its presence is denoted as a tendon. Due to the different manufacturing processes, its characteristics is not uniquely described by the yield strength. The strength of a prestressed tendon is thus typically reported as $f_{p0,1k}$, representing the stress at 0.1% inelastic strain of the steel.

2.3.1 Prestressed concrete

By prestressing concrete, the aim is to cancel part of the loading on the structure. Essential here is the compressive load-effect from the prestress, which shall counteract the present tensile stresses. Prestressed concrete is then also utilized to control deformations within a structure. An illustration of the concept is given in Figure 2.5, showing its performance compared to an ordinary reinforced concrete beam in an exaggerated manner.

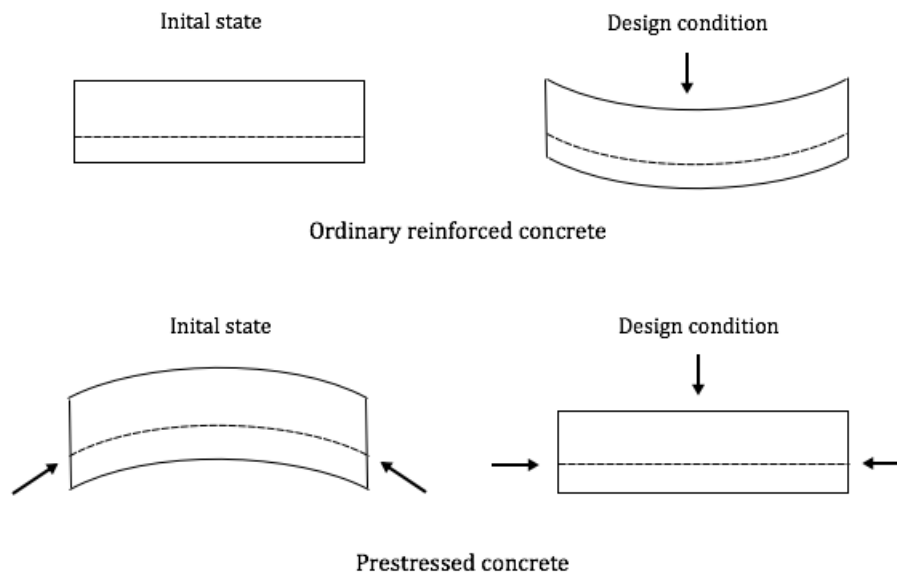


Figure 2.5: Behavior of a reinforced concrete beam versus a prestressed concrete beam.

The prestressing force is achieved by a process of either pre-tensioning or post-tensioning the tendons. As the name of the methods suggests, the main difference is whether you stress the reinforcement prior or post to casting of the concrete. In both of these methods tension in steel turns into concrete compression. For the pre-tensioning approach, the steel is first jacked to a desirable value of strain. After casting of surrounding concrete, the tendons are cut and the steel will try to compress in order to reach its equilibrium state. As a function of the concrete-steel

bond strength, this transfers as a compressive force into the concrete. The magnitude of this force is controlled by means of the jacking procedure.

When post-tensioning, tendons are guided through ducts previously casted into the concrete. By anchoring the steel to the end of the casted structure followed by a steel jacking, compressive point forces are obtained at the anchoring zones transferring into the concrete. If the ducts further are injected with some type of grout, this will establish a bond between concrete and steel denoting a bonded solution which ensures further compatibility in the strains.

An important application of this principle is within structures externally loaded in bending, which gives a varying stress distribution over the cross section. Since the primary target is to cancel the tensile stresses, it is preferred to introduce a similar, but opposite in magnitude stress variation by means of prestressing. This is obtained by placing the steel with an eccentricity to the center of gravity, COG. In addition to the constant compressive stress introduced, the eccentricity will then produce an eccentricity moment. An illustration can be seen in Figure 2.6.

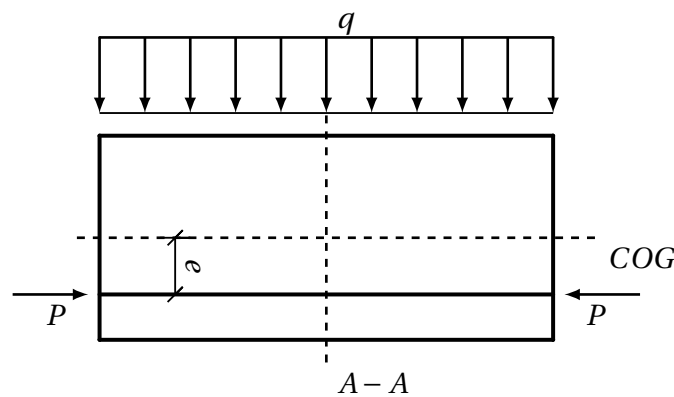


Figure 2.6: Eccentric prestressed beam loaded in bending.

Since the stress distribution in an externally loaded structure often varies over the element length, it is advisable to introduce an equivalent load from the prestressing that varies along the element. This can be obtained by prestressing tendons with changing eccentricity along the structure. As stated by (Sørensen, 2013, Part 2), the steel profile should have the same layout as the moment distribution from the external loading in order to completely counteract it. An illustration is given as Figure 2.7.

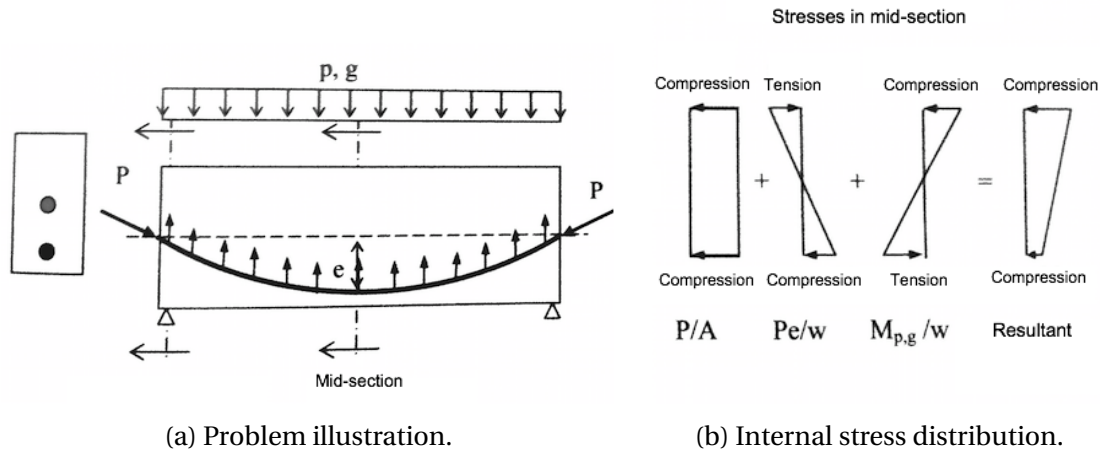


Figure 2.7: Beam prestressed with varying eccentricity loaded in bending, (adapted from Sørensen, 2013, p. 201).

Losses in prestress

The amount of prestress, as introduced by jacking of the steel, will in reality be lesser than the reported jacking stress. These losses of prestress arise due to a contraction of the steel. Although its causes depends on whether the tendons are pre- or post-tensioned, they may be differentiated with respect to a short-term and long-term perspective.

Losses due to anchor set and friction are denoted as short-term causes present for post-tensioned tendons. Due to the initial lack of concrete-steel bond, the following gradually jacking procedure introduces an anchorage slip as well as friction between the duct and steel. Within the long-term perspective present for both construction methods, creep and shrinkage as presented in Section 2.1 contracts the steel even further. Due to tendons subjected to a constant elongation throughout a long time period, the steel will experience a decrease in the appearing stress. This phenomena is recognized as steel relaxation.

These effects are further described by (Sørensen, 2013, Chapter 5). It shows how to account for the prestress losses individually and in an approximate compact manner with a reference to NS-EN-1992-1 (2008).

Chapter 3

Precast concrete tanks for smolt breeding

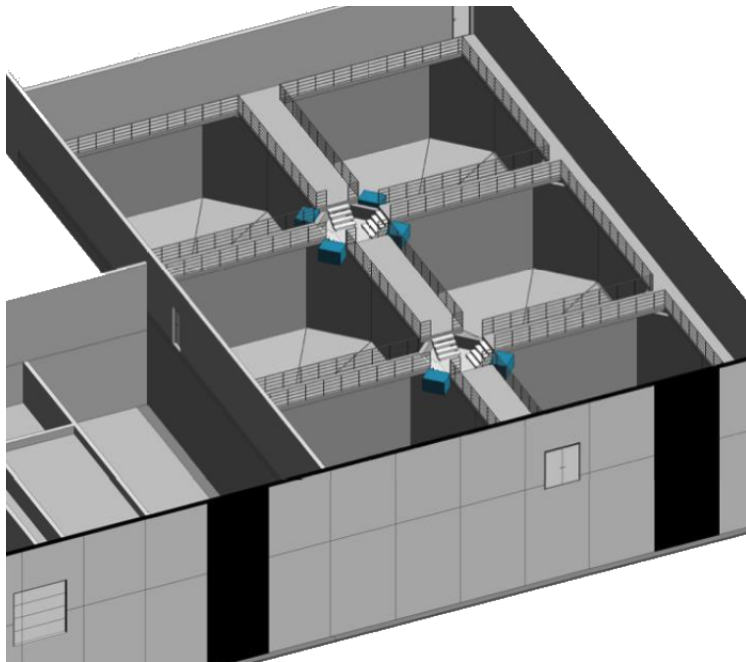


Figure 3.1: Modern smolt breeding plant currently under construction, OverhallaBetongbygg (2015)

Figure 3.1 shows part of a modern smolt breeding plant which at the time of writing is under construction. This design, as formulated by Overhalla Betongbygg, will be used as a reference when considering some of the boundary conditions applying for the precast concrete panels.

3.1 Polygonal shaped tanks

As the volume of the tanks defines the capability of the plant, this becomes the parameter of importance for the farming company. By use of precast concrete panels, the preferred volume may be obtained from different structural configurations. For a restriction on the diameter, the most efficient way to increase the volume is to construct the tank from high panels. The width of the panels then states the polygonal order of the tank influencing the global load-transferring.

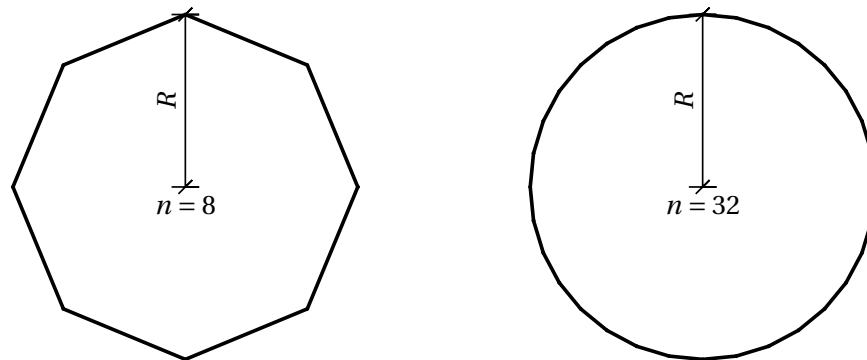


Figure 3.2: Polygonal shape of a tank as a function of the number of equal panels, n .

Figure 3.2 shows two geometrical unequal tanks with the same diameter. The tanks are assembled by n equally concrete panels reflecting the polygonal order. For increasing number of concrete panels, implying decreasing panel width, the shape tends towards more or less circular. Solutions making use of geometrically unequal elements, such as the configuration in Figure 3.1 are not further investigated.

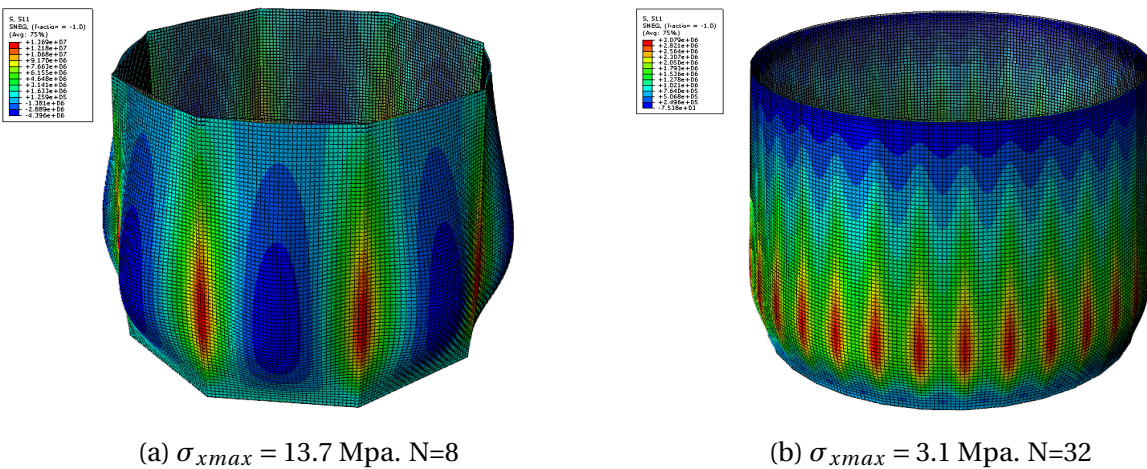


Figure 3.3: Comparison of stress along the perimeter within tanks constructed of n equal concrete panels.

For a given height and diameter of the tank, the number of elements primarily affects the load transferring. The panels act as two-way slabs taking the load by bending action in both principal directions. For an increasing number of elements, implicating decreasing panel width, more of the load along the perimeter is taken by membrane action. Figure 3.3 shows that the maximum resulting stress amplitude along the perimeter, as found by a global analysis in Abaqus/CAE, lowers when increasing the number of panels. These results states the beneficial circumferential load-carrying effect appearing when increasing the polygonal order.

3.2 Load conditions

As the tank performance is evaluated from a local consideration of the individual panels, the main geometry may be expressed by the span-ratio defined as $\frac{L_y}{L_x}$. The x-direction hereby denotes the local distance along the width of a panel, or globally as the distance along the perimeter of the tank. The y-direction is along the panel height, or globally the distance along tank depth. Figure 3.4 defines the span of the panel.

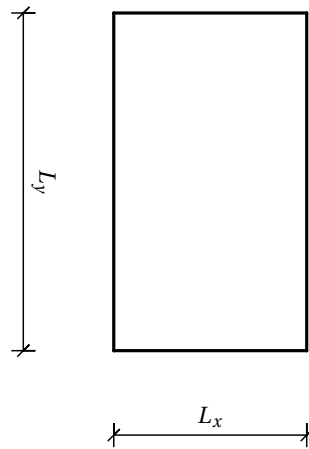


Figure 3.4: Definition of the span-directions within a concrete panel.

3.2.1 Self-weights

As soon as it is casted, the self-weight of the panel contributes to the loading. The magnitude and distribution of this load-effect depends on the panel orientation. When horizontally oriented, which is governing for the casting process, the panel experiences a uniform lateral load with a resultant force given as Equation (3.1).

$$F_g = \rho_c \cdot L_x \cdot L_y \cdot t \cdot g \quad [N] \quad (3.1)$$

ρ_c represent the concrete density, t the governing panel thickness and g the acceleration of gravity. For the panel in operation oriented vertically, its self-weight act as in-plane compressive forces. The distribution may be taken as more or less linearly throughout the height with a resultant as for the horizontally oriented panel given by Equation (3.1).

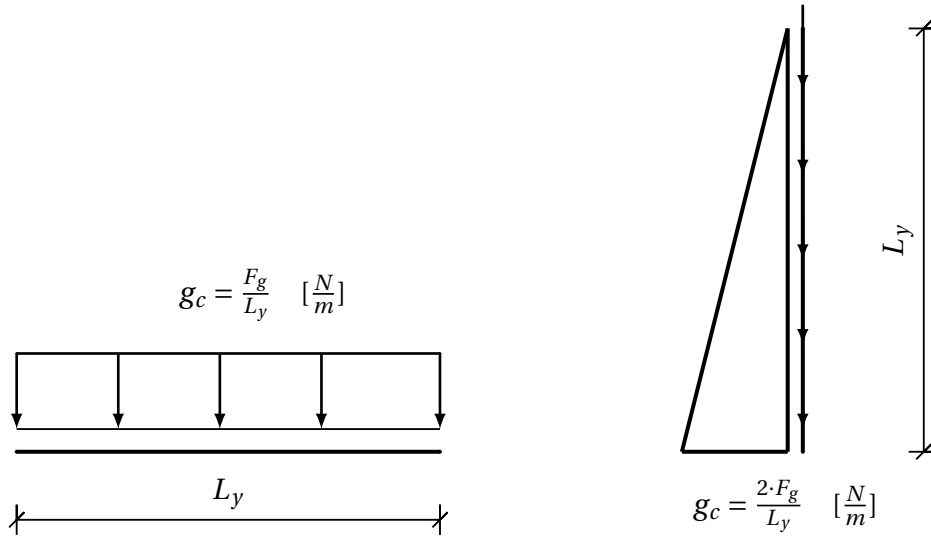


Figure 3.5: Self-weight distribution for different orientations of a concrete panel.

The tank should also carry a pedestrian bridge at the upper edge for inspection purposes. Its presence introduces additional compressive forces dependent on the weight of the bridge. The distribution may be taken as uniform while the magnitude is not further considered. However, the load-effect is qualitatively introduced for the relevant parts of the study.

3.2.2 Prestress as external edge loads

The individual panels are intended to be prestressed occurring as a load-effect prior to the operational phase. Basically prestressed steel contributes as an additional internal resistance of the concrete section. The effect may however be captured by considering equivalent external compressive forces. Since the panels span in two directions, it may be of interest to make use of prestressed steel in both principal directions. Regardless of the type of prestressing, in terms of either pre-tensioning or post-tensioning the steel as mentioned in Section 2.3, the load effect remains the same. For a concrete panel uniformly prestressed at the short edge, the equivalent load picture can be seen in Figure 3.6.

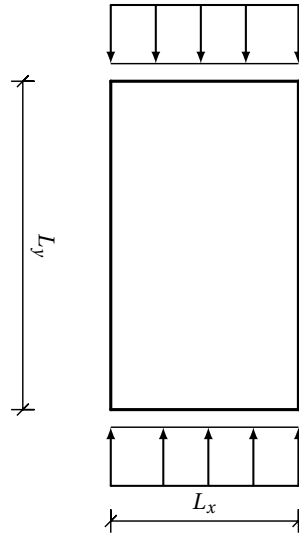


Figure 3.6: Prestress captured as external compressive loads acting at the edge of the concrete panel.

3.2.3 Hydrostatic pressure

When operating, the tank is subjected to a hydrostatic pressure from the containing water. This type of loading shows a triangular distribution along the depth, and therefore a function of the water level. As specified in (NS-EN-1991-4, 2010, Chapter 3), this level should comply with the overall height of the tank for ultimate strength considerations. The magnitude of this pressure acting at the tank bottom is recognized as Equation (3.2).

$$p = \rho_w \cdot g \cdot L_y \quad (3.2)$$

Where ρ_w denotes the density of freshwater.

3.3 Static model

Another issue when establishing the structural model is the boundary conditions. Dependent of the interconnection given by the joint solution, an additional restraint at the long edges must be introduced. The same holds for the connection with the bottom slab, where the connection is dependent of the panel-base solution. As stated by Bergin et al. (2011), it is challenging to fix this connection. A typical solution makes use of an in-situ cast beam, denoting a workmanship carried out at the building site, for the uptake of lateral forces. The resulting eccentricity moment will due to this solution transfer to the bottom slab.

The pedestrian bridge is said to connect two adjacent concrete panels, as is the case in Figure 3.1. In terms of boundary conditions, this will introduce a restraint for out-of-plane movement at the upper edges. A statical model under the governing boundary conditions, not considering the effect from prestress, is shown in Figure 3.7.

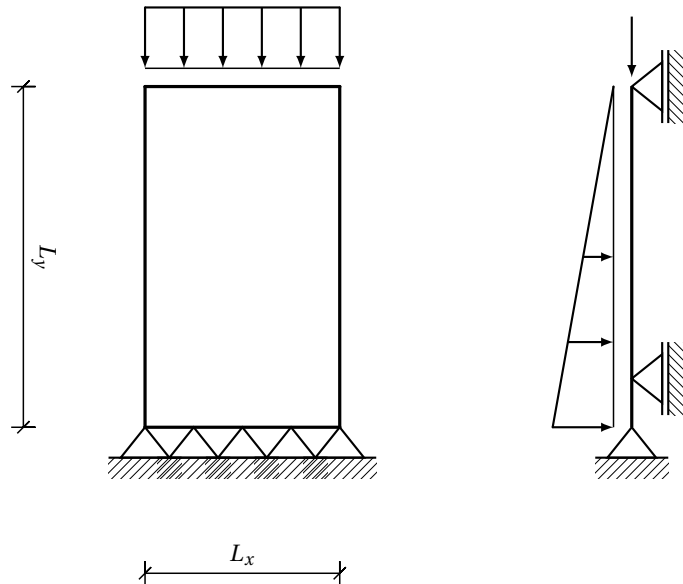


Figure 3.7: A concrete panel on a base foundation subjected to in-plane compressive loads and a triangular distributed pressure.

Figure 3.7 shows a simplified model of a prefabricated concrete panel subjected to compressive loads and a hydrostatic pressure. From a structural point of view it may be recognized as a shell structure. The loading is taken by a flexural slab action and a membrane behavior, which states the structural classification governing for the design checks.

3.4 Design checks

Such as all other load-carrying structures, a liquid-retaining concrete tank must fulfill requirements related to overall strength. The design is typically done within the ultimate limit state, denoted ULS. In addition to these general requirements there exist some rules depending on the purpose of the structure. For a tank within the field of aquaculture, it is crucial that it remains watertight. Although the ultimate capacity checks are satisfied, this does not imply that the structure remains functional throughout the lifetime. These types of requirements are considered within the serviceability limit state, denoted SLS.

According to Table 4.1 in NS-EN-1992-1 (2008) sorting structures into classes of exposure, the tank may be classified as XS2. This class is used as a reference for the given environmental condition, with relevance for parts of the design procedure.

3.4.1 Ultimate limit state

As shown in Figure 3.7, a precast concrete tank may be decomposed into panels loaded in-plane and laterally. The flexural behavior will then introduce bending moments and shear forces in the structure, which must be checked against the corresponding capacity. For this evaluation, the concrete compressive capacity, f_{ck} , and the yield strength for steel, f_{yk} , are the governing strength parameters. In ULS, these capacities are relaxed through material factors, specified in NS-EN-1992-1 (2008) as following.

$$f_{cd} = \alpha \cdot \frac{f_{ck}}{\gamma_c} \quad (3.3)$$

$$f_{yd} = \frac{f_{yk}}{\gamma_s} \quad (3.4)$$

$\alpha = 0.85$ takes into account unfavorable effects depending on the way of loading

$\gamma_c = 1.5$ material factor for concrete

$\gamma_s = 1.15$ material factor for reinforcement steel

Figure 3.8 shows a reinforced concrete cross-section derived from a strip of the panel, which will be used as reference throughout this chapter. The following considerations are based on material from NS-EN-1992-1 (2008) and Sørensen (2013).

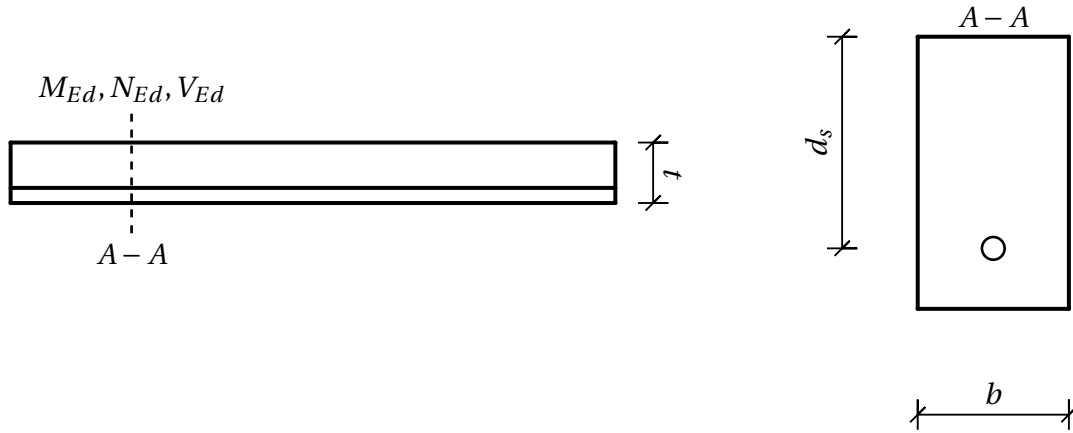


Figure 3.8: A strip of a concrete panel acting as reference for the ultimate strength considerations.

Flexural capacity

The panels must be able to resist the bending moments present. This requirement is formally stated as Equation (3.5), where the design capacity, M_{Rd} , should be greater than or equal to the design load, M_{Ed} .

$$M_{Ed} \leq M_{Rd} \tag{3.5}$$

The flexural capacity of a reinforced concrete section is reached when the compressive strain in the outer fiber becomes ϵ_{cu} , the strain value for compressive crushing. In terms of moment, the capacity M_{Rd} may be derived by considering equilibrium in Figure 3.9.

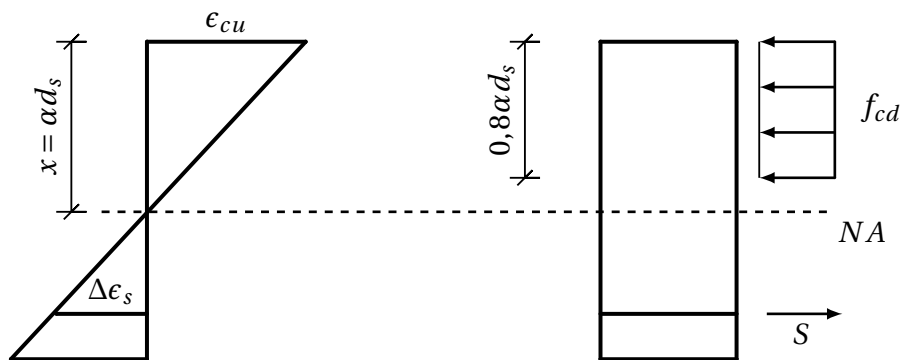


Figure 3.9: Strains and corresponding internal forces within the reference strip section at flexural failure.

The internal forces contributing to this capacity are the concrete compression, f_{cd} , as well as tension in the ordinary reinforcement, S . As seen in the figure, the compression zone is approximated by a rectangular block. The length of this block is set to $0,8\alpha d_s$ in agreement with NS-EN-1992-1 (2008). From moment equilibrium of the internal forces, Equation (3.6) may be established.

$$M_{Rd} = 0,8 \cdot \alpha \cdot (1 - 0,4 \cdot \alpha) \cdot f_{cd} \cdot b \cdot d_s^2 \quad (3.6)$$

The value of α is found by considering horizontal equilibrium, and thus dependent of the amount of reinforcement. As mentioned in Section 2.2, it is beneficial to choose an amount such that the reinforcement yields at a stage before compressive failure. This will then give a warning in terms of deflection prior to collapse. For a value $\alpha = 0,4$, typically within this ductile range, the capacity becomes as Equation (3.7).

$$M_{Rd} = 0,8 \cdot (1 - 0,4 \cdot 0,4) \cdot 0,4 \cdot f_{cd} \cdot b \cdot d_s^2 = 0,269 \cdot f_{cd} \cdot b \cdot d_s^2 \quad (3.7)$$

When intending to use prestressed steel within a structure, this capacity check must be revised. From describing the flexural resistance as a design moment capacity, the design now governs the use of M-N diagrams. By exposing the cross-section to different strain conditions corresponding to concrete crushing, the belonging axial force and moment can be calculated. These pairwise values are then plotted to construct an M-N diagram unique for the cross-section. An example of such a diagram is given in Figure 3.10.

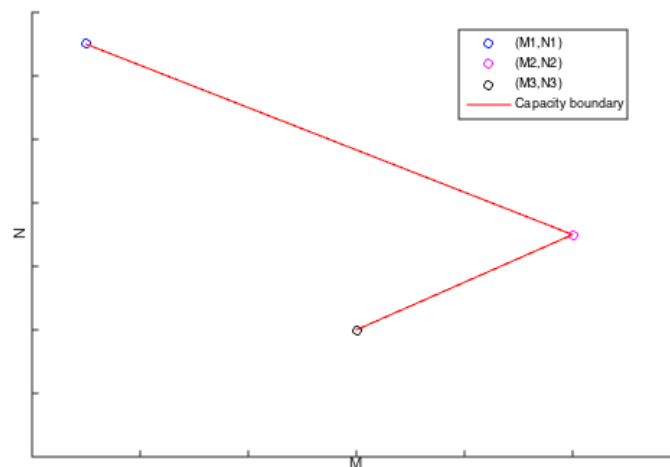


Figure 3.10: Illustration of an M-N diagram specifying the design capacity for a combination of axial forces and moments.

The red line gives the boundary of the capacity. A formal requirement for the cross-section to have sufficient capacity, may be expressed as Equation (3.8).

$$(M_{Ed}, N_{Ed}) \in (M_{Rd}, N_{Rd}) \quad (3.8)$$

A load-condition in the inner domain of this boundary does not violate the capacity of the member. Vice versa for loads outside this boundary, which will result in a structural failure. When applying prestressed steel, the axial force N_{Ed} is typically governed by the amount of prestress. If the section is eccentricity loaded by the prestressing force, an eccentricity moment together with other external bending contributions gives the value of M_{Ed} .

Resistance for shear

In addition to the bending moment present, the lateral load introduces shear stresses in the tank. For the panels to carry these forces, the requirement in Equation (3.9) must be fulfilled.

$$V_{Ed} \leq V_{Rd} \quad (3.9)$$

The shear capacity, V_{Rd} , may be found by considering the formulation of diagonal cracks. This failure mode appears when the principal stress, majorly influenced by the present shear force, reaches the axial tensile strength of concrete. NS-EN-1992-1 (2008) presents Equation (3.10), an empirical formula for determination of the shear capacity.

$$V_{Rd,c} = [C_{Rd,c} \cdot k \cdot (100 \cdot \rho_L \cdot f_{ck})^{\frac{1}{3}} + k_1 \cdot \sigma_{cp}] \cdot b_w \cdot d_s \quad (3.10)$$

f_{ck} = characteristic compressive cylinder strength [$\frac{N}{mm^2}$]

$$k = 1 + \sqrt{\frac{200}{d_s}} \leq 2,0 \text{ [mm]}$$

$\rho_L = \frac{A_{sL}}{b_w d_s} \leq 0,02$ is the ratio of steel [-]

$b_w = 1$ is the unit width when considering a panel strip [mm]

$C_{Rd,c} = \frac{k_2}{\gamma_c}$ where $k_2 = 0,18$ according to national annex [-]

$\sigma_{cp} = \frac{N_{Ed}}{A_c} < 0,2 f_{cd}$ where N_{Ed} is an external axial force [$\frac{N}{mm^2}$]

$k_1 = 0,15$ for compression and $0,3$ for tension [-]

A minimum value of the shear capacity is however limited according to Equation (3.11).

$$V_{Rd,c} = v_{min} \cdot b_w \cdot d_s \quad (3.11)$$

Where v_{min} is given as $0,035 \cdot k^{1,5} \cdot f_{ck}^{0,5}$.

This set of formulas is based on structures with lack of shear reinforcement. Within the panels, introduction of shear reinforcement will most likely not be feasible due to the slender properties. Equation (3.10) and (3.11) will thus be governing when designing for shear failure.

3.4.2 Serviceability limit state

For liquid-retaining structures the ultimate capacity is rarely the governing design issue. A complete design must cover issues in the operational conditions, such that the structure remains functional and sustainable. This design considerations are handled within the SLS.

At this limit state, in contrast to the ULS, the response quantities are investigated considering the actual value of the external loads. Dependent of the appearing concrete tensile stress, the cross-sectional characteristics may differ as cracking occurs. The calculations are therefore sorted for two different phases, prior and post to cracking as specified by the characteristics tensile strength, f_{ctm} .

Deformation control

When calculating this response quantity, time-dependent effects such as creep and shrinkage become important. Creep is introduced when the loading is more or less permanent providing some additional deformation as time goes by. Due to the purpose of smolt breeding, the tanks hold water throughout long periods making this a relevant issue. As mentioned in Section 2.1, the effect may be captured by making use of a long-time concrete modulus of elasticity.

NS-EN-1992-1 (2008) states a maximum allowable deformation as $\delta = \frac{L}{250}$. Here L denotes the length of a beam, or equivalently the shortest span-direction of the panel. The governing design requirement is then described as Equation (3.12).

$$\delta_{max} = \min\left[\frac{L_x}{250}, \frac{L_y}{250}\right] \quad (3.12)$$

A deflection amplitude larger than this value is said to damage the esthetics or primary purpose of the structure.

Control of cracking

In general, crack-width limitations are governing for all structures to maintain sustainability throughout the lifetime. The maximum width of a crack is given according to the degree of exposure. A concrete tank for smolt breeding was previously classified as XS2. For this type of structure, the maximum crack-width is dependent on whether or not the reinforcement is bonded. For prestressed members with bonded tendons, the criteria relates to maintaining a certain zone of compression, stated as "Decompression" in Figure 3.11.

Exposure Class	Reinforced members and prestressed members with unbonded tendons	Prestressed members with bonded tendons
	Quasi-permanent load combination	Frequent load combination
X0, XC1	0,4 ¹	0,2
XC2, XC3, XC4	0,3	0,2 ²
XD1, XD2, XS1, XS2, XS3		Decompression
<p>Note 1: For X0, XC1 exposure classes, crack width has no influence on durability and this limit is set to guarantee acceptable appearance. In the absence of appearance conditions this limit may be relaxed.</p> <p>Note 2: For these exposure classes, in addition, decompression should be checked under the quasi-permanent combination of loads.</p>		

Figure 3.11: Recommended values for maximum crack-width, w_{max} (mm), sorted for exposure classes, (NS-EN-1992-1, 2008, p. 119).

A flexural member carries the loading by a combination of tension and compression in the section, as seen by the strain distribution in Figure 3.12. The illustration is based on a strip formulation of the concrete panel.

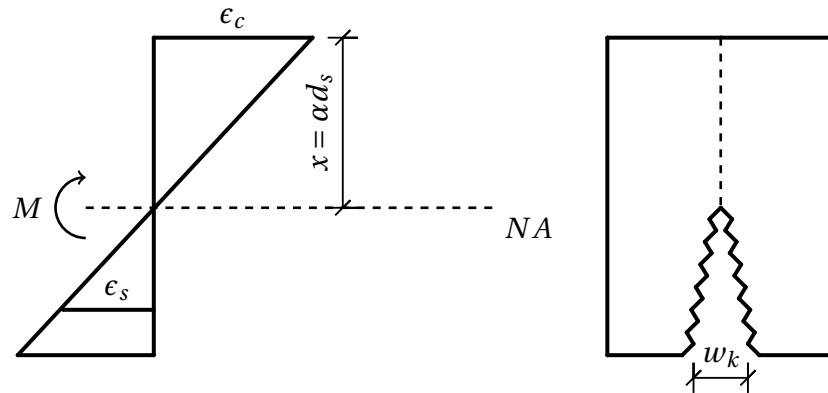


Figure 3.12: A section of the reference strip loaded in bending developing a flexural crack.

The tensile side of the section may easily be subjected to cracks as the concrete possess low tensile strength. However, as part of the section stays in compression, the crack nose meets resistance when trying to penetrate through this compressive zone. Dependent of the size of this zone, the crack may lock meaning no further propagation.

A section loaded in pure tension experiences a different crack pattern, as can be seen in Figure 3.13. The loading introduces a uniform tensile strain, which gives the crack propagation equal resistance throughout the thickness. The result is then a through-thickness crack with a magnitude governing for the design. The self-healing concept, stating that a crack will heal itself up to a certain value of w_k , may be utilized.

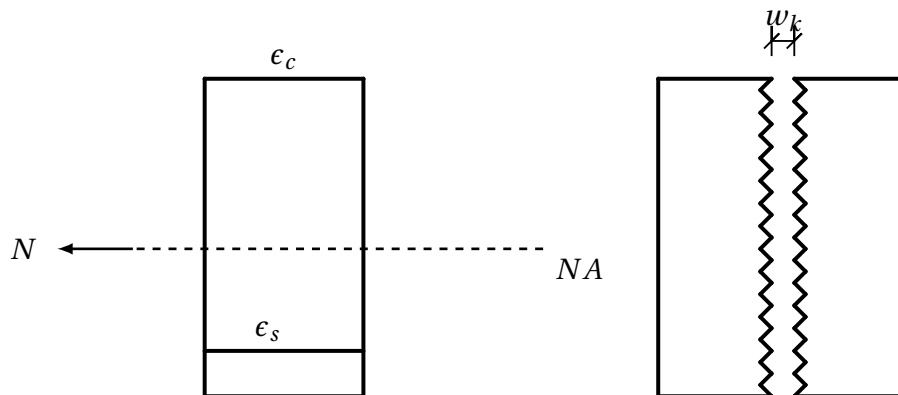


Figure 3.13: A section of the reference strip loaded in tension developing a through-thickness crack.

A conservative design strategy aims to fully prohibit cracks. This is obtained by forcing the tension in concrete to stay beyond its level of cracking, or more extremely by keeping the whole section in compression. Although this may be seen as the most secure philosophy, it is often related to high economical costs and unpractical layouts. A thicker section introduces a higher

internal resistance to prohibit cracks, but implies higher material costs. Reinforcement also serves as a resistance to cracking, as it carries the tensile part of the loading. Slender elements do however set restrictions on the use of this type of reinforcement, as it is difficult to satisfy the required concrete cover.

Crack-width limitations exist for all concrete structures so to remain sustainable. However, due to the purpose of the structure, it is essential that the limitation of cracks relates to a watertightness-criterion. Liquid-retaining concrete structures are therefore given special care in NS-EN-1992-3 (2009). The standard operates with tightness classes specifying the degree of protection against leakage required. As seen in Figure 3.14, these classes range from 0-3 stating having different requirements within each.

Tightness Class	Requirements for leakage
0	Some degree of leakage acceptable, or leakage of liquids irrelevant.
1	Leakage to be limited to a small amount. Some surface staining or damp patches acceptable.
2	Leakage to be minimal. Appearance not to be impaired by staining.
3	No leakage permitted

Figure 3.14: Classification of tightness in accordance to requirements for leakage, (NS-EN-1992-3, 2009, p. 10).

While tightness class 0 allows some degree of leakage, a structure within class 3 must remain completely watertight. A concrete tank for smolt breeding purposes is typically within the latter. Cracks and leakage within this structure introduces loss of water, as well as a degree of pollution in the farming. It is worth mentioning that this classification may be somewhat relaxed, as Solstad (2015) states that the structures typically are protected with an inner coating.

As tightness class 3 does not allow any leakage, NS-EN-1992-3 (2009) suggests special measures in order to fulfill this criteria. The use of prestressed steel is mentioned, and typically the governing solution for such problems. By combining prestressed steel with the reinforced concrete section properties, one may obtain a solution meeting the leakage requirement by a reasonable economic cost. The concept is called partially prestressing, covered later on.

For a flexural member within tightness class 3, acting as the categorization of the concrete tank panels, leakage is avoided by controlling the compressive zone, x , shown in Figure 3.12. The typical design procedure considering limitation of crack-widths is then abandoned. NS-EN-1992-3 (2009) gives the recommended value for this zone, denoted x_{min} , as the lesser of 50mm and 0,2 times the thickness.

3.5 Prestressed concrete tanks

There exist several concepts for the purpose of retaining liquid in concrete tanks by the use of prestressed steel. Regardless of the type of liquid, the pressure introduce forces which must be carried by the same principles. These prefabricated polygonal tanks take the loading by a two-way flexural action.

Two existing approaches are presented in the following. The solution stated by Abetong is especially suited for water storage, while the XPREStank covers more general applications. These two concepts reflects the current practices and intentions when using prestressed concrete for storage. For both cases, the panels are joined together at a base slab casted in situ.

3.5.1 Abetong

Figure 3.15 shows the overall aim as proposed by Abetong (2015), when utilizing prestressed steel in the liquid-retaining applications. The arrows illustrate the load-effect by prestressing the tank in both principal directions.

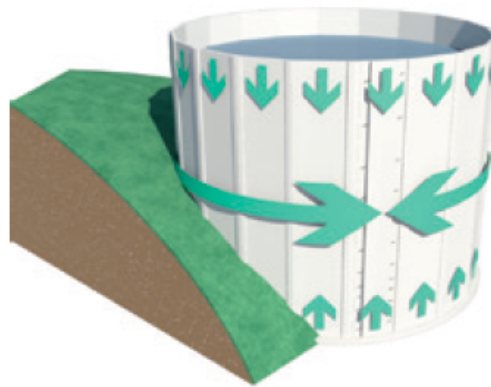


Figure 3.15: The structural effects arising when prestressing a precast concrete tank in both directions, Abetong (2015).

The panels are first vertically prestressed in fabric by means of pre-tensioning. In this process concrete is casted in forms which surrounds the priorly jacked steel. After a while, the steel is relaxed thereby trying to counteract the initial strains. Through the established concrete-steel bond, these strains transfer as compressive forces to concrete. Figure 3.16 shows the different steps in the operation. The product is a one-way prestressed panel to be transported to site for further post-tensioning along the perimeter.

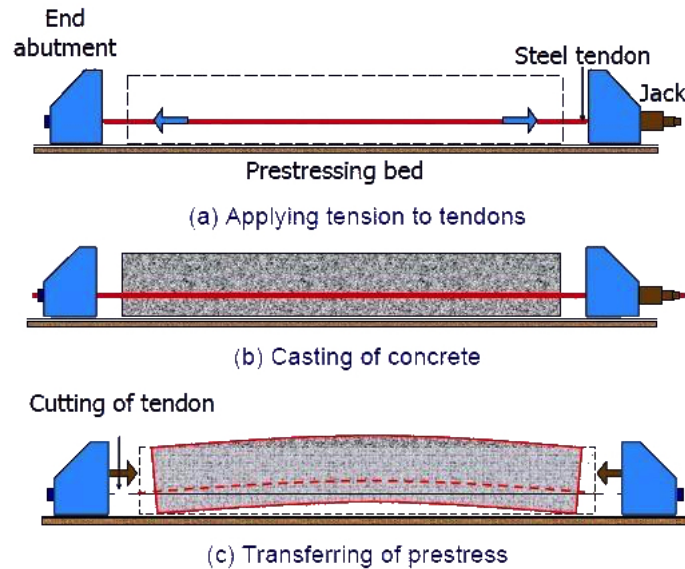


Figure 3.16: Illustration of the pre-tensioning process during casting of a concrete panel at fabric, CivileA (2015).

In contrast to the vertically prestressed steel, the prestressing force along the perimeter is introduced after casting of the concrete. The process is known as post-tensioning, denoting the prestressing force as post to the casting. In order to do this, the panels are equipped with previously casted ducts in this direction. When the panels then are assembled forming a polygonal tank, steel tendons are guided through the ducts along the circumference of the tank. While the vertical prestressing affects the panels individually, prestressing along the perimeter is done in one operation. This process can be seen in Figure 3.17, where the red arrows highlight the applied tendon forces.

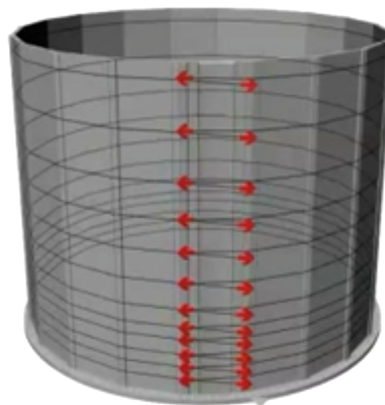


Figure 3.17: Illustration of post-tensioning along the perimeter covering all precast concrete panels in one operation, Abetong (2015).

When tendons as placed within the ducts are prestressed, this will introduce compression into concrete. Grout may then be injected to establish a bond between concrete and steel ensuring further compatibility in the strains. In addition to the load-carrying effect, this type of prestressing also introduces compressive forces across the vertical joints of the panels. As joints are potentially weak spots in such structures, the effect is beneficial when considering watertightness.

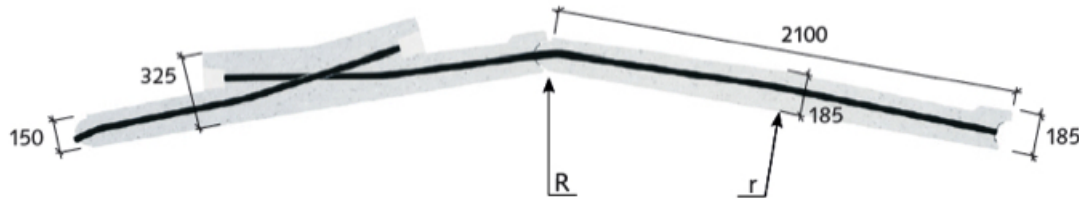


Figure 3.18: Layout of post-tensioned steel inside a horizontal section of two adjacent concrete panels, Abetong (2015).

3.5.2 XPREStank

The XPREStank is a concept developed by the Consolis Group. It covers applications for storage of both liquids and solids. Compared to the solution stated by Abetong, this concept only applies for a limited range of tank dimensions.

Individual panels are pre-tensioned vertically in the same manner as illustrated in Figure 3.16. For load-carrying along the perimeter, the solution differs from the one previously presented. Instead of placing steel within previously casted ducts, tendons are now located on the outside of the tank. Since the tendons are separated from the concrete section, the effect from the following prestressing will not be the structural characteristics obtained from the concept proposed by Abetong (2015). Figure 3.19 shows the tendon orientation in relation to a section of a panel.

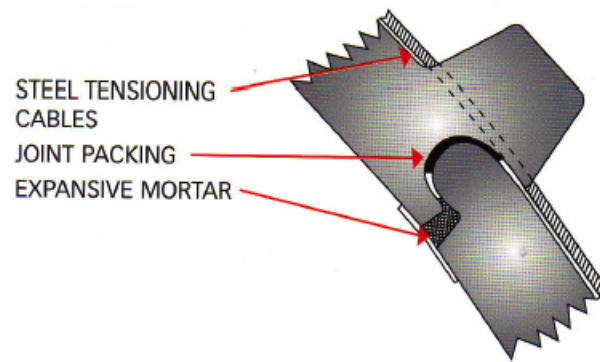
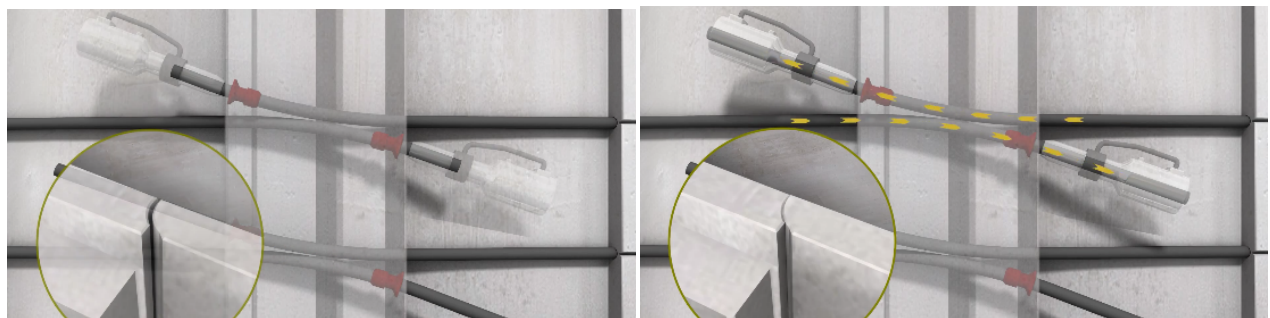


Figure 3.19: Steel tendons placed at the outside of a concrete tank prepared for tensioning, MooreConcrete (2015).

The main purpose by the placement of these tendons is related to the joint performance. As the tendons along the perimeter gets tensioned, the tank as a whole tries to contract as a result of the contact force between steel and concrete surface. Due to the matching geometry at the long sides of the panels, the joints now in compression get nearly sealed. This effect will then act to obtain a watertight joint solution.



(a) Opening in highlighted joint before tensioning. (b) Sealed highlighted joint after tensioning.

Figure 3.20: Sealing a vertical joint by post-tensioning the steel tendons placed at the outside of a concrete tank, ConsolisGroup (2015).

Although this solution does not give the same structural properties as an ordinary prestressed element, it will be beneficial for closure of the vertical joints. This approach does not require casting of ducts neither such a following demanding prestress operation, which can be seen as an economical and therefore competitive solution.

Part II

Investigation of large concrete panels

Chapter 4

Buckling of large prestressed concrete panels

The buckling analyses are performed by use of finite shell elements primarily within Abaqus/-CAE. By a linear perturbation analysis step, this software considers linearity when solving the eigenvalue problem. The explicit formulation adopted from Abaqus (2013) is reproduced in Equation (4.1).

$$(K_0 + \lambda_i K_\Delta) v_i = 0 \quad (4.1)$$

Here K_0 denotes the initial stiffness matrix of the panel. The stiffness contribution from the loading is captured by the term K_Δ . λ_i states the corresponding eigenvalues acting as the scale factor for the base load, Q . By an iterative solution method, the specified number of eigenvalues are calculated. To obtain the corresponding buckling stress, the eigenvalues are multiplied with the reference load as in Equation (4.2).

$$Q_{crit(i)} = \lambda_i Q \quad (4.2)$$

The reference load is specified as a shell edge load with unit $[\frac{N}{m}]$, which then states the response unit reported by Abaqus/CAE. In the following case studies, the buckling performance is given as stresses $[\frac{N}{mm^2}]$. This is simply done by dividing the results from the software by the governing thickness of the panel.

4.1 Problem description

The reference panel, further denoted as Panel 1, is shown in Figure 4.1. The panel height $L_y = 6m$ and width $L_x = 3m$ gives a span-ratio of $\frac{L_y}{L_x} = 2$. Panel thickness is given as $300mm$.

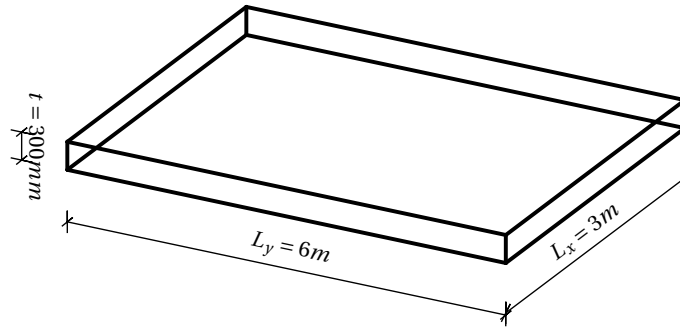


Figure 4.1: The geometry of the panel used as reference for the buckling analyses.

Table 4.1 presents the material properties of the concrete panel.

Parameter	Value
Poisson's ratio (ν)	0.15
Concrete modulus of elasticity (E_c)	$35 \cdot 10^3$ Mpa
Density of concrete (ρ)	$2400 \frac{kg}{m^3}$

Table 4.1: Material properties of concrete panel.

With increasing span-ratio and decreasing value of thickness, the concrete panels get more vulnerable to instability problems. This chapter deals with a study regarding buckling strength of prestressed concrete panels.

The study is differentiated with respect to three load cases as basis for the buckling analyses.

- Vertical prestressing in fabric, i.e panel subjected to compressive stress at the short edges
- Further prestressing at site along the perimeter, i.e panel subjected to biaxial compression
- Design condition, i.e biaxial compressed panel subjected to a lateral pressure

In fabric, prestress is applied in the direction of the longest span during casting of the panels. Prior to the water supply, the panels are further prestressed along the perimeter reflecting a biaxial state of compression. The last case considers the presence of hydrostatic pressure, which together with the state of prestress represents the design condition. In this stage, the panels are also loaded by a pedestrian bridge resting on the upper edge.

4.1.1 Simplification of reinforced concrete properties

A reinforced concrete panel, denoted RC, consists of both reinforcement steel and concrete which forms an inhomogeneous material. The presence of reinforcement will distract the overall stiffness of the panel, affecting its behavior. Isotropicity suggests that an element has equal material properties in the principal directions. For an RC panel, this is typically not the case. In addition to the amount of steel, the presence of cracks also differs in each direction. These effects result in directional material properties stating an anisotropic material. However, while the amount of steel is chosen initially, cracking is a consequence of the appearing loads. It is therefore apparent that an element may crack in only one direction resulting in a more complex situation.

The transition from an uncracked to a cracked section does in reality happen seamlessly in terms of structural behavior. When it comes to numerical modeling, this is however defined as two different states. In the following, these states are presented as representatives for the two ways of approximating the RC panel cross-sectional properties. The following formulation is adapted from (Sørensen, 2013, Chapter 5).

Uncracked section

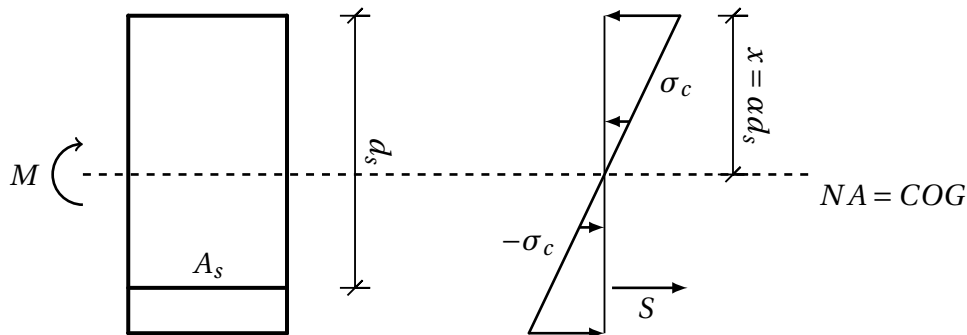


Figure 4.2: Internal forces for an uncracked section of a strip of the concrete panel loaded in bending.

Figure 4.2 shows the first stadium, which reflects no cracking within the concrete. The maximum tensile stress is then beyond the corresponding concrete strength. Since the cross section still is intact reflecting a homogenous property, every part of it will contribute in terms of stiffness. As the section is reinforced, an additional stiffness contribution is provided from the steel reinforcement. The moment of inertia may be calculated separately for both the concrete and steel as shown in Equation (4.3) and (4.4).

$$I_c = \frac{b \cdot h^3}{12} + b \cdot h \cdot \left(\alpha \cdot d_s - \frac{h}{2} \right)^2 \quad (4.3)$$

$$I_s = A_s \cdot (d_s - \alpha \cdot d_s)^2 \quad (4.4)$$

A consequence of the uncracked cross section is the coincident neutral axis, NA , and center of gravity, COG . The height of the compressive zone, x , may thus be found by considering the area moments. The resulting expression, where $\eta = \frac{E_s}{E_c}$ represents the ratio of material stiffness, is given in Equation (4.5).

$$\alpha \cdot d_s = \frac{A_c \cdot 0.5 \cdot h + \eta \cdot A_s \cdot d_s}{A_c + \eta \cdot A_s} \quad (4.5)$$

The bending stiffness of a reinforced uncracked section is further found by a superposition of the separate bending stiffnesses, as shown in Equation (4.6).

$$E \cdot I = E_c \cdot I_c + E_s \cdot I_s \quad (4.6)$$

Cracked section

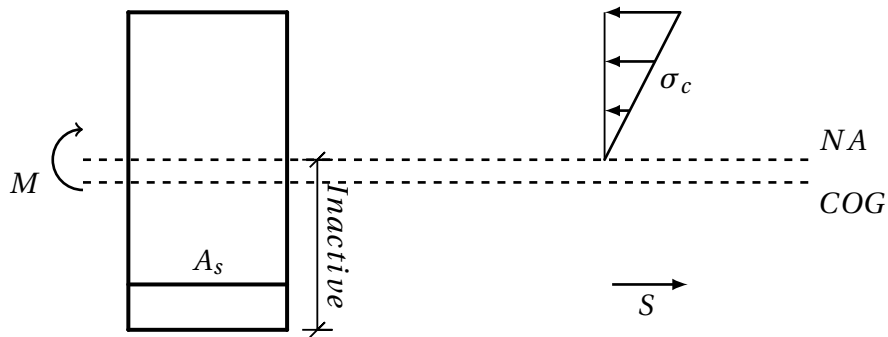


Figure 4.3: Internal forces for a cracked concrete section of a strip of the concrete panel loaded in bending.

When the forces in the tensile part of the concrete section exceeds its tensile strength, the result is a cross sectional configuration as shown in Figure 4.3. The concrete part in the tensile zone has now cracked as indicated by the inactive notation. In terms of concrete structural resistance, this is now only provided by the concrete in compression.

There are several ways to express the moment of inertia for a reinforced cracked concrete section. Equation (4.7) gives an equivalent concrete moment of inertia, when incorporating the stiffness from the reinforcement steel.

$$I_{c-eq} = \frac{1}{2} \cdot \alpha^2 \cdot \left(1 - \frac{\alpha}{3}\right) \cdot 10^3 \cdot d_s^3 \quad (4.7)$$

As a result of cracking, NA moves away from the COG to maintain equilibrium between internal and external forces. The height of the compressive zone is found by considering force equilibrium in the axial direction. The result is presented as Equation (4.8), where $\rho = \frac{A_s}{bd_s}$ denotes the ratio of reinforcement.

$$\alpha \cdot d_s = d_s \cdot \left(\sqrt{(\eta \cdot \rho)^2 + 2 \cdot \eta \cdot \rho} - \eta \cdot \rho\right) \quad (4.8)$$

The bending stiffness may then be expressed as Equation (4.9).

$$E \cdot I = E_c \cdot I_{c-eq} \quad (4.9)$$

As concrete possess a low tensile strength, this structural configuration is typically governing. For cases where the concrete section really stays uncracked, the approximation introduced by this model provides safety in the design.

By using a homogenous and isotropic material model in the buckling analysis, the stiffness contribution from reinforcement and the presence of cracks are not accounted for. A modification of this approach may however be done from a strip-consideration of the panel. This theory suggests that the load-transferring may be captured by dividing the panel into strips, acting as structural beams.

(NS-EN-1992-1, 2008, Chapter 5) states that a simply supported panel may be considered as one-way load-transferring as long as the span-ratio is larger than two. The governing direction for load-carrying within the examined panel considered as simply supported, is then along the short edge. This approximation can also be supported by compatibility in the deflections. As an intersection point between a strip in x-direction and another in y-direction must deflect equally, this indicates differences in the curvatures. The shortest strip located along the x-direction experiences greatest curvature, which gives rise to the largest bending moment.

For a simply supported panel, the idea is to assume uptake of forces only for the x-directional strips. For a homogenous uncracked concrete strip, the moment of inertia may be expressed as (4.10).

$$I = \frac{10^3 \cdot t^3}{12} \quad (4.10)$$

According to this equation, the moment of inertia may be manipulated by a change in the thickness. This fact is used in the following when approximating the cracked section properties. By setting Equation (4.10) equal to (4.7), i.e the moment of inertia of a homogenous concrete strip section equal to the moment of inertia of a cracked RC strip section, Equation (4.11) is obtained.

$$t_{eq} = \sqrt[3]{\frac{12 \cdot I_{c-eq}}{10^3}} \quad (4.11)$$

Table 4.2 presents the data needed to calculate the equivalent thickness.

Parameter	Value
E_s , steel modulus of elasticity [Mpa]	$195 \cdot 10^3$
E_c , concrete modulus of elasticity [Mpa]	$35 \cdot 10^3$
b , plate strip width [mm]	1
d_s , distance from steel to section surface [mm]	280
A_s , area of reinforcement [$\frac{mm^2}{m}$]	510

Table 4.2: Material and geometrical parameters to determine the equivalent concrete panel thickness.

The area of reinforcement is chosen as the minimum value given by Equation (4.12), taken from (NS-EN-1992-1, 2008, Chapter 9).

$$A_{s,min} = 0,26 \cdot \frac{f_{ctm}}{f_{yk}} \cdot b \cdot d_s > 0,0013 \cdot b \cdot d_s \quad (4.12)$$

Where $f_{ctm} = 3,5\text{Mpa}$ is the mean value axial strength of concrete, while $f_{yk} = 500\text{Mpa}$ gives the characteristic yield strength of the reinforcement. d_s must be chosen in accordance to required concrete cover. A typical value is given as $c_{nom} = c_{min} + \Delta c_{dev}$. c_{min} is related to degree of exposure, with a minimum value of 10mm. Δc_{dev} may be taken as 10mm as proposed by the national annex in NS-EN-1992-1 (2008). d_s is then calculated as thickness less than the concrete cover, $d_s = t - c_{nom}$.

The equivalent moment of inertia may then, after some intermediate steps, be calculated according to Equation (4.7) as $I_{c-eq} = 1,85E08\text{mm}^4$. By utilizing Equation (4.11), the equivalent thickness is given as $t_{eq} = 130,4\text{mm}$.

This particular thickness value may then be used to perform a simplified buckling analysis of an RC panel subjected to cracks. However, the strip theory suggests one-way load-transferring when boundaries are simply supported. As this is an ideal condition rather than a practical one, it may not be satisfied for the cases considered in the following buckling analysis. The interpretation of this equivalent thickness, which neglects load uptake from the y-directional strips, will then be rough and highly conservative.

In order to relax these assumptions, the study considers the use of $t = 200\text{mm}$, stating a value somewhere between the equivalent and the true one. Although this modification is not further supported by structural considerations, it aims to investigate the reduce of stiffness when a reinforced concrete panel is loaded above its tensile capacity.

4.2 Case study

For each case corresponding to a stage in the construction, the performance is evaluated with increasing height of Panel 1. By keeping the panel width constant, representing a certain polygonal structure, the effect of increasing span-ratio $\frac{L_y}{L_x}$ is investigated. The effect in terms of buckling capacity by changing the panel thickness is shown within the first case study. Table 4.3 presents the panel geometries that are considered.

Panel	1	2	3	4
Height [m]	6	8	10	12
Span-ratio [-]	2	2,67	3,33	4

Table 4.3: Panel geometries considered in the buckling analyses.

4.2.1 Concrete panel subjected to monoaxial compressive stress

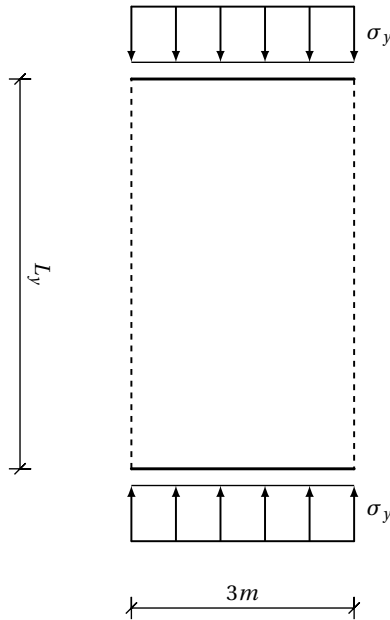
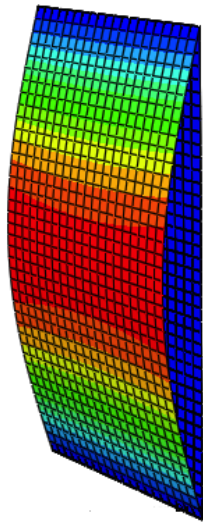
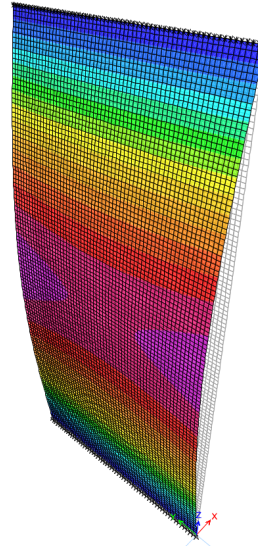


Figure 4.4: Concrete panel prestressed with a uniform distribution at the short edges.

Prior to the tank assembly, the concrete panels are prestressed in fabric. Reinforcement steel placed in the y-direction are then tensioned to a certain level before casting of surrounding concrete in prestressing beds. As this force is intended to be uniformly introduced, it favors the use of equally spaced prestressed steel tendons. Figure 4.4 may then be considered as representative for this stage of the construction. The dashed lines indicates free movement, acting as the governing boundary condition at the long sides when prestressing panels in forms at fabric.

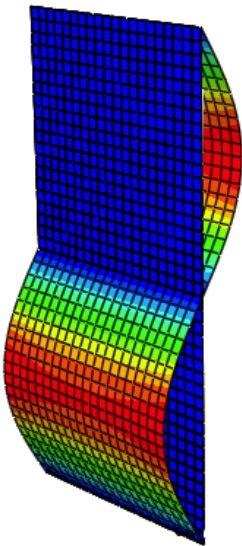


(a) First eigenmode as visualized by Abaqus.

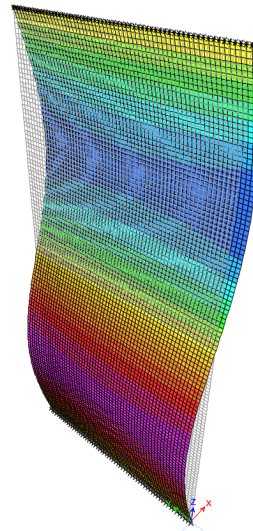


(b) First eigenmode as visualized by Etabs.

Figure 4.5: First eigenmode for Panel 1 within the first case study.



(a) Second eigenmode as visualized by Abaqus.



(b) Second eigenmode as visualized by Etabs.

Figure 4.6: Second eigenmode for Panel 1 within the first case study.

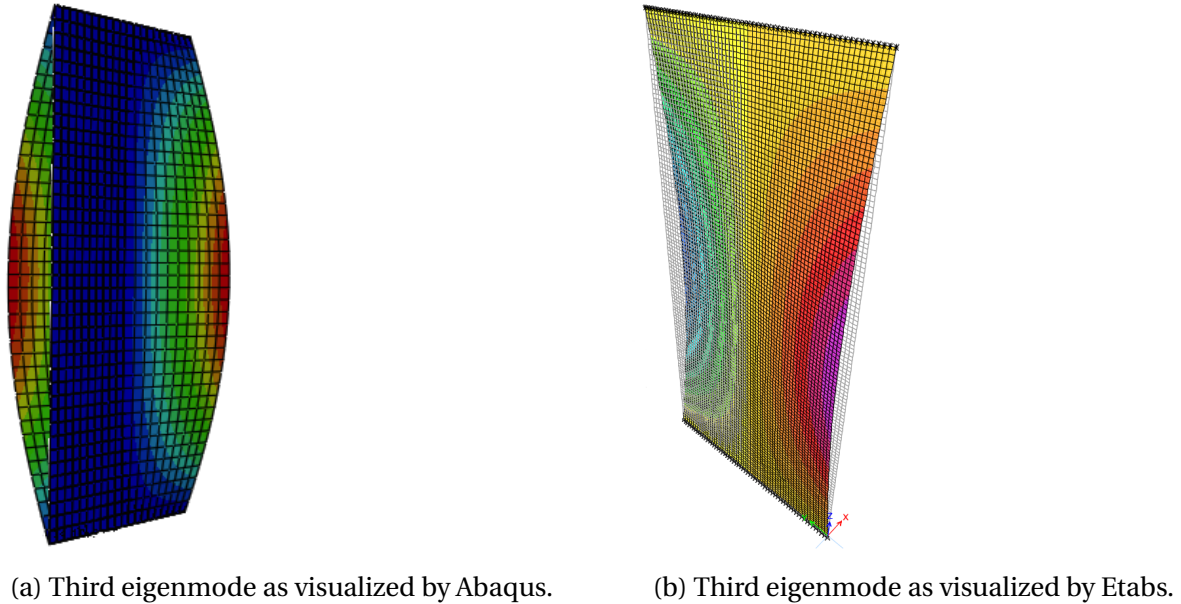


Figure 4.7: Third eigenmode for Panel 1 within the first case study.

Eigenmode	Buckling stress [Mpa]	
	Abaqus	Etabs
1st	32.1	31.8
2nd	128.5	128.5
3rd	281.5	287.0

Table 4.4: Buckling strength corresponding to the three first eigenmodes of Panel 1.

Figure 4.5, 4.6 and 4.7 shows the corresponding shapes of the three first eigenmodes for Panel 1. As the first mode shows the lowest buckling strength, this turns out as the critical one with respect to buckling when prestressing the panels at short edges. The first eigenmode corresponds to a deflection in one half-wave, as seen in Figure 4.5. Increasing eigenmodes reflect increasing buckling capacities thus not that easily triggered. For each mode, the results are validated by reporting the modes as calculated by Abaqus and Etabs. Table 4.4 shows that the buckling capacities correlate well across the softwares.

With increasing span-ratio according to Table 4.3, the panels show a natural decreasing trend regarding buckling capacity. Appendix A.1 presents the eigenmodes for these other examined panels. The results are given for the first eigenmodes as these are most easily triggered in terms of compressive stress. Independent of the span-ratio, the lowest modes are still governed by a deflection in one half-wave. Despite of the equality in buckling shape, the corresponding buckling stresses decrease considerably with increasing span-ratio as noted by an evaluation of the results in Table 4.5.

Panel	1	2	3	4
Buckling stress by Abaqus [Mpa]	32.1	18.1	11.6	8.0
Buckling stress by Etabs [Mpa]	31.8	17.8	11.4	7.9

Table 4.5: Buckling stress corresponding to the lowest eigenmode for the evaluated panels.

Contribution from self-weight of the panel

Panel self-weight may additionally be introduced as a base load. The distribution of this load component is dependent of the panel orientation, as discussed in Section 3.2.1. For a panel within this stage, its horizontally orientation suggests a lateral self-weight component. This component acts in the opposite direction of the deformation as a stabilizing issue during the casting process. However, as the one-way prestressed panel at a certain point in time will be vertically oriented, self-weight as in-plane compressive forces is considered as the governing issue.

Panel	1	2	3	4
Buckling stress [Mpa]	32.0	18.0	11.5	7.8
Percentage reduction [%]	0.31	0.55	0.86	2.50

Table 4.6: Buckling stress corresponding to the lowest eigenmode for the evaluated panels when incorporating panel self-weight.

Table 4.6 shows the buckling stress for the evaluated panel when accounting for self-weight. Compared to the results provided in Table 4.5, the influence from this additional load-component on the buckling performance is rather minor. However, as the buckling capacity decreases considerably with increasing span-ratio, the load-effect from panel self-weight increases in importance as presented by the percentage reduction. This compressive force component may then for an even larger precast panel become decisive for its performance.

Effect from panel slenderness

The panels are modeled with an equivalent thickness aiming to incorporate the stiffness effect from reinforcement steel as well as cracking of concrete. As previously discussed, this represents an approximation which really damage the validity of the results. While the primary target for this investigation is to capture the buckling performance for varying panel slenderness, the results will also show the sensitivity and thereby a potential accumulation of errors in the use of

an equivalent thickness. Figure 4.8 presents the buckling strength for the examined panels with varying thicknesses.

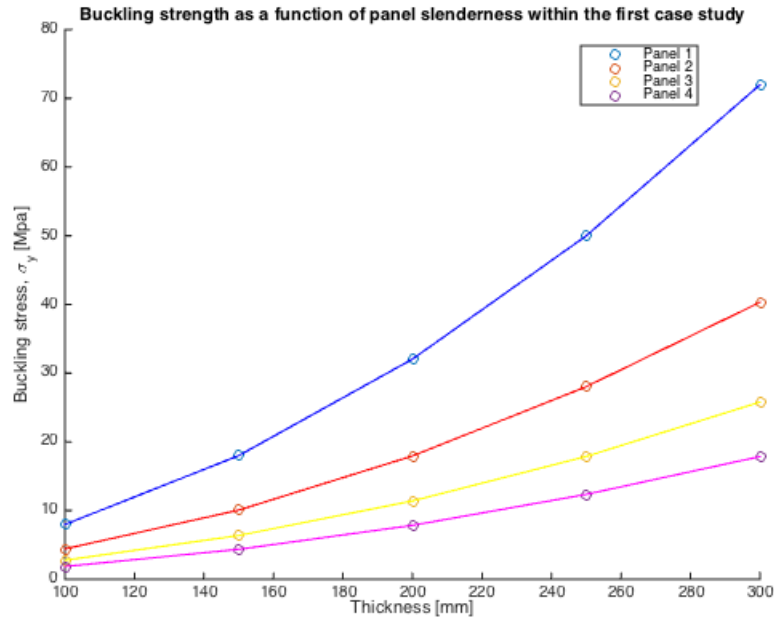


Figure 4.8: Buckling stress as a function of panel slenderness within the first case study.

An increase in panel thickness strengthens the buckling capacity considerably. This trend is governing independent of the span-ratio. However, the positive correlation between thickness and buckling performance reduces for increasing span-ratios. This is recognized by the blue line in the figure, representing the buckling strength for Panel 1, which shows a greater gradient than the other performances.

When decreasing the panel thickness from 300mm to 200mm, representing the approximation of a cracked reinforced concrete section, the panels experience a major change in buckling strength. The decrease may be taken as twice the initial value, as interpreted from Figure 4.8.

The results state the importance of the panel thickness to resist buckling. As increased panel thickness implies larger material costs, the correlation with buckling capacity is an important issue in order to optimize costs and structural capacity. Parallel with the great correlation between buckling strength and panel slenderness, this finding also states the sensitivity for errors when approximating reinforced concrete properties by an adjustment in thickness.

4.2.2 Concrete panel subjected to biaxial compressive stress

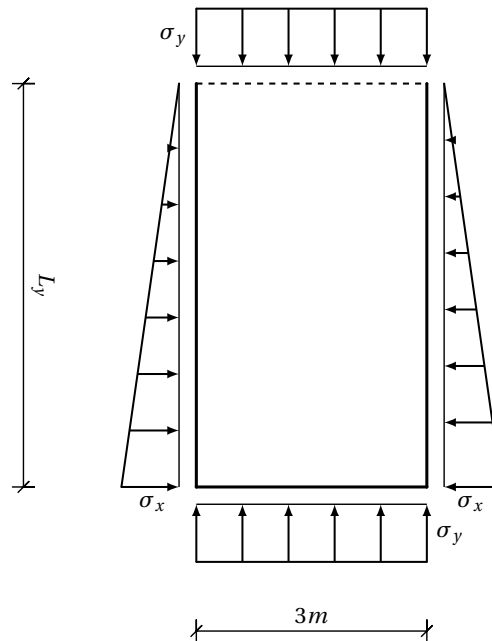


Figure 4.9: Concrete panel with a uniform prestress at short edges and a linearly distributed prestress at long edges.

The second stage relates to the connection of the panels at site, prior to the supply of water. In addition to the vertical prestress appearing from the previous stage, the panels are now also stressed at the long edges. As it should act over a large distance, it may now be considered practical to introduce a linear force distribution by the application of prestress. The equivalent load picture is reproduced in Figure 4.9, where a concrete panel is subjected to a biaxial compressive stress. As indicated by the dashed line, the upper edge is free to move. The long sides are connected to the adjacent panels by keeping the boundaries fixed in the y -direction and for out-of-plane movement.

Buckling analyses in this stage are performed by varying the degree of vertical prestress accumulated from the previous stage. This amount characterizes the initial deformed shape, influencing the resulting buckling shape and thereby capacity. The degree of vertical prestress is stepped through an interval containing the panel buckling stress for pure vertical compression calculated previously. By doing this, the analysis covers the biaxial buckling strength with various initial degree of prestress at short edges.

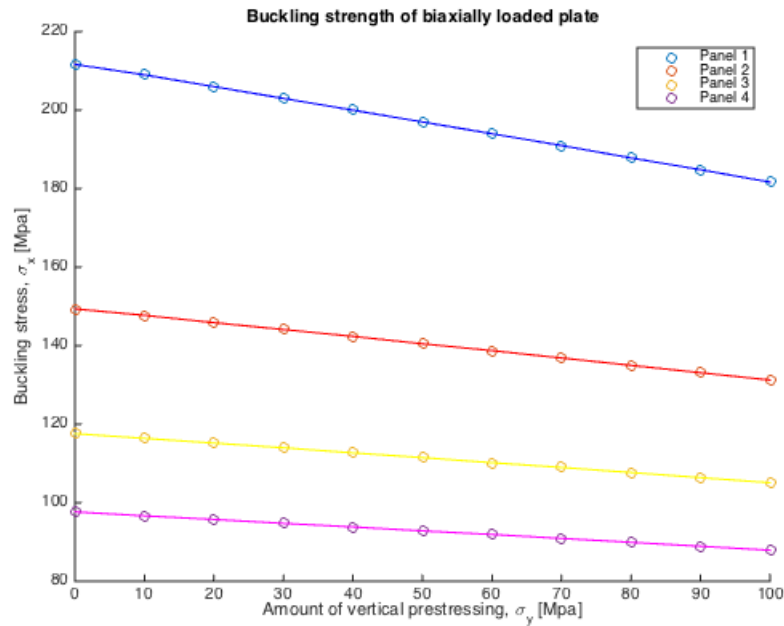


Figure 4.10: Buckling stress for concrete panels within the second case study.

Figure 4.10 shows the buckling strength for the panels given in Table 4.3, as a function of the vertical prestress. The results are presented graphical for a uniform compressive stress at short edges ranging from 0Mpa to 100Mpa. The procedure then contains the buckling strength for pure vertical compression as calculated for the first case. As well as a large decrease of buckling capacity for increasing span-ratios, the results state the panel performance when increasing the degree of compression at short edges. As represented by the blue dots in the figure, Panel 1 shows the greatest negative correlation with this increasing degree. For increasing span-ratio, the relationship between the biaxial buckling strength and amount of vertical prestress gets somewhat more relaxed.

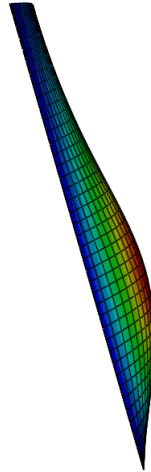


Figure 4.11: Lowest eigenmode for Panel 1 within the second case study experiencing minor influence from the vertical prestress.

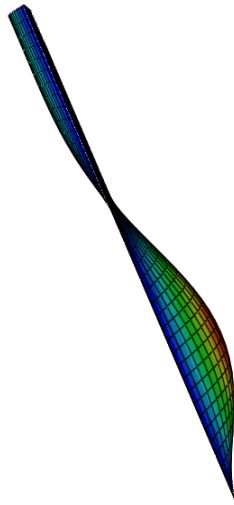


Figure 4.12: First eigenmode for Panel 1 within the second case study experiencing major influence from the vertical prestress.

Along the interval of vertical prestress presented in Figure 4.10, the biaxial buckling capacity is characterized by different buckling shapes. As the degree of compression at short edges increases, this load shows a stronger influence on the activated buckling mode. For a panel with acting loads as in the left region of the figure, the contribution from this stress component is of minor importance. This statement can be justified by Figure 4.11, presenting the buckling shape at this state of prestress. The activated mode seems to be dominated by the compression

at long edges, as the panel buckles with a deflection maximum near the resultant for the linear force distribution.

With increasing amount of vertical compression, reflecting a movement to the right in Figure 4.10, the biaxial buckling strength decreases for each of the panels. Figure 4.12 shows the buckling mode for Panel 1 when experiencing a large degree of stress at short edges. The shape suggests a major contribution from this force component as it provides a deflection at the upper edge. This initial deformation is then more easily amplified by the compression at the long edges, resulting in a lowered biaxial buckling strength. The overall deflection is now governed by two-half waves.

While the arguments are based on results from Panel 1, the same story applies for the other evaluated panels. Appendix A.2 shows the buckling shapes for Panel 2, 3 and 4 considering both minor and major influence from compression at short edges. With increasing span-ratio, the vertical prestress tends to activate an initial deflection more easily triggered by a compression at the long edges. The buckled shapes are now however characterized by increasing half-waves as the panel height increases.

4.2.3 Biaxially loaded concrete panel subjected to a triangular lateral pressure

When in design condition, the biaxially compressed concrete panel will be subjected to a water pressure as illustrated in Figure 4.13. A part of the vertical compressive load, σ_y , is here governed by the resting pedestrian bridge.

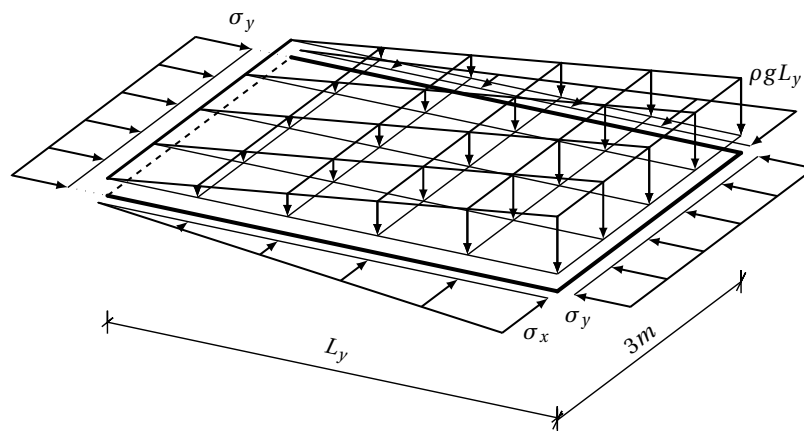


Figure 4.13: Two-way prestressed concrete panel subjected to a hydrostatic pressure.

The boundary conditions correspond to the ones presented in Figure 3.7. The free upper edge is now constrained by the pedestrian bridge, which only allows moment vertically. At the base slab, a ring beam resist lateral movement a certain distance above the depth. The height of the ring beam is taken as $\frac{1}{10}$ of the vertical span, stating the height of panel area which is laterally constrained utilized in this buckling analysis.

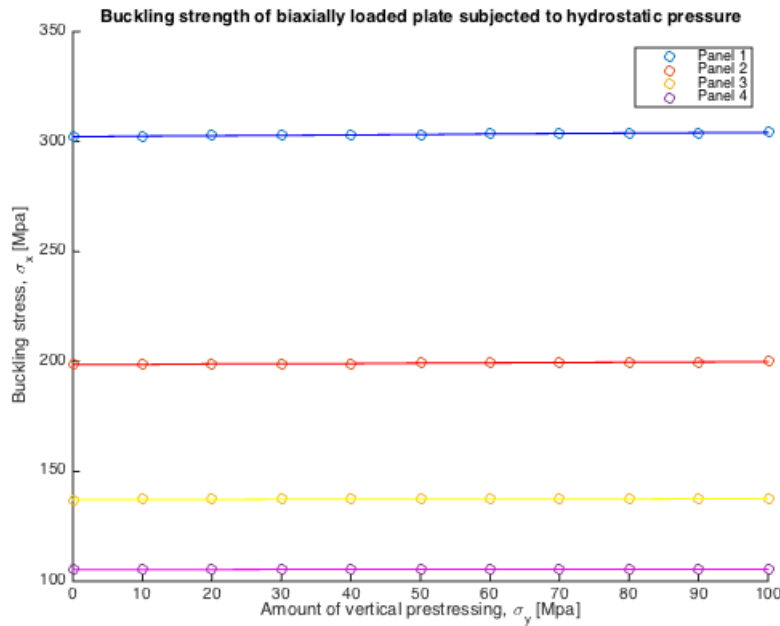


Figure 4.14: Buckling stress for concrete panels within the third case study.

Figure 4.14 presents the results in the same manner as previously, by stepping the amount of vertical prestress through an interval. Compared to Figure 4.10, the biaxial buckling strength increases for each of the examined panels. It also shows that the capacity is nearly independent of the amount of vertical compression, which here really is the sum of vertical prestress and self-weights.

Throughout the presented load-conditions, the buckled shape remains consistent as Figure 4.15 shown for the reference panel. The buckling modes corresponding to the other examined panels are given as Appendix A.3.

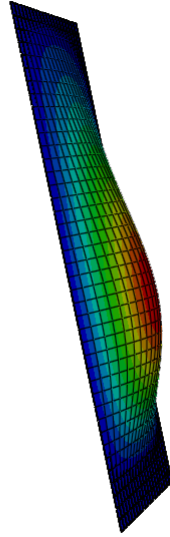


Figure 4.15: Lowest buckled shape for Panel 1 within the third case study.

These findings states the beneficial stiffening effect from both the pedestrian bridge and the ring beam. Although the hydrostatic pressure introduces a destabilizing effect, this is really not present under the governing boundary conditions. While the upper edge remained free during the previous stages of prestress, the pedestrian bridge now provides a constraint that increases the buckling capacity. The other stiffening effect appears from the ring beam, which through the uptake of lateral forces provides the panel with beneficial characteristics. In this stage, as well as in the previous one, the great buckling performance suggests that compressive crushing of concrete becomes the governing failure mode.

Chapter 5

Flexural cracking of concrete

A general design issue, independent of the panel geometry, is related to cracking of concrete. While the ultimate strength of a liquid-retaining concrete tank often is sufficient, the operational condition may suffer from cracks followed by leakage. Larger concrete tanks panels implies higher loads, making the cracking limit state even more important.



Figure 5.1: Cracking of concrete panel in a liquid-retaining concrete tank followed by a leakage, AlchemyPolymers (2015).

5.1 Design philosophies

There are several design philosophies governing the cracking limit state. In order to keep up with the crack restrictions, concrete elements have typically been designed by means of either ordinary reinforcement or by prestressed steel. For a large reinforced concrete tank, the cross sectional properties to resist leakage are primarily governed by the member thickness. This may lead to an unreasonable design with high material costs. Figure 5.2 shows the resulting stress distribution for a strip of an ordinary reinforced concrete panel in flexure.

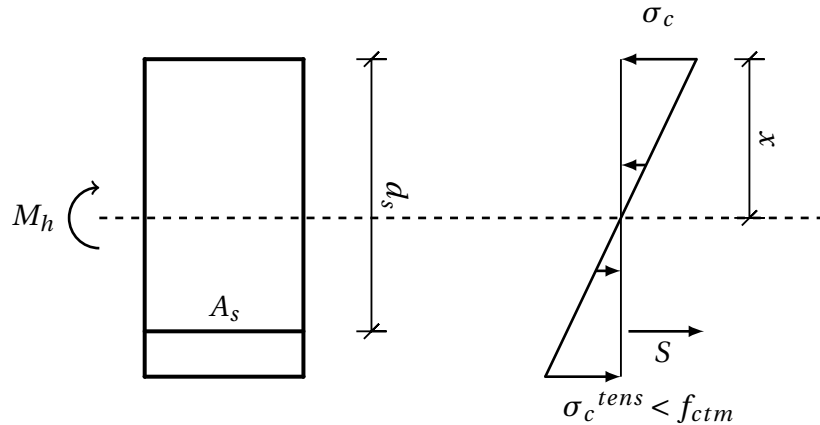


Figure 5.2: Controlling cracking by ordinary reinforcement, $\sigma_c^{tens} < f_{ctm}$.

When using prestressed steel, the purpose is typically to counteract the tensile stress present. This leads to an element subjected to pure compression, such that no cracking is apparent. It is noted that this is a conservative approach, as leakage could be avoided in a more relaxed manner. The stress distribution and its components for the same strip now eccentrically prestressed, are shown in Figure 5.3. Here the moment, M_h , represents the resultant from the hydrostatic pressure. Prestressing with an eccentricity, e , leads to a stress distribution which can be divided into two contributions. A uniform compressive stress is introduced as the term $\frac{P}{A_c}$. The bending contribution resulting from the eccentricity moment given as $M_p = P \cdot e$, is represented by the linear stress contribution in the figure.

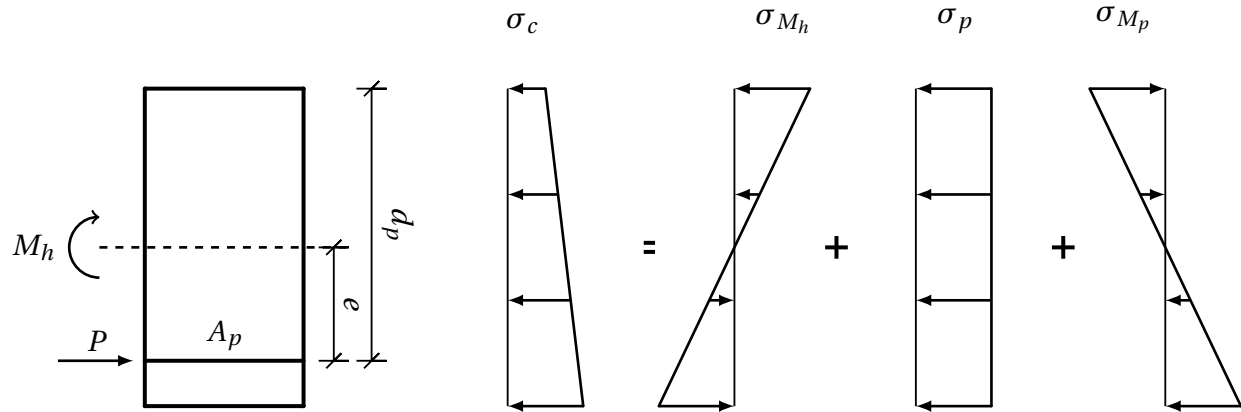


Figure 5.3: Controlling cracking by prestressed reinforcement, $x \rightarrow \infty$.

A large concrete panel acts as a flexural member under influence of the hydrostatic pressure. As mentioned in Section 3.4.2 for a structure within tightness class 3, the cracking limit state may be handled by triggering a certain zone of compression. When using ordinary reinforcement as shown in Figure 5.2, the required structural properties to resist leakage may be not applicable within practical limits. A fully prestressed approach given in Figure 5.3 introduces a residual compressive stress, which is recognized as an infinitely large zone of compression. Cracking is thus not present, making the structure theoretically watertight.

In between these design philosophies, a possibility is to make use of both ordinary and prestressed reinforcement. The idea is then to utilize the characteristics from these two types of reinforcement simultaneously, denoted partial prestressing. Since ordinary reinforcement provides its best characteristics when subjected to tension, it is beneficial to keep a part of the section in this configuration even after prestress is introduced. Figure 5.4 shows a concrete section utilizing ordinary and prestressed reinforcement to obtain the required zone of compression, x_{min} .

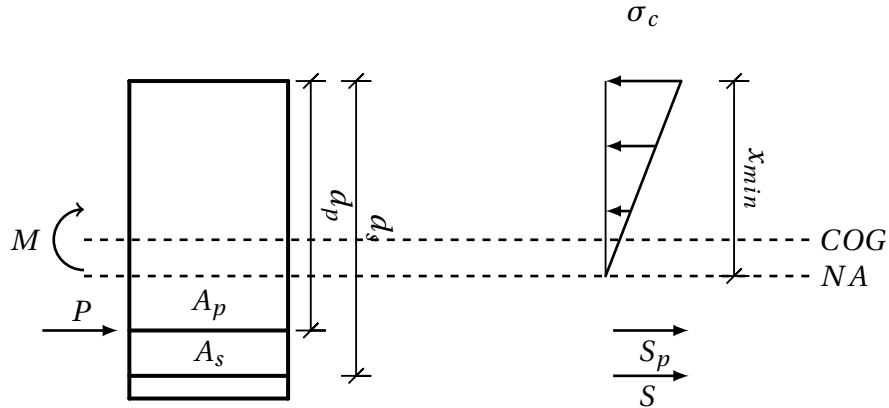


Figure 5.4: Controlling cracking by combining the use of ordinary and prestressed reinforcement.

Rashed et al. (2002) presents a study on the parameters in Figure 5.4 to determine their relative influence on this zone. One important parameter is the amount of prestressed steel to ordinary reinforcement, denoting the degree of partial prestress. It shows that an efficient design considering cracking as well as the ultimate strength, combines these types of reinforcement. By allowing a certain degree of tension in the ordinary reinforcement, the criterion of no leakage is satisfied by maintaining a certain height of the compressive zone due to prestress, even under the influence of cracks. The eccentricity, e , is one effective tool to control the compressive zone.

As Rashed et al. (2002) describes, crack design has typically been performed by keeping track of the stress in the ordinary reinforcement. Since this approach often results in low utilization of the ordinary reinforcement, it can not be seen as an efficient design. An optimal solution utilizes both types of reinforcement intended to reach their strength simultaneously.

5.2 Parameter study regarding the zone of compression, χ

In the following, parts of the parameter study from Rashed et al. (2002) are reproduced on a strip of a concrete panel. The aim is then to do a more specific investigation on some parameters influence on the compressive zone. For this purpose, a routine incorporating the calculation model is established in Matlab attached as Appendix C.1.

The calculation model

The panels are intended to be partially prestressed, so that the calculations include prestressed as well as ordinary reinforcement. The latter is also introduced in the compressive zone of the cross-section, A_{sc} , as this often is practical. Figure 5.5 shows the basis for the calculation model, which is adapted from Sørensen (2013). The idea is to capture the eccentricity moment from prestressing together with the contribution from the hydrostatic pressure, in one single load. This is done by loading the section by the prestressing force P , a distance a from the neutral axis. The parameter $a = \frac{M_h - M_p}{P} = \frac{M}{P}$ then states an equivalent eccentricity by similarity in the produced moment.

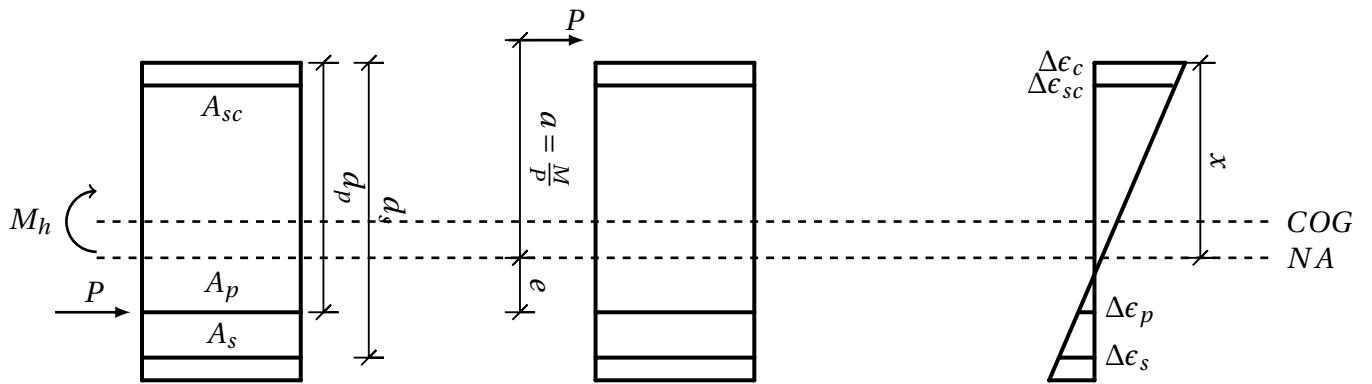


Figure 5.5: Cross-sectional calculation model as basis for the parameter study on the compressive zone, x .

By considering horizontal force equilibrium in this model, Equation (5.1) is obtained.

$$P = T_c + S_c - S_p - S \quad (5.1)$$

The internal forces may so be found by considering the materials to be in the elastic regime. A linear elastic material follows Hookes law, such that the stresses may be written as $\Delta\sigma = E \cdot \Delta\epsilon$. By further multiplying with the respective areas, the forces can be written as follows.

$$P = \frac{1}{2} \cdot E_c \cdot \Delta\epsilon_c \cdot x \cdot b + E_s \cdot \Delta\epsilon_{sc} \cdot A_{sc} - E_p \cdot \Delta\epsilon_p \cdot A_p - E_s \cdot \Delta\epsilon_s \cdot A_s \quad (5.2)$$

The idea now is to establish a relation between the concrete strain at the upper edge, ϵ_c , and the corresponding strains at the locations for the reinforcement. From the Navier/Bernoulli hypothesis, stating that plane sections remains plane, these relations may be expressed through a constant curvature approach as Equation (5.3), (5.4) and (5.5).

$$\Delta\epsilon_p = \left(\frac{d_p - x}{x}\right) \cdot \Delta\epsilon_c \quad (5.3)$$

$$\Delta\epsilon_s = \left(\frac{d_s - x}{x}\right) \cdot \Delta\epsilon_c \quad (5.4)$$

$$\Delta\epsilon_{sc} = \left(\frac{d_s + x - t}{x}\right) \cdot \Delta\epsilon_c \quad (5.5)$$

Now by substituting these relations into Equation (5.2).

$$P = \frac{1}{2} \cdot E_c \cdot \Delta\epsilon_c \cdot x \cdot b + E_s \cdot \left(\frac{d_s + x - t}{x}\right) \cdot \Delta\epsilon_c \cdot A_{sc} - E_p \cdot \left(\frac{d_p - x}{x}\right) \cdot \Delta\epsilon_c \cdot A_p - E_s \cdot \left(\frac{d_s - x}{x}\right) \cdot \Delta\epsilon_c \cdot A_s \quad (5.6)$$

Every term now contains the concrete strain, ϵ_c . By some reformulation followed by a division with the concrete stress amplitude at upper edge, $\Delta\sigma_c$.

$$\frac{P}{\Delta\sigma_c} = \frac{1}{2} \cdot x \cdot b + \frac{E_s}{E_c} \cdot \left(\frac{d_s + x - t}{x}\right) \cdot A_{sc} - \frac{E_p}{E_c} \cdot \left(\frac{d_p - x}{x}\right) \cdot A_p - \frac{E_s}{E_c} \cdot \left(\frac{d_s - x}{x}\right) \cdot A_s \quad (5.7)$$

This equation can be simplified slightly when introducing the material stiffness ratio, $\eta_1 = \frac{E_s}{E_c}$ and $\eta_2 = \frac{E_p}{E_c}$.

$$\frac{P}{\Delta\sigma_c} = \frac{1}{2} \cdot x \cdot b + \eta_1 \cdot \left(\frac{d_s + x - t}{x}\right) \cdot A_{sc} - \eta_2 \cdot \left(\frac{d_p - x}{x}\right) \cdot A_p - \eta_1 \cdot \left(\frac{d_s - x}{x}\right) \cdot A_s \quad (5.8)$$

Equation (5.8) then serves as the main equation for force equilibrium. Here both $\Delta\sigma_c$ and the compressive zone, x , are unknowns. In order to solve this equation for x , we are in the need of an additional equation. By considering moment equilibrium, here chosen at the location for prestressed reinforcement, this additional condition is obtained.

$$P \cdot (e + a) = T_c \cdot \left(d_p - \frac{1}{3} \cdot x\right) + S_c \cdot (d_s + d_p - t) + S \cdot (d_s - d_p) \quad (5.9)$$

Analogous as for the force equilibrium, the forces may be expressed in terms of strains.

$$P \cdot (e+a) = \frac{1}{2} \cdot E_c \cdot \Delta \epsilon_c \cdot x \cdot b \cdot \left(d_p - \frac{1}{3} \cdot x\right) + E_s \cdot \left(\frac{d_s + x - t}{x}\right) \cdot \Delta \epsilon_c \cdot A_{sc} \cdot (d_s + d_p - t) + E_s \cdot \left(\frac{d_s - x}{x}\right) \cdot \Delta \epsilon_c \cdot A_s \cdot (d_s - d_p) \quad (5.10)$$

Which again can be normalized with respect to $\Delta \sigma_c$, and simplified in the same manner as the equation considering force equilibrium.

$$\frac{P}{\Delta \sigma_c} = \frac{1}{(e+a)} \left[\frac{1}{2} \cdot x \cdot b \cdot \left(d_p - \frac{1}{3} \cdot x\right) + \eta_1 \cdot \left(\frac{d_s + x - t}{x}\right) \cdot A_{sc} \cdot (d_s + d_p - t) + \eta_1 \cdot \left(\frac{d_s - x}{x}\right) \cdot A_s \cdot (d_s - d_p) \right] \quad (5.11)$$

By setting Equation (5.11) equal to (5.8), one may now solve for both x and $\Delta \sigma_x$. This is done iteratively by stepping x through an interval. The iteration is said to be completed when the difference between these two equations is below a specified limit. The routine will then return the value of the compressive zone, x . A graphical presentation of this process is shown in Figure 5.6.

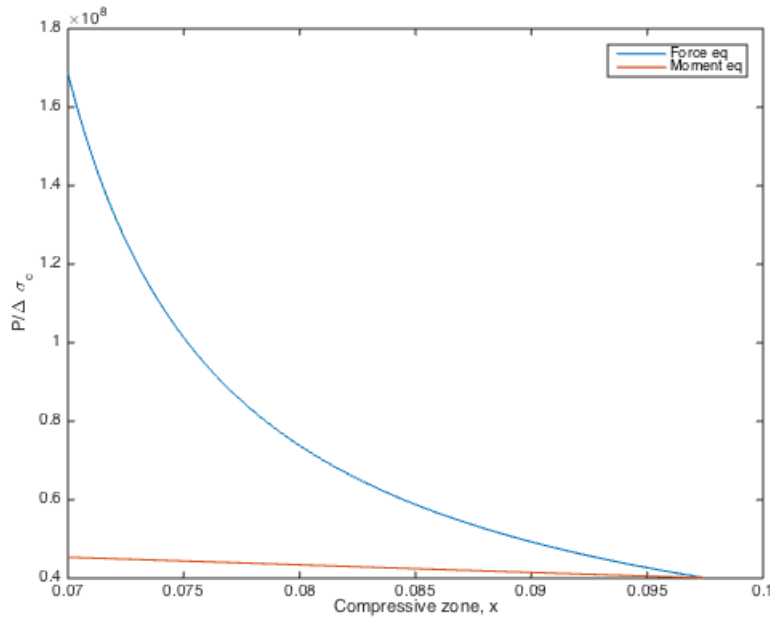


Figure 5.6: Graphic illustration of the iteration process utilized when solving for the compressive zone, x .

The calculation includes some parameters which are held constant. The constant lengths and areas are presented in Table 5.1. The compressive reinforcement is taken as the minimum

value from Equation (4.12). Table 5.2 presents the modulus of elasticity for the materials involved.

Parameter	Value
Width of plate strip, b [mm]	1
Panel thickness, t [mm]	300
Distance to ord. reinforcement, d_s [mm]	280
Area of compressive reinforcement, A_{sc} [$\frac{mm^2}{m}$]	510

Table 5.1: Constant lengths and areas used for calculation of the compressive zone

Elastic modulus [Mpa]	Value
Ordinary steel	$200 \cdot 10^3$
Prestressed steel	$195 \cdot 10^3$
Concrete	$35 \cdot 10^3$

Table 5.2: Elastic modulus of materials

P denotes the compressive force from prestressing calculated as Equation (5.12).

$$P = \sigma_p \cdot A_p \quad (5.12)$$

NS-EN-1992-1 (2008) limits this force by specifying a maximum value of the steel stress due to the jacking procedure. This restriction is given as Equation (5.13).

$$\sigma_{p,max} = \min[0.8f_{pk}; 0.9f_{p0,1k}] \quad (5.13)$$

Here $f_{pk} = 1700\text{Mpa}$ is the characteristic tensile strength of the prestressed steel, while $f_{p0,1k} = 1550\text{Mpa}$ represents the same parameter adjusted by a 0.1% tensile strain limit. The force P used in the calculations is then obtained by setting $\sigma_p = \sigma_{p,max} = 1360\text{Mpa}$ further multiplied with the area of the prestressed steel, $P = \sigma_{p,max} \cdot A_p$. M_p may so be calculated as $M_p = P \cdot e$, representing the eccentricity moment arising from this force.

The parameter a , denoting the equivalent eccentricity for the compressive force, is calculated as $a = \frac{M_h - M_p}{P}$. M_h represents the moment from the hydrostatic pressure acting on the evaluated strip of the panel. As noted in the following, this magnitude is really not of importance as part of the parameter study investigates the residual moment, $M_h - M_p$.

5.2.1 Degree of partial prestress

Variable	Value
Degree of partial prestress, $\frac{A_p}{A_s}$ [-]	$\frac{A_p}{A_s}$
Distance to prestressed reinforcement, d_p [mm]	280

The first parameter study considers the reinforcement ratio, $\frac{A_p}{A_s}$. As initial amounts, $A_p = 100 \frac{mm^2}{m}$ and $A_s = 3500 \frac{mm^2}{m}$. The study is then performed by increasing A_p with $100 \frac{mm^2}{m}$ up to $A_p = 1200 \frac{mm^2}{m}$. The corresponding amount of ordinary reinforcement may then be found by setting a restriction on the total amount of reinforcement, or by enforcing equality in the steel tensile capacity as adapted from Rashed et al. (2002). Here the latter condition is utilized, this by making use of Equation (5.14).

$$\omega = A_s \cdot f_{ys} + A_p \cdot f_{pk} \quad (5.14)$$

The utilized data points are given in Table 5.3.

Data point	$A_p [\frac{mm^2}{m}]$	$A_s [\frac{mm^2}{m}]$
1	100	3500
2	200	3190
3	300	2880
4	400	2570
5	500	2260
6	600	1950
7	700	1640
8	800	1330
9	900	1020
10	1000	710
11	1100	400
12	1200	90

Table 5.3: Combinations of A_p and A_s used in calculations of the compressive zone, x.

When increasing $\frac{A_p}{A_s}$, there are several effects appearing acting to either increase or decrease the compressive zone. These effects are more easily describable if the load components are sorted into bending and axial contributions. The contributions for bending, giving rise to a linear stress distribution in the elastic regime, may be seen as a corresponding sum of the hydrostatic pressure and the eccentric prestress as presented in Figure 5.7.

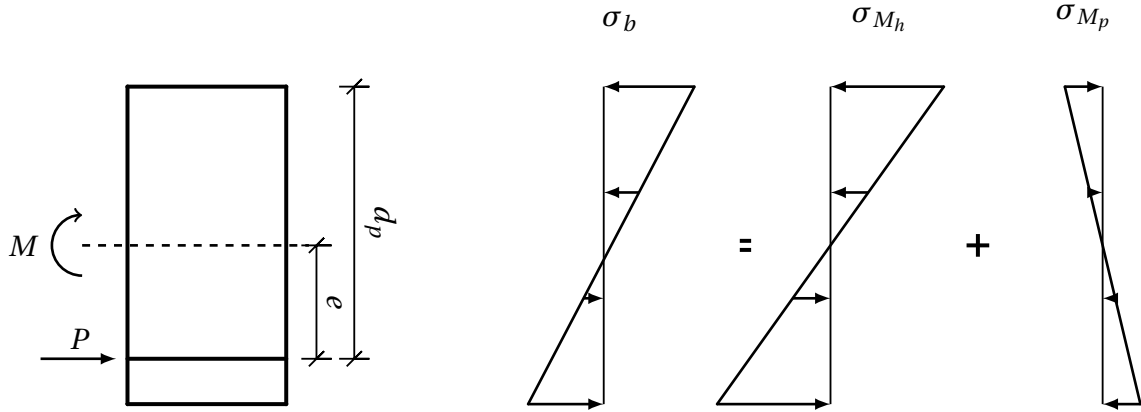
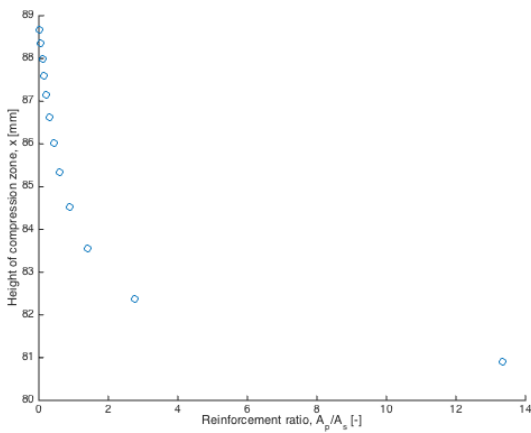


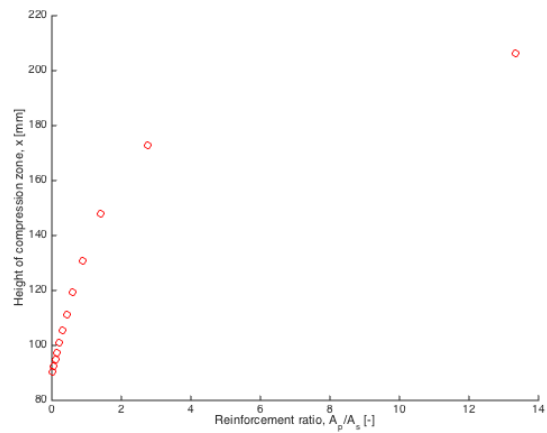
Figure 5.7: Residual bending stress distribution within a strip section of a prestressed concrete panel loading in bending.

With decreasing amount of A_s , the neutral axis changes so to decrease the compressive zone for maintaining equilibrium. The effect is then a cross-section with a reduced zone of compression. When A_p increases, this introduces a larger eccentricity moment. The sum of these effects results in a cross-section with reduced compressive zone experiencing a certain value of bending stress.

The residual bending stress, σ_b , further acts as a reference when adding the normal stress distribution, σ_p , appearing from the prestressing force. The degree of influence on the compressive zone from this component is thus dependent on the residual bending stress. As this is a defining issue, the study is performed for both minor and major amount of σ_b . The amount is here controlled by varying the hydrostatic moment, M_h .



(a) High residual bending stress.



(b) Low residual bending stress.

Figure 5.8: Effect on the compressive zone with increasing reinforcement ratio, $\frac{A_p}{A_s}$.

The results from the study can be viewed in Figure 5.8, presenting the effect on the compressive zone for cross-sections with both high and low residual bending stress. For the case with a large hydrostatic moment as in the left figure, x decreases throughout the interval. This states a dominating negative effect on the zone of compression when decreasing A_s . As the value of σ_b is high, the corresponding increase in A_p does not change the compressive zone considerably. The other case considers a low residual stress, giving the normal stress distribution more freedom to increase the compressive zone as A_p increases. The result is then a greater zone of compression as the reinforcement ratio, $\frac{A_p}{A_s}$, increases.

5.2.2 Eccentricity of prestressed reinforcement

Variable	Value
Degree of partial prestress, $\frac{A_p}{A_s}$ [-]	$\frac{A_p}{A_s}$
Distance to prestressed reinforcement, d_p [m]	d_p

In the previous investigation, d_p was taken as 280mm , corresponding to the eccentricity of the ordinary reinforcement, d_s . An increase of this parameter largens the eccentricity moment for a given value of $\frac{A_p}{A_s}$, further influencing the residual bending stress. Figure 5.9 extend the previous parameter study by considering the effect from changing d_p . By stepping this parameter through an interval ranging from $\frac{t}{2}$ to t , the height of compressive zone is evaluated at each ratio of reinforcement.

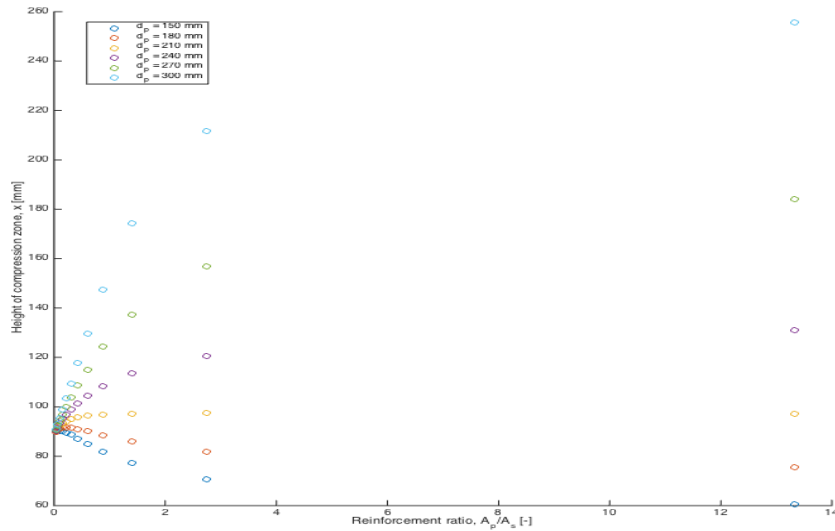


Figure 5.9: Effect on the compressive zone with increasing eccentricity of the prestressed steel, d_p .

Figure 5.9 shows that above a certain value of d_p , the height of this zone increases monotonically with $\frac{A_p}{A_s}$. Below this value, approximately given along the yellow data points, the effect on x by increased ratio of reinforcement is negatively correlated.

The findings from this study may be explained analogous as in the previous parameter study. As d_p increases, the eccentricity moment giving rise to σ_{M_p} as presented in Figure 5.7, increases in magnitude becoming a more dominating term. For a given value of the hydrostatic bending stress, σ_{M_h} , this increase tends to relax the resulting residual bending stress, σ_b .

The residual bending stress resulting from an eccentricity according to the yellow data points, states the transition between two major findings. For an eccentricity lower than this value, the downward trend is governed by the decrease in A_s , which decreases the zone of compression. By choosing an eccentricity higher than this transition value, the relaxed residual bending stress gives the normal stress component, σ_p , an advantage in increasing the compressive zone. With increasing $\frac{A_p}{A_s}$, the trend then shows an increasing zone.

An illustration of these characteristics are given in the following figures, showing the stress distribution for two different eccentricities at a given ratio of $\frac{A_p}{A_s}$. Compared to Figure 5.10, Figure 5.11 shows how easily the compressive zone may be changed with increasing eccentricity.

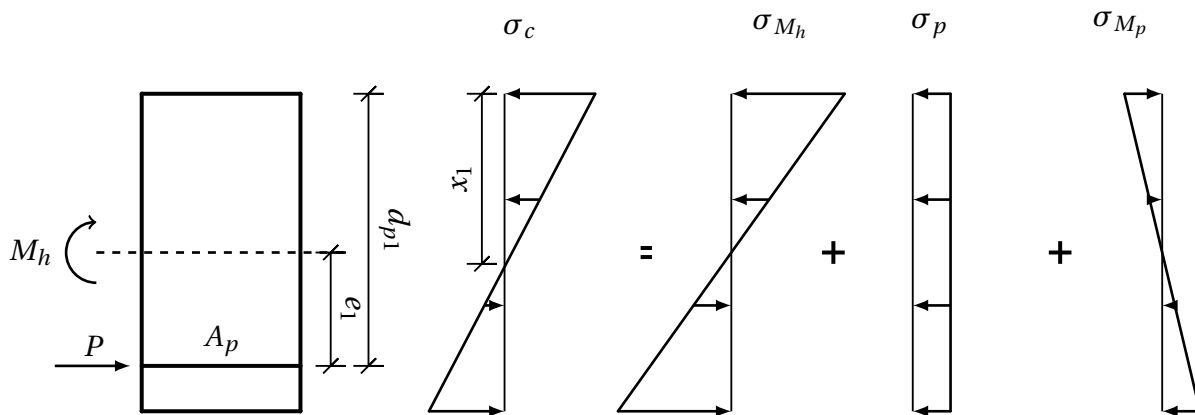


Figure 5.10: Resulting stress distribution and height of compressive zone for prestressing with $d_{p1} < d_{p2}$.

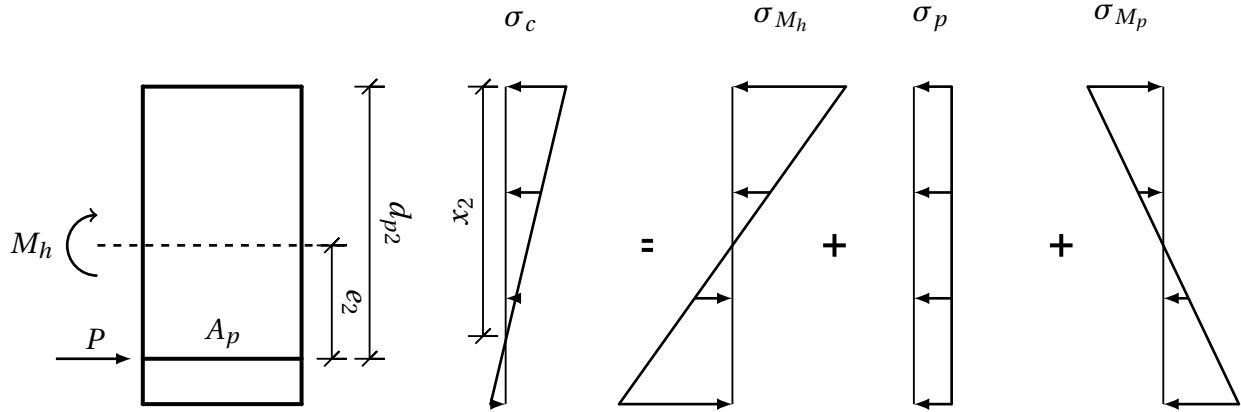


Figure 5.11: Resulting stress distribution and height of compressive zone for prestressing with $d_{p2} > d_{p1}$.

The studies suggest an efficient way to control the compressive zone as choosing a tendon eccentricity giving a bending stress contribution, σ_{M_p} , close to the external, σ_{M_h} . Larger panels implies greater external loads. The eccentricity should then be chosen in accordance with the governing load-condition. A use of this strategy results in a residual bending stress contribution low in magnitude more easily influenced by the normal stress contribution. The amount of prestress, stating the degree of this normal stress component, may so become an efficient and powerful tool in manipulating the compressive zone.

As there are requirements related to concrete cover so to avoid corrosion and following degradation of the steel tendons, the desired eccentricity may not be applicable. This could turn the cross-section into a configuration where the compressive zone decreases with increasing $\frac{A_p}{A_s}$, as presented in the Figure 5.8. In this case, the zone is more sensitive against change in the ratio of reinforcement, $\frac{A_p}{A_s}$. A following use of the strategy considering low residual stress, may then become more complex and not that powerful. To still provide the section with efficient characteristics, the effect on the compressive zone for varying ratios of reinforcement should be examined more closely.

Part III

Design for a watertight concrete panel

Chapter 6

Non-prestressed concrete panel

Part II investigated some special design issues when dealing with large concrete panels. The studies considered a buckling assessment to determine a potential limitation when prestressing large concrete panels, as well as a parameter study on how to efficiently control the compressive zone within a member. The idea is now to include these findings in a prestressing design of a large watertight precast concrete panel. The following should be considered as a conceptual issue as it makes use of strip-theory as reference for the cross-sectional characteristics.

6.1 Design condition

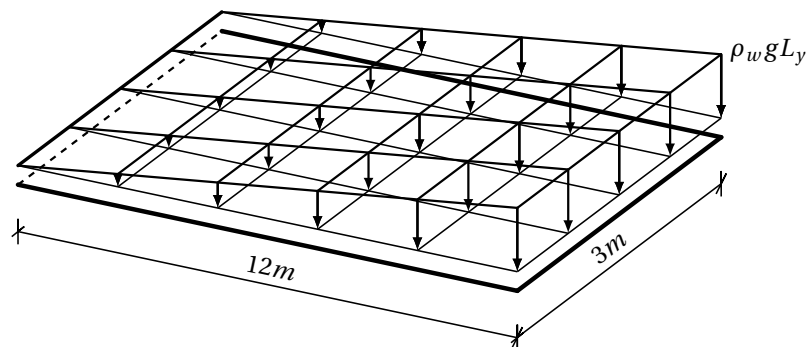


Figure 6.1: Non-prestressed concrete panel subjected to a hydrostatic pressure as the design condition.

Figure 6.1 shows the evaluated panel corresponding to Panel 4 in Part II of this thesis. The boundary conditions correspond to the tank in design condition as described in Section 3.2.

The height of the ring beam is still taken as $\frac{1}{10} \cdot L_y = 1.2m$, stating the height of the panel area above foundation constrained for lateral deformations.

The design is governed by the containing water subjecting the panel to a pressure. The hydrostatic pressure is triangularly distributed along the depth with a magnitude according to Equation (6.1). As the self-weights introduce beneficial compressive forces, these loads will not be covered in the design condition. The effect will however be considered as a part of the required prestress.

Parameter	Value
$\rho_w [\frac{kg}{m^3}]$	1000
$g [\frac{kg \cdot m}{s^2}]$	9.81
$L_y [m]$	12

Table 6.1: Data for calculation of the hydrostatic pressure.

$$p = \rho_w \cdot g \cdot L_y = 117720 [\frac{N}{m^2}] \tag{6.1}$$

6.1.1 Moment distribution

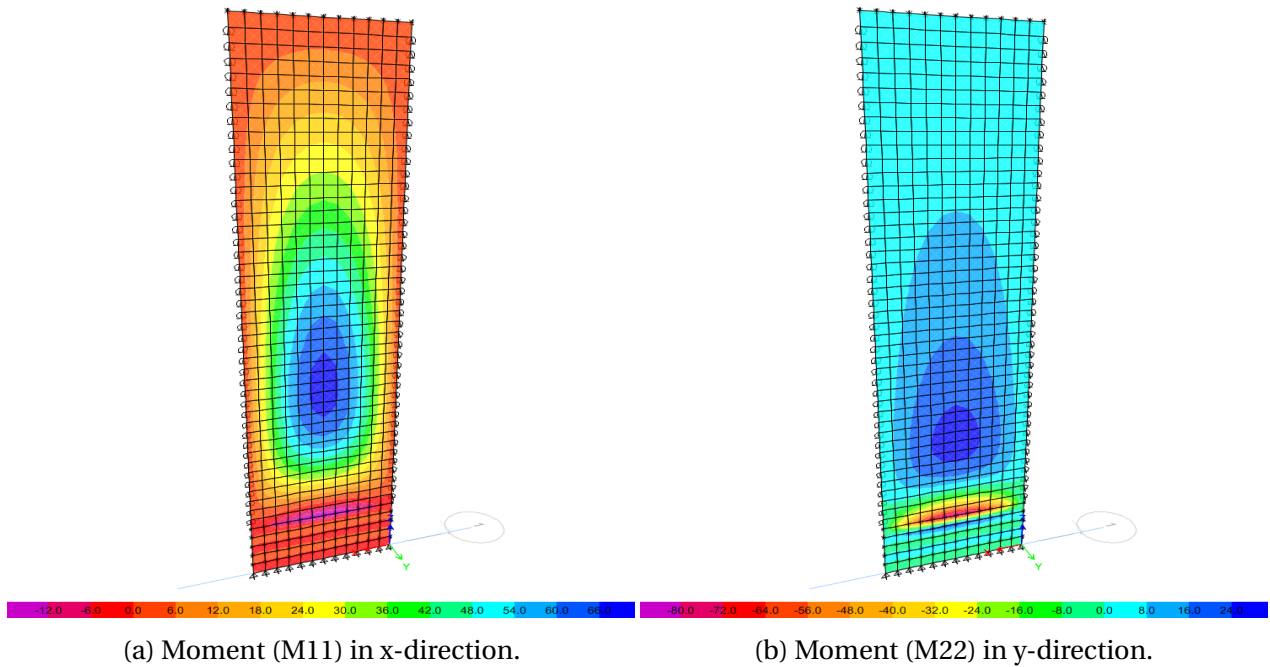


Figure 6.2: Distribution of moments throughout the concrete panel due to the hydrostatic pressure.

The load-effect in terms of moment resulting from the hydrostatic pressure, is presented as Figure 6.2. As the panel acts as a two-way slab, the load is taken by bending in two principal directions. The left subfigure shows the moment distribution along the the x-direction, denoting the direction along the shortest span. The most loaded strip of the panel is located at a depth of $y = 7.5m$. For the acting moments in the longest direction of the span, i.e y-direction, the right subfigure shows the results. The constraint from the foundation beam introduces a strip behavior close to fixed.

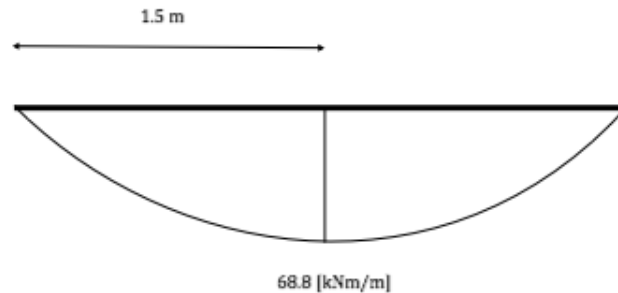


Figure 6.3: Moment distribution throughout the critical x-directional strip of the concrete panel.

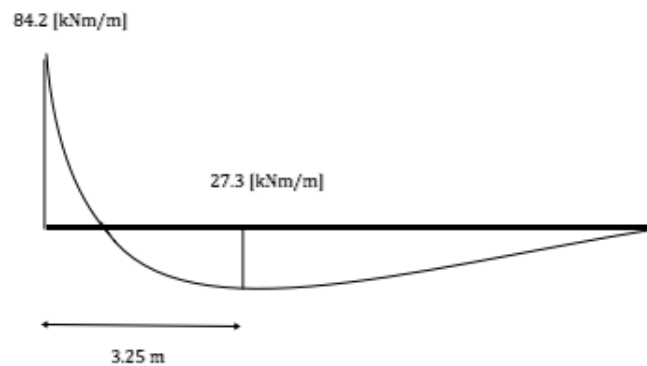


Figure 6.4: Moment distribution throughout the critical y-directional strip of the concrete panel.

The moment distribution throughout the critical strips are given in Figure 6.3 and 6.4. With these strips as references, the stress distribution and height of compressive zone at the respective critical locations may be calculated. The calculation model includes a minimum reinforcement according to Equation (4.12) in both the tensile, A_s , and compressive side, A_{sc} , of the section.

6.1.2 Assessment of the compressive zone as design basis

Figure 6.5 shows the internal forces for a cracked reinforced concrete section. The model is reproduced from the Matlab routine given in Appendix C.1. From force equilibrium, the height of the compressive zone, x , is assessed. The appearing stresses in concrete and reinforcement are then easily calculated.

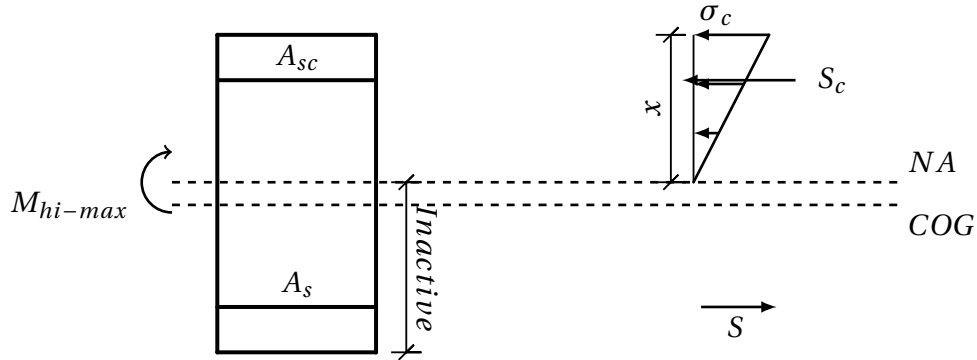


Figure 6.5: Internal forces within a section of the critical strip of the concrete panel as basis for the design.

From axial equilibrium of the internal forces, Equation (6.2) is established.

$$\frac{1}{2} \cdot \sigma_c \cdot x \cdot b + S_c - S = 0 \quad (6.2)$$

Now by assuming the concrete and steel to be in the elastic regime following Hookes law, the stress components can be expressed as $\Delta\sigma = E \cdot \Delta\epsilon$.

$$\frac{1}{2} \cdot E_c \cdot \Delta\epsilon_c \cdot x \cdot b + E_s \cdot \Delta\epsilon_{sc} \cdot A_{sc} - E_s \cdot \Delta\epsilon_s \cdot A_s = 0 \quad (6.3)$$

The cross-sections are assumed to obey Navier hypothesis, stating that plane sections remains plane. The strain-relations in Equation (6.4) and (6.5) may then be utilized.

$$\Delta\epsilon_s = \left(\frac{d_s - x}{x} \right) \cdot \Delta\epsilon_c \quad (6.4)$$

$$\Delta\epsilon_{sc} = \left(\frac{d_s + x - t}{x} \right) \cdot \Delta\epsilon_c \quad (6.5)$$

By substituting these relations into the expression for axial equilibrium, Equation (6.6) is obtained.

$$\frac{1}{2} \cdot E_c \cdot \Delta\epsilon_c \cdot x \cdot b + E_s \cdot \left(\frac{d_s + x - t}{x}\right) \cdot \Delta\epsilon_c \cdot A_{sc} - E_s \cdot \left(\frac{d_s - x}{x}\right) \cdot \Delta\epsilon_c \cdot A_s = 0 \quad (6.6)$$

Which further simplifies into Equation (6.7), giving a 2nd order equation.

$$\frac{1}{2} \cdot E_c \cdot x^2 \cdot b + E_s \cdot (A_s + A_{sc}) \cdot x + E_s \cdot [d_s \cdot (A_{sc} - A_s) - t \cdot A_{sc}] = 0 \quad (6.7)$$

The appearing stresses may then be found by utilizing the moment-curvature relation in Equation (6.8).

$$\kappa = \frac{M}{E_c \cdot I_{c-eq}} \quad (6.8)$$

Here the equivalent directional bending stiffness, $E_c \cdot I_{c-eq}$, is calculated as described in Section 4.1.1 for a cracked section modification. By an adoption from Sørensen (2013, p. 116), the curvature can be described by the concrete strain, $\Delta\epsilon_c$, as Equation (6.9).

$$\kappa = \frac{\Delta\epsilon_c}{x} \quad (6.9)$$

Setting these equations equal to each other, results in Equation (6.10) giving the strain at concrete top.

$$\Delta\epsilon_c = \frac{M \cdot (d - x)}{E_c \cdot I_{c-eq}} \quad (6.10)$$

The corresponding stress at this location is then found from Hookes law as $\sigma_c = E_c \cdot \Delta\epsilon_c$.

Direction of plate strip	Height of compressive zone [mm]	Concrete stress [Mpa]
x	36.4	14.1
y	36.4	17.3

Table 6.2: Height of compressive zone and concrete stress in critical plate strips.

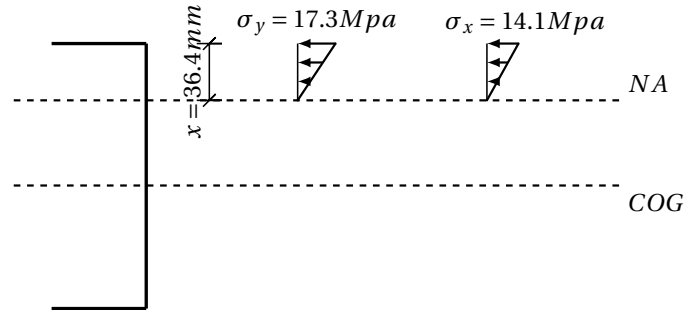


Figure 6.6: Concrete stress distribution throughout the compressive zone in the critical strips.

Table 6.2 presents the height of the compressive zone as $x = 36.4\text{ mm}$ for the cracked reinforced concrete panel. Figure 6.6 shows that the concrete stress is largest in the critical strip spanning in the y -direction. As the loading throughout the panel differs, some part of it may in reality stay uncracked leading to a somewhat larger compressive zone. However, conservatism related to concrete cracking is preserved when allocating these critical plate strips as design states for the two span directions of the panel.

6.2 Controlling the compressive zone by application of prestress

As mentioned in Section 3.4.2, NS-EN-1992-3 (2009) states that watertightness may be fulfilled by maintaining a compressive zone of $\min(50\text{ mm}, 0.2t)$. The governing concrete panel has a thickness of 300 mm , which turns the criterion into a minimum compressive zone, $x_{\min} = 50\text{ mm}$. As the cracked panel in the design condition experiences a zone of smaller magnitude than this requirement, the idea now is to control it by introducing compressive forces. The prestressing forces are introduced as point loads along the edges. Dependent of their relative magnitudes and mutual spacing, the loads form distributions along the edges comparable to the cases investigated in the buckling analysis.

6.2.1 Prestressing y -directional strips of the panel

The right part of Figure 6.2 shows the distribution of moments in y -direction. By prestressing the panel along the width of the panel, giving rise to forces in the y -direction, the aim is to control this directional load-transferring. As this prestress should be distributed along relatively short edges, it may be practical to introduce the load as uniformly. This is obtained by jacking equally spaced steel tendons to the same value of strain. The prestressed steel are further chosen to lay in the centroid of the panel, $\frac{t}{2}$, which do not introduce any eccentricity moment.

To calculate the necessary amount of vertical prestress giving the magnitude of the edge load, the results from the critical y-directional strip in Table 6.2 are considered. The evaluated location along the strip corresponds to the most loaded one as shown in Figure 6.4.

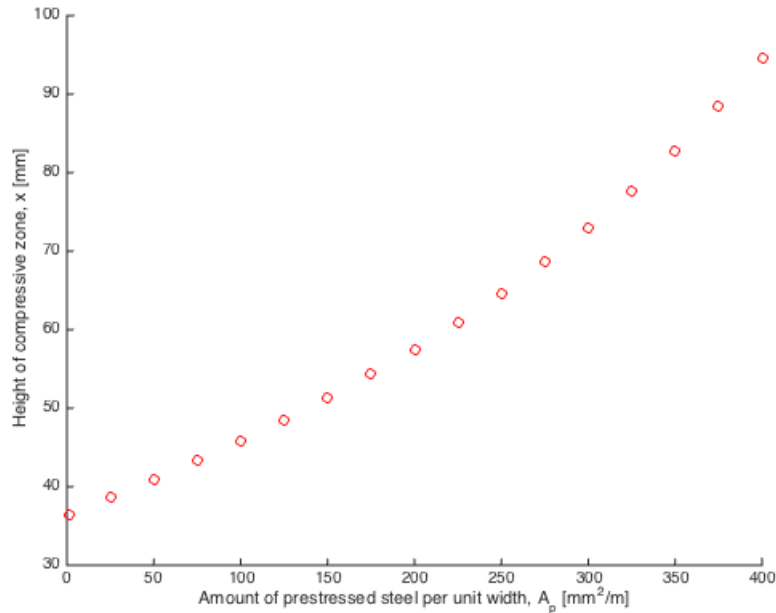


Figure 6.7: Height of compressive zone at the most loaded location of the critical y-directional strip for increasing amount of prestress.

Figure 6.7 shows how the compressive zone gets manipulated by increasing the amount of non-eccentric prestressed steel. The y-crossing represents the height of the compressive zone in the non-prestressed case with a value $x = 36.4\text{mm}$. With increasing amount of prestressed steel, the trend is characterized by an increase of this zone. To maintain a zone of $x = 50\text{mm}$, the results suggest a minimum amount of approximately $A_p = 150[\frac{\text{mm}^2}{\text{m}}]$.

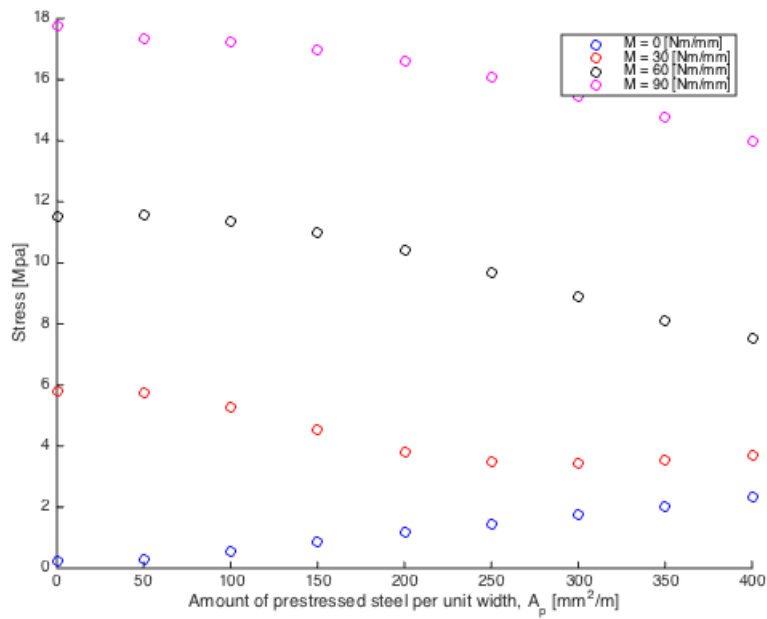


Figure 6.8: Resulting stress at concrete top due to y-directional prestress.

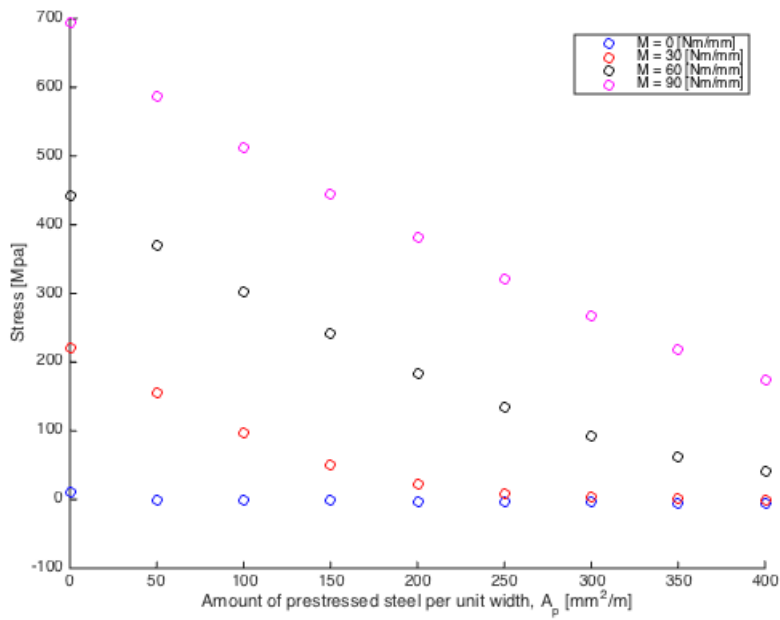


Figure 6.9: Resulting stress in ordinary reinforcement steel due to y-directional prestress.

Figure 6.8 shows the appearing stress at concrete top with varying amount of prestress. The results are shown within a range of the external hydrostatic moment, as this covers the load-conditions, M_{hy} , acting at different locations of the critical strip. The pink dots indicates approximately the condition at the most loaded location governing for the design. Within the presented range of applied prestress, the concrete stress decays and stays beyond its compressive capacity. The concrete used, C40, possess a compressive strength of $f_{ck} = 40\text{Mpa}$.

Figure 6.9 considers the same calculation model, presenting the stress in the ordinary reinforcement within the same range of external hydrostatic moment. This type of reinforcement typically has a strength, $f_{yk} = 500\text{Mpa}$, governing the first yield of the steel. Providing the critical strip with the required amount of prestress, $A_p = 150[\frac{\text{mm}^2}{\text{m}}]$, gives a steel stress of approximately $\sigma_s = 450\text{Mpa}$. An increasing amount of prestress will further lower this stress component.

6.2.2 Prestressing x-directional strips of the panel

The left part of Figure 6.2 shows the distribution of moments in x-direction, which varies considerably throughout the height. As prestress should be introduced along these long edges, a non-uniform distribution becomes rather practical. This variation is intended to be linear as utilized in the buckling analyses.

Figure 6.10 illustrates two approaches suggested by the author to obtain a linear force distribution along an edge. The former makes use of equally spaced prestressed tendons. To obtain this desired force variation, tendons must be post-tensioned in a linear sequence along the depth. The result is then a correlation between prestressing force and depth, stating that $F_1 < F_2 < .. < F_N$. The approach may be further denoted as equally spaced.

This method could become unpractical as it is time consuming to prestress the tendons in this individually manner. The second solution suggests an approach where to prestress the steel to the same level, which may further be recognized as equally jacked. The linear force distribution is then obtained by providing linear varying spacing between the prestressed tendons. Near the panel bottom, where the accumulation of loading is high, the spacing should be correspondingly small.

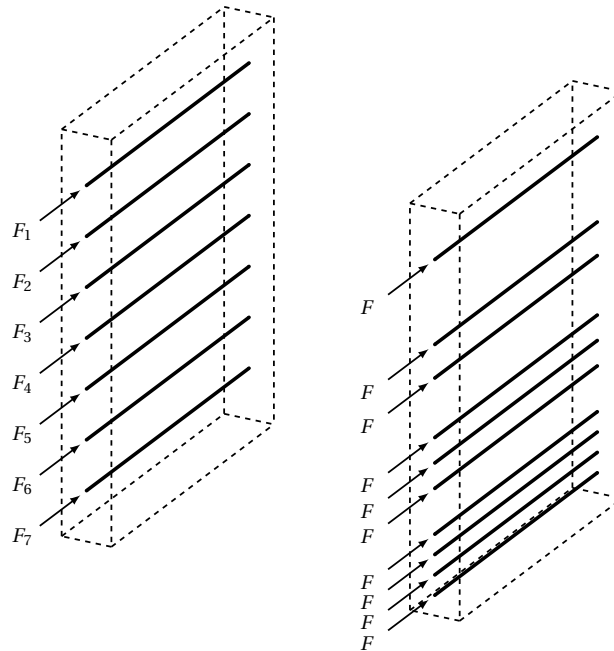


Figure 6.10: Two approaches to obtain a linear force distribution from the process of post-tensioning along long edges.

In contrast to the vertical prestress introduced within each panel during fabrication, compressive forces at the long edges are introduced as single jacking operations. As mentioned earlier, this is typically done by guiding steel through priorly poured ducts around the perimeter of the panels, now connected into a polygonal tank. When post-tensioning these tendons by a jacking sequence, the compressive loads are obtained within each panel.

As the tank is polygonal shaped, stating a discontinuity in panel orientation at the vertical joints, a secondary lateral load effect could arise during the application of prestress. This may lead to local failure as the tendons breaks out through the inside cover. In order to prohibit this failure mode, NS-EN-1992-3 (2009) suggests that the prestressing steel should be placed in the outer third of the panel section. For the following design procedure, the location of these prestressed tendons is considered as $d_p = 220\text{mm}$. This will additionally relax the residual bending stress, an issue covered in Part II of the thesis.

An equally-jacked procedure may now be utilized by sorting the panel into x-directional unit strips. A reference amount, which defines the slope of the linear force distribution, is determined by a compressive zone control of the critical strip shown in Figure 6.3.

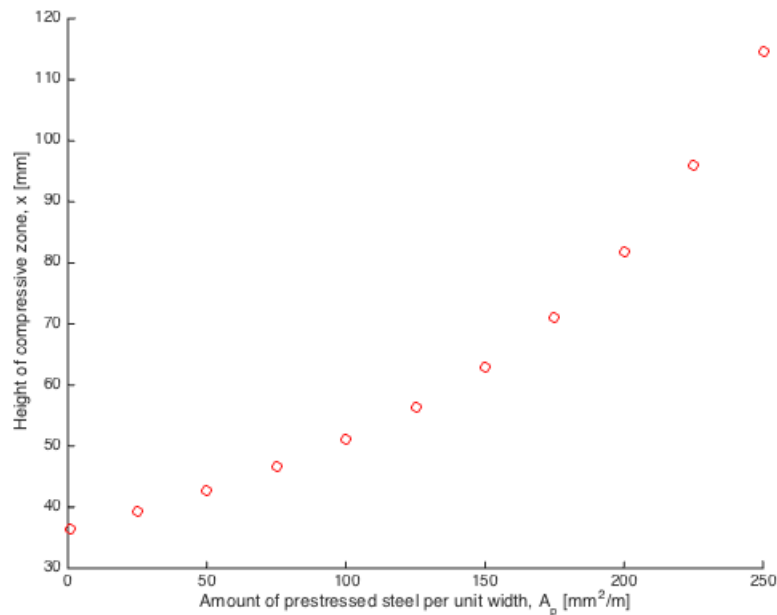


Figure 6.11: Height of compressive zone at the most loaded location of the critical x-directional strip for increasing amount of prestress.

Figure 6.11 shows the increase of compressive zone as a function of the amount of eccentric prestress. The non-prestressed initial condition is once again recognized by the y-crossing, stating this height as $x = 36.4\text{mm}$. Compared to the other principal direction, the eccentric location of the tendons relaxes the external bending stress contribution. A marginal increase in the amount of prestress will thus trigger a larger zone of compression. The effect is recognized by the gradient in Figure 6.11, which is considerably steeper than the y-directional investigation in Figure 6.7.

This compressive zone control suggests an amount of prestressed steel as approximately, $A_p = 125[\frac{\text{mm}^2}{\text{m}}]$. When providing an quantity greater than this, the cracking limit state in terms of required compressive zone, $x > 50\text{mm}$, is fulfilled.

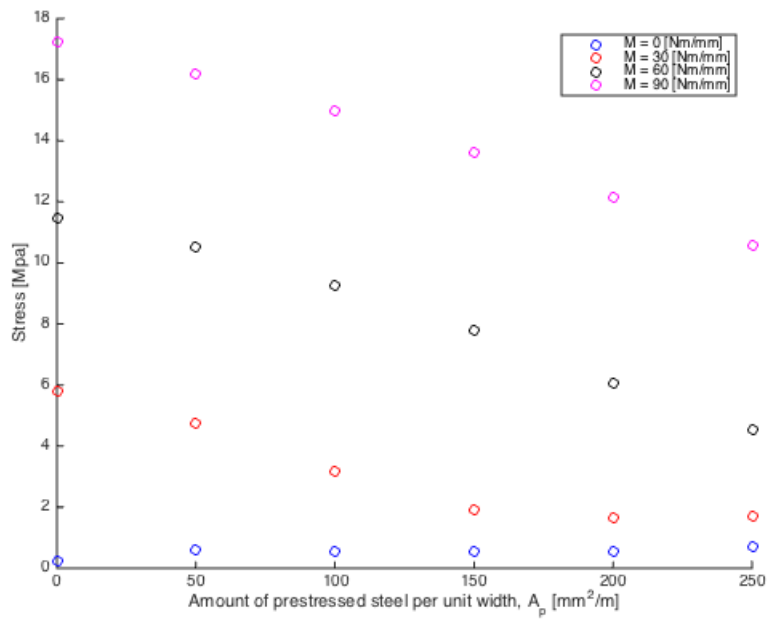


Figure 6.12: Resulting stress at concrete top due to x-directional prestress.

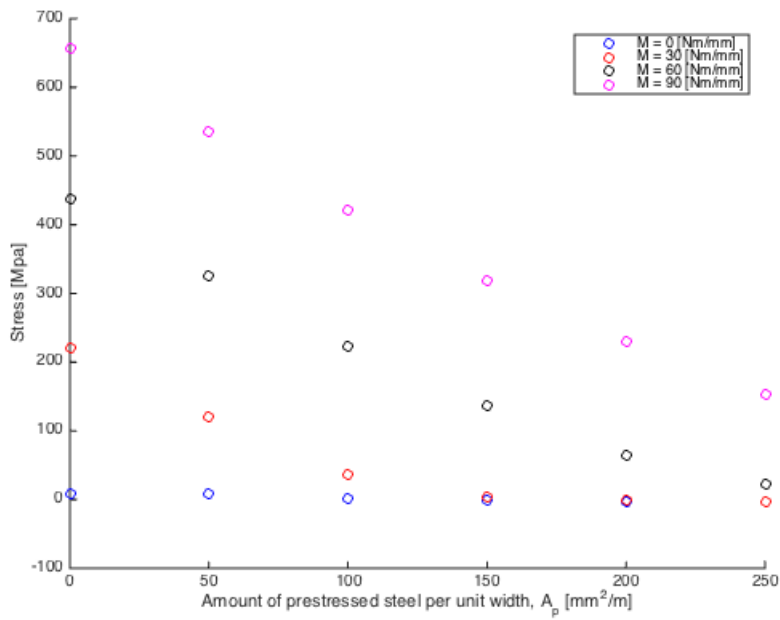


Figure 6.13: Resulting stress in ordinary reinforcement steel due to x-directional prestress.

Figure 6.12 shows the resulting stress at concrete top with varying amount of the eccentric prestressed steel. The results are once again shown for a range of the external hydrostatic moment, M_{hx} , covering this directional load-conditions throughout the strip. The condition for the critical location lies close to the black dots. Within the presented amount of prestressed steel, the concrete stress decays and stays within reasonable limits. As stated previously, the chosen type of concrete possess a compressive strength of $f_{ck} = 40\text{Mpa}$.

Figure 6.13 considers the same calculation model, presenting the stress in the ordinary reinforcement. This type of reinforcement typically has a strength, $f_{yk} = 500\text{Mpa}$, governing the first yield of the steel. Providing the critical strip with the minimum required amount of prestress, $A_p = 125[\frac{\text{mm}^2}{\text{m}}]$, results in an steel stress of approximately $\sigma_s = 200\text{Mpa}$. Increasing the amount of prestressed steel, will then further lower the steel stress.

Chapter 7

Two-way prestressed concrete panel

The following design approval considers a plain concrete panel. As stated by Solstad (2015), the inner surface of the tank is typically treated with epoxy. Dependent of its performance, the coating will increase watertightness characteristics of the panel. By considering the main issue as keeping the zone of compression greater than 50mm, the solution really applies for non-treated concrete panels. However, an incorporating of this strategy when surface finished will provide conservatism in terms of watertightness.

7.1 The design proposition

7.1.1 Y-directional prestressed steel

Prestressing along short edges aims to control the load-transferring in y-direction. These directional prestressed tendons are equally spaced and jacked, placed along the middle of the panel. The result is a uniform distribution of compressive loads, σ_y . As found in the previous study, a minimum amount of $A_{py} = 150[\frac{mm^2}{m}]$ is required. The corresponding minimum amount of compressive stress is then given as Equation (7.1).

$$\sigma_y = \frac{\sigma_{pmax} \cdot A_{py}}{t} = 0.68Mpa \quad (7.1)$$

A part of this required force is provided by the panel self-weight and the resting pedestrian bridge. The panel self-weight may be calculated according to Equation (3.1). For a panel vertically oriented, this force is distributed more or less linearly along the depth. At the foundation, the support introduces a magnitude according to Equation (7.2).

$$\sigma_{y,g} = \frac{F_g}{L_x \cdot t} = 0.28 \text{ Mpa} \quad (7.2)$$

The design of a pedestrian bridge is not considered in this study meaning no assessment of this additional self-weight component. However, the sum of these contributions relaxes the necessary amount of vertical prestress. As increased compressive stress leads to a decrease of the resulting stress parameters shown in Figure 6.8 and 6.9, the effect may be considered as beneficial for reasonable magnitudes.

The critical buckling stress for the panel by pure vertical compression were found to be $\sigma_y = 7.9 \text{ Mpa}$, as presented in Appendix A.1. By providing the panel with the minimum amount of vertical prestress, $\sigma_y = 0.68 \text{ Mpa}$, the solution will not violate the limitations for buckling. As the self-weight of the panel corresponds to approximately half of this value, this interpretation will still give a stress beyond the corresponding critical buckling stress.

By introducing steel with diameter, $\phi = 14 \text{ mm}$, the area of the prestressed reinforcement is calculated as Equation (7.3).

$$A_{py} = \pi \cdot \frac{\phi^2}{4} = 153.9 \left[\frac{\text{mm}^2}{\text{m}} \right] \quad (7.3)$$

This directional amount of prestressed steel provides a sufficient zone of compression under the governing assumptions. The resulting stresses in ordinary reinforcement and concrete top will further stay within reasonable limits. Figure 7.1 shows this directional design, specifying the amount and placement of ordinary and prestressed reinforcement.

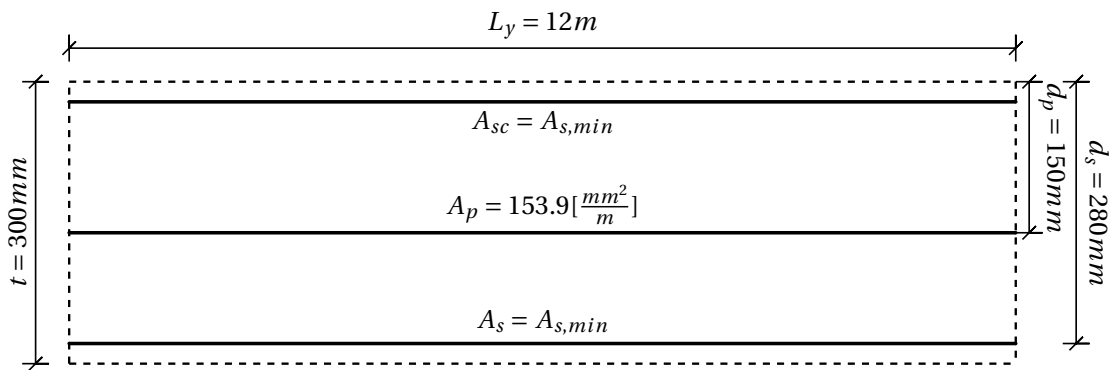


Figure 7.1: Resulting reinforcement design for load-transferring in y-direction.

7.1.2 X-directional prestressed steel

Due to the long span, the loads on x-directional strips varies considerably throughout the panel depth. A linear varying prestressing force, introduced at the long edges intends to capture this issue. The distribution is obtained by varying the spacing between tendons having the highest density near the panel bottom, while jacking them to the same value of strain. The prestressed steel are placed with an eccentricity relative to the COG, such that the risk of tendons breaking out of the inside cover reduces.

The minimum amount of prestressed steel as found in the design study was approximately given as, $A_{px} = 125[\frac{mm^2}{m}]$.

$$\sigma_x = \frac{\sigma_{pmax} \cdot A_{px}}{t} = 0.57 Mpa \quad (7.4)$$

Equation (7.4) states the equivalent minimum value of prestress to maintain the required compressive zone within the critical strip. The resulting value is taken as the amplitude in the linear prestress distribution acting on long edges of the panel. A combination of this edge load with the results from the vertical prestressing design, states a condition of biaxial compression. The corresponding buckling strength was investigated in Part II for both the prestressing state and the design condition. Figure 4.10 shows that the maximum linear prestressing amplitude for minor degree of prestress at short edges, lies close to $\sigma_x = 100 Mpa$. As this is not an accessible value within practical limits, buckling of the panel in these conditions is really not governing for the design.

By choosing prestressed steel with diameter, $\phi = 14 mm$, the total steel area within the critical x-directional strip may be calculated according to Equation (7.5)

$$A_{px} = \pi \cdot \frac{\phi^2}{4} = 153.9[\frac{mm^2}{m}] \quad (7.5)$$

This value states the magnitude of the linear distribution of steel area throughout the long edges of the panel. Therefore, the corresponding prestressing steel area is given as $A_{px} = 153.9 \cdot \frac{y}{12}[\frac{mm^2}{m}]$, where y denotes the panel depth. Figure 7.2 shows the proposed design for x-directional load-transferring.

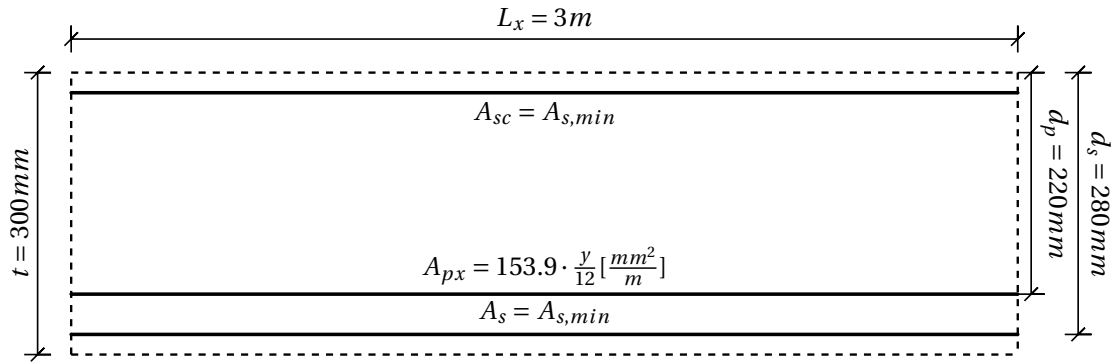


Figure 7.2: Resulting reinforcement design for load-transferring in x-direction.

7.2 Finite element analysis in Etabs

The solution is now to be approved by a finite element analysis, FEA, in Etabs. In this analysis, the panel is concerned with its actual thickness, $t = 300\text{mm}$. To reflect the cracked section properties of concrete, Etabs provides the opportunity to modify the relevant stiffnesses. CSi-wiki (2015) suggests scaling the out-of-plane bending stiffness 0.25 times the initial value which will give reasonable values regarding deflection of the panel.

7.2.1 Shell element modeling

The FEA makes use of shell elements to approximate the behavior of the panel. These elements takes the loading by a combination of membrane and bending response, which states the governing condition for a prestressed panel subjected to a hydrostatic pressure. For a non-curved shell within linear theory governing for the examined panel, these effects are captured by a superposition of the characteristics from plate and plane-stress elements. This is provided by the homogenous shell option in Etabs. In the following, the element formulation and usage are presented by statements adopted from Leira (2011). For a further reference to finite element analysis in Etabs, the reader is recommended to look into the documentation manual (CSi, 2013, Chapter X).

A panel in design condition is primarily loaded by a hydrostatic pressure represented by a bending action. This behavior is approximated by a plate formulation with internal load-components as seen in Figure 7.3.

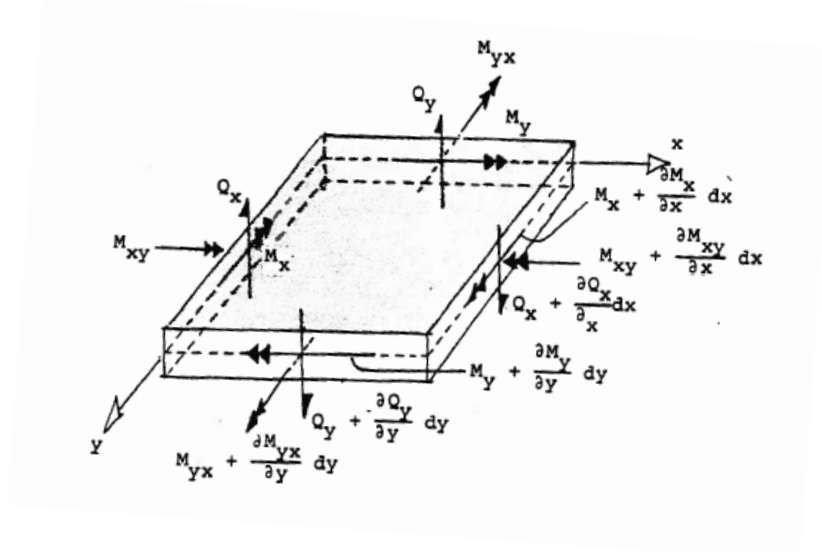


Figure 7.3: Forces acting within a plate element, Leira (2011) .

$$\frac{\partial^2 M_x}{\partial x^2} + 2 \frac{\partial^2 M_{xy}}{\partial x \partial y} + \frac{\partial^2 M_y}{\partial y^2} + p(x, y) = 0 \quad (7.6)$$

Consistent with Hooke's law, which gives the stress-strain relation, this equation can be formulation into the differential equation for a plate as given in Equation (7.7). The plate stiffness is shown as Equation (7.8).

$$\nabla^4 w = \frac{p(x, y)}{D} \quad (7.7)$$

$$D = \frac{Et^3}{12(1 - \nu^2)} \quad (7.8)$$

The differential equation acts as basis for the finite element formulations. As other FEM softwares, Etabs provides the opportunity to choose between different theories for formulation of the plate elements.

$$\begin{aligned} \frac{t}{L_i} < 0.1 & \quad \text{Thin plate} \\ 0.1 < \frac{t}{L_i} < 0.4 & \quad \text{Moderate thick} \\ \frac{t}{L_i} > 0.4 & \quad \text{3D solid} \end{aligned}$$

The thin-plate formulation refers to Kirchhoff plate theory which neglects the transverse shear deformations. For the examined panel, $\frac{t}{L_x} < 0.1$, which suggests the use of a thin-plate formulation. A moderate thick panel makes use of Mindlin/Reissner theory accounting for the transverse shear deformation. For a even larger value of $\frac{t}{L_i}$, the panel should typically be characterized as a 3D solid.

A panel loaded by in-plane compressive forces, as for the application of prestress, is concerned by a membrane action. To represent this behavior, it is convenient to make use of plane stress elements. These elements represents a physical matter where the thickness is much smaller then the span, such that the stress components normal to the element are close to zero. The internal stresses in these element can be seen in Figure 7.4, where the in-plane definition is recognized by the stresses acting in plane.

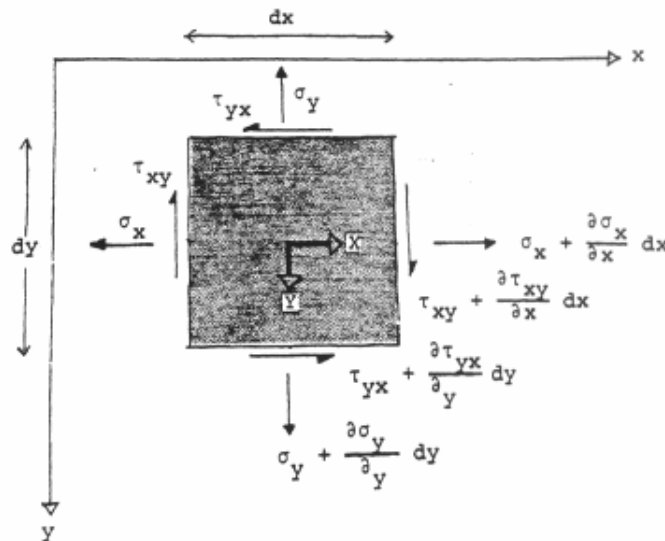


Figure 7.4: Stresses acting within a plane stress element, Leira (2011) .

Shell elements incorporates the plate and plane-stress element characteristics. The governing shell element used within Etabs is shown in Figure 7.5. This element is denoted S4, recognized by the four corner nodes. Quadratic interpolation polynomials approximates the in-plane membrane behavior, while the out-of-plane displacement is given a cubic variation.

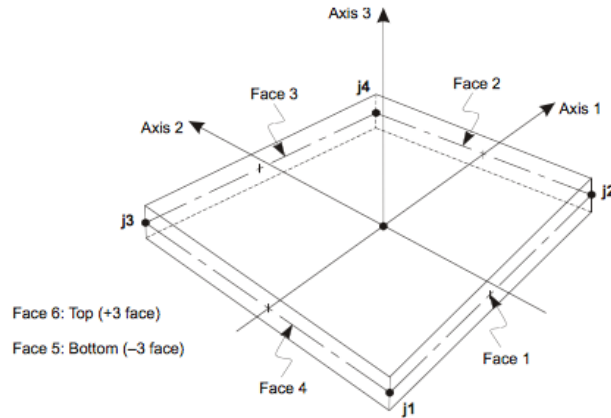


Figure 7.5: The four-node quadrilateral shell element used in Etabs, CSI (2013).

7.2.2 Modeling prestress as compressive point loads

Figure 7.6 highlights the proposed arrangement of prestressed steel throughout the panel. The structural effects of prestressed steel are considered as external compressive point loads. As the spacing between each individual tendon is not specified, the effect is said to be captured by point loads reflecting the amount of prestressed steel per unit width.

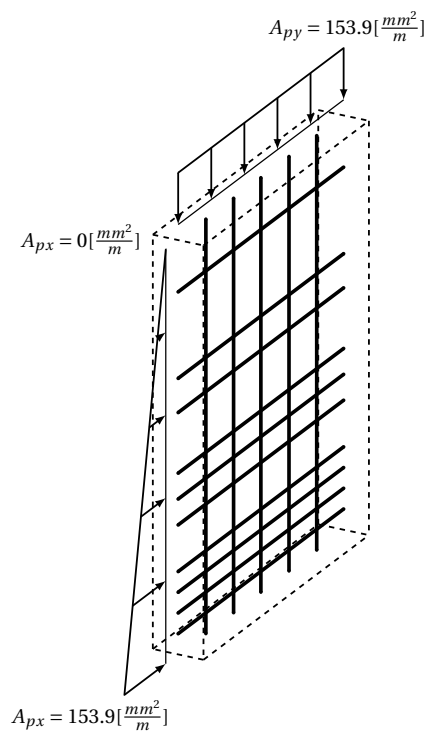


Figure 7.6: Distribution of prestressed steel throughout the panel.

The vertical prestressed reinforcement are introduced as non-eccentric point loads. Equation (7.9) calculates the magnitude which is equal for all these compressive loads due to the constant tendon spacing.

$$P_y = \sigma_{pmax} \cdot A_{py} = 1360 \frac{N}{mm^2} \cdot 153.9 \frac{mm^2}{m} \cdot 10^{-3} = 209.3 \frac{kN}{m} \quad (7.9)$$

The x-directional prestressed reinforcement introduces point loads as well as eccentricity moments. Due to the linear spacing, the magnitude will differ throughout the height of the panel. Equation (7.10) calculates the magnitude for the point loads, while Equation (7.11) gives the corresponding eccentricity moment.

$$P_x = \sigma_{pmax} \cdot A_{px} \cdot \frac{y}{L_y} = 1360 \frac{N}{mm^2} \cdot 153.9 \frac{mm^2}{m} \cdot \frac{y}{12} \cdot 10^{-3} = 209.3 \frac{kN}{m} \cdot \frac{y}{12} \quad (7.10)$$

$$M_{px} = \sigma_{pmax} \cdot A_{px} \cdot e \cdot \frac{y}{L_y} = 1360 \frac{N}{mm^2} \cdot 153.9 \frac{mm^2}{m} \cdot 0.07m \cdot \frac{y}{12} \cdot 10^{-3} = 14.7 \frac{kNm}{m} \cdot \frac{y}{12} \quad (7.11)$$

These forces, in addition to the hydrostatic pressure, states the governing load-condition for the panel in design condition.

7.2.3 Response of the prestressed solution

Stresses

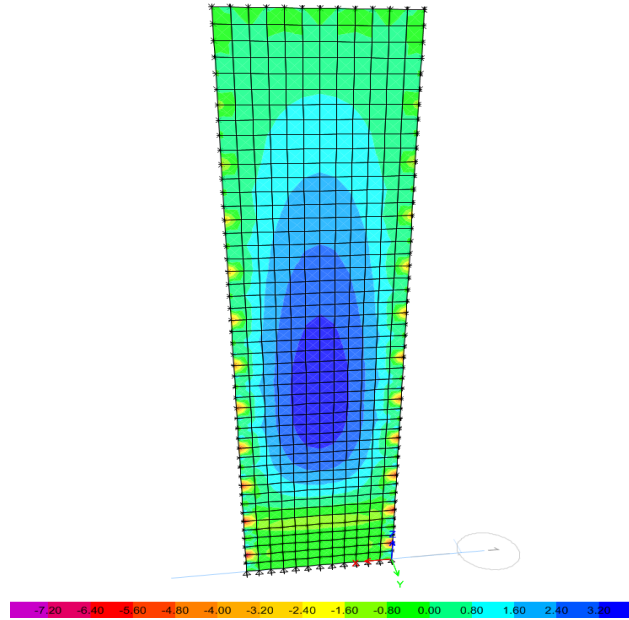


Figure 7.7: Stress distribution in x-direction for the prestressed concrete panel.

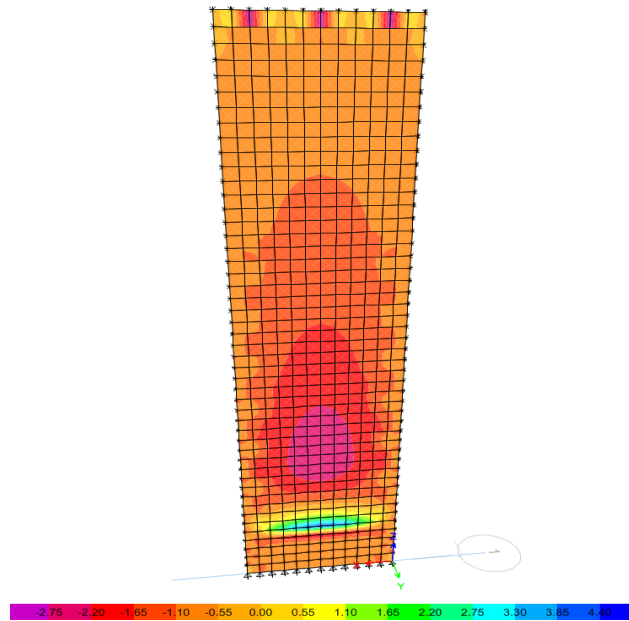


Figure 7.8: Stress distribution in y-direction for the prestressed concrete panel.

Figure 7.7 and 7.8 shows the stress distribution in each principal direction of the prestressed panel. The values are reported for the side of the panel corresponding to tensile stress at the critical locations. Appendix B.2 provides the compressive stress at the opposite sides.

Compared to the response quantities for the non-prestressed case as given in Appendix B.1.1, the maximum tensile stresses are now lowered. These reductions corresponds to the biaxial compressive forces introduced by prestressing the concrete.

Panel condition	Non-prestressed	Prestressed
Tensile stress [Mpa]	4.59	3.79
Compressive stress [Mpa]	4.59	4.55

Table 7.1: Maximum stress values in x-direction at the critical section.

Panel condition	Non-prestressed	Prestressed
Tensile stress [Mpa]	5.61	4.16
Compressive stress [Mpa]	5.61	5.99

Table 7.2: Maximum stress values in y-direction at the critical section.

As Etabs assumes uptake of tensile forces in the concrete, the resulting stresses will not be directly comparable with the results from the routine used in the prestressing design. However, as the value of tensile stress still exceeds the characteristics tensile strength of concrete, $f_{ctm} = 3.5\text{Mpa}$, cracking will be present which further validates the design assumptions.

Deflection of panel

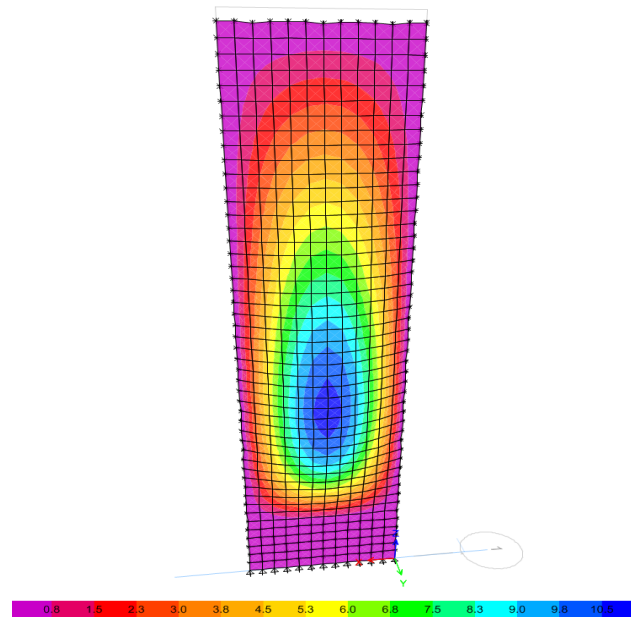


Figure 7.9: Out-of-plane deformations for the prestressed concrete panel.

Figure 7.9 shows the resulting deformation of the prestressed concrete panel by contours. Due to the eccentric x-directional tendons, the maximum deformation lowers as compared to the non-prestressed case in Appendix B.1.2.

Panel condition	Non-prestressed	Prestressed
Deformation [mm]	12.3	10.9

Table 7.3: Maximum lateral deformation for concrete panel.

As presented in Section 3.4.2, the allowable deformation is limited to $\min[\frac{L_x}{250}, \frac{L_y}{250}]$. The distance along the shortest span is 3m turning the criteria into $\delta_{max} < 12\text{mm}$. As the two-way prestressed panel experiences a deflection magnitude less than 12mm, this criteria is fulfilled.

$$\left(1 - \frac{10.9}{12.3}\right) \cdot 100\% = 11.4\% \quad (7.12)$$

Equation (7.12) gives the percentage reduction of the deflection amplitude due to the transition from a non-prestressed panel to the governing prestressed solution. The model does not consider long-term effects such as concrete creep and shrinkage, neither the different losses of prestress. To incorporate these matters, a staged-construction sequence as given by (CSI, 2013, Chapter XXIII), is required.

Due to the model limitations, the resulting deformation will be smaller than the actual value. However, as neither of these two cases considers creep or shrinkage, the decreasing deflection trend may still be valid when considering the compressive forces as the net value of prestress.

The effect of creep may be approximated by a long-time concrete modulus of elasticity as discussed in Section 2.1. The creep coefficient due to the hydrostatic pressure is found by use of Figure 3.1b in NS-EN-1992-1 (2008). Figure 7.10 illustrates the scheme when approximating the creep factor reflecting the long-time presence of water.

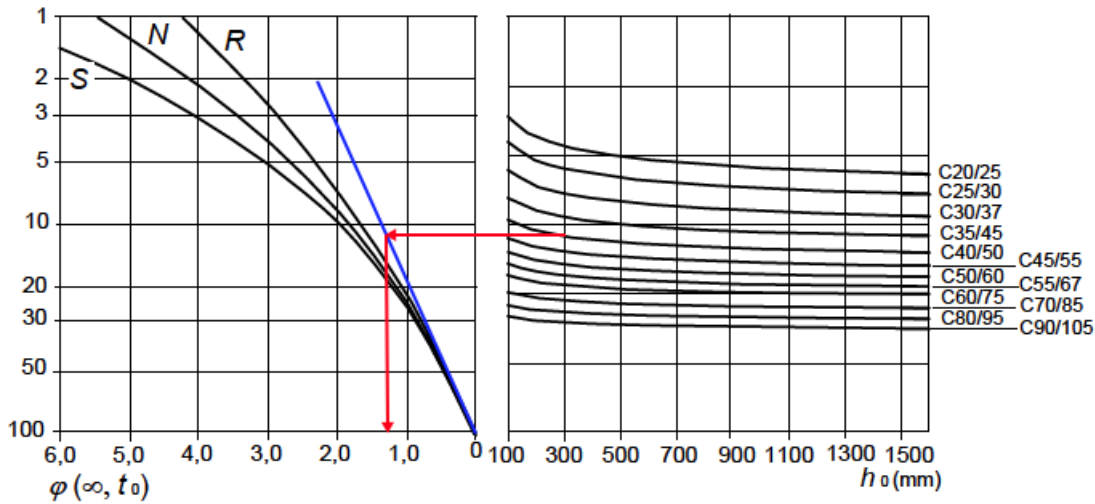


Figure 7.10: Illustration of the scheme used to approximate the creep coefficient, (NS-EN-1992-1, 2008, Section 3)

As the tanks consist of precast panels, the concrete will age a considerable amount of time before the applied loading, t_0 . These facts state the use of the blue tangent line. For the governing concrete class, C40, and by approximating h_0 as the panel thickness, the creep coefficient is found as, $\phi(\infty, t_0) = 1.2$.

$$E_{cl} = \frac{35}{1 + 1.2} = 15.9Gpa \tag{7.13}$$

Equation 7.13 gives the resulting long-time concrete modulus of elasticity. Now by making use of this value as E_c in the analysis, the maximum deflection increases considerably for both the non-prestressed and the prestressed solution as seen in Table 7.4.

Panel condition	Non-prestressed	Prestressed
Deformation [mm]	27.0	23.9

Table 7.4: Maximum lateral deformation for concrete panel when accounting for creep behavior.

$$\left(\frac{23.9}{10.9} - 1\right) \cdot 100\% = 119.3\% \quad (7.14)$$

Equation (7.14) shows the percentage increase in deflection maximum for the prestressed panel. The proposed way of creep estimation shows that this effect has a great influence on the deflection. As the allowable deformation now is violated, it may be of interest to further iterate on an optimal prestressed solution. Prestressing with an eccentricity along the short edge may be seen as an efficient way to reduce the deflection amplitude even further.

Chapter 8

Summary and Recommendations for Further Work

8.1 Conclusions

In general, local capacities such as flexural and shear resistance governs the design for concrete elements. The solution is then further approved in the serviceability limit state by deformation control and crack-width calculations. When operating in liquid-retaining applications the attention is typically given the latter. In addition to a degradation of the structure, the formulation of cracks may lead to a certain degree of leakage. NS-EN-1992-3 (2009) propose a classification of liquid-retaining structures with respect to a watertightness criterion. For the most conservative classes denying any degree of leakage, this standard propose the use of prestressed steel to maintain a sufficient compressive zone in the member.

The structural effects from prestressing were throughout the study handled as external compressive forces. With increasing size of the precast concrete panels, formulated through the span-ratio, buckling was further investigated as a potential failure mode. The study investigated this capacity within three different cases representative for the stages in construction.

- Vertical prestressing in fabric \Rightarrow panel subjected to compressive stress at the short edges
- Further prestressing at site along the perimeter \Rightarrow panel subjected to biaxial compression
- Design condition \Rightarrow biaxially compressed panel subjected to a hydrostatic pressure

Prestressing at a casting bed in fabric represented the least stiff configuration. The corresponding buckling load for Panel 4 with a span-ratio of $\frac{L_y}{L_x} = 4$, was found as $\sigma_y = 7.9\text{Mpa}$. This stage turned out to be the most critical one, as the others showed a buckling performance with mag-

nitudes way beyond practical prestressing limits. In the design condition, the analyses also considered the presence of a hydrostatic pressure from the containing water. Even though this typically destabilizes the structure, the stiffening effect from the resting pedestrian bridge and the ring beam at the foundation lead to a net increased buckling strength.

A design proposition for the amount and cross-sectional placement of prestressed tendons then followed. According to the class of watertightness, a preservation of a compressive zone greater than 50mm was considered as the main design issue. For panels treated with an inner coating which typically is a relevant issue, this criterion will be relaxed. Since the design proposal did not consider the presence of this beneficial effect, the solution may really be considered as conservative. However, as parts of the design procedure are conceptual it may be easily adopted so to account for this issue in future studies.

The design was based on acting moments as given from an analysis in the design condition performed in Etabs. For the vertical load-transferring, further strip considerations proposed the use of a uniform prestress along the short edges. For an amount greater than $A_{py} = 150 \frac{mm^2}{m}$, a sufficient height of the compressive zone was said to be preserved. A comparison with the buckling capacity within the first stage showed that this amount of prestress, acting as compressive loads in collaboration with the panel self-weight, would not violate this limit. With an even further increase in the slender properties, the study however revealed the fact that this directional prestress will be limited by the buckling capacity within the first stage of the construction.

The prestressing design at the long edges made use of a varying tendon spacing. The following process of post-tensioning was said to introduce a linear compressive force distribution. As the design was performed for the critical directional strip, located near the panel bottom, the corresponding amount of prestressing steel defined the magnitude of the force distribution. The minimum amount was found as $A_{px} = 125 \cdot \frac{y}{12} [\frac{mm^2}{m}]$, where y denotes the depth of the panel. Near the foundation, where $y = 12m$, the necessary amount of prestressing steel would then be $A_{px} = 125 [\frac{mm^2}{m}]$ as found for the critical strip. As the tendons were suggested to lay in outer third of the cross-section, the following prestress would introduce an additional eccentricity moment beneficial for the panel performance.

The solution was then implemented and approved by a FEA in Etabs. Shell elements were considered as representative for the governing flexural and membrane action. As the software assumes uptake of tensile stresses in the concrete, the resulting stress distribution could not be further approved. For deflection purposes the concrete cracking was introduced as a scaling of the shell stiffness. The maximum deflection experienced a major increase when accounting for creep deformation, which really violated the allowable deformation. A further iteration on a prestressing design should be performed in order to fulfill this criteria.

8.2 Strength and limitations

The thesis is based on an investigation of concrete panels as modules of a polygonal tank. The examined panel dimensions are primarily chosen so to investigate the effect of increasing span-ratio. However, to maintain reasonability with respect to production and transportation, the height and width are within limits according to information given by Solstad (2015).

The study may be classified as a local analysis, as it considers the individual panels with a given connection to the adjacent structure and the foundation. These connections are defining for each stage of the construction, such that the results and conclusions do not apply for other boundary conditions. However, the parameter study on the compressive zone stays valid independent of the governing connections, as the hydrostatic moment can be varied according to the user. As mentioned in the study, the boundary conditions are given as extreme values. This means that translational and rotational degrees of freedom are either free or fixed. In reality, these values are intermediates, which can be modeled by springs with certain stiffnesses.

In the buckling analysis, panels were given homogenous and isotropic material properties. The use of an equivalent thickness aimed to incorporate both the stiffness contribution from reinforcement, as well as the cross-sectional degradation resulting from cracking. As the panel carries the load in two principal directions, the cracking behavior may in reality differ in each direction interfering with the assumptions. In terms of modeling, this is only accounted for by considering anisotropic material properties.

The interpretation of an equivalent thickness may be considered as the weakest part of the study. As the result from the cracked-section methodology is highly conservative, the thickness was really given a value somewhere between the equivalent and the true one. As the buckling stress shows a strong positive correlation with panel slenderness, the interpretation of $t_{eq} = 200\text{mm}$ will cause inaccuracies.

The design was performed with a reference at the most loaded areas in the respective directions. It proposes the use of strip theory within a cracked concrete calculation model established as a Matlab routine. It may be noted that this is conservative strategy in determining the amount of prestress.

In addition to an amount of prestressed steel, the proposed design for cracking limit state makes use of a minimum reinforcement for beams as given in NS-EN-1992-1 (2008). This amount should really be determined from a flexural design in the ULS, as described in Section 3.4.1. Since this thesis does not cover ultimate design, the minimum amount is utilized per unit width as compressive and tensile reinforcement in both span-directions of the panel. The proposed design shows however that the appearing stresses in concrete and reinforcement are beyond the

respective capacities, which states a certain reasonability by the use of this quantity.

As presented in Part I, time-dependent effects such as creep and shrinkage of concrete give additional deformation within the structure. Losses of effective force may suggest that the amount of prestress should be increased somewhat. As these effects are not entirely assessed in the study, the closing design should be considered as a conceptual issue rather than a complete design.

8.2.1 Non-linear effects

Throughout this study, linearities have been assumed when examining the concrete panels. These procedures include some assumptions related to the stress-strain relationship, as well as the magnitude of the deformations. In terms of non-linearities, the effect of concrete cracking may be seen as a special case. However, as this is unique for concrete, it is not dealt with in the same manner as the other general effects.

In a linear model, the stress-strain relationship is described by Hookes law expressing a linear relationship. As the strain reaches the yield limit, this statement will be interrupted and rather defined by the strain-hardening properties, also known as plasticity. The stress increment due to an increment in strain, is then expressed by $\Delta\sigma = E_t\Delta\epsilon$. Here E_t is denoted as tangential modulus. An illustration of this concept is given as Figure 8.1.

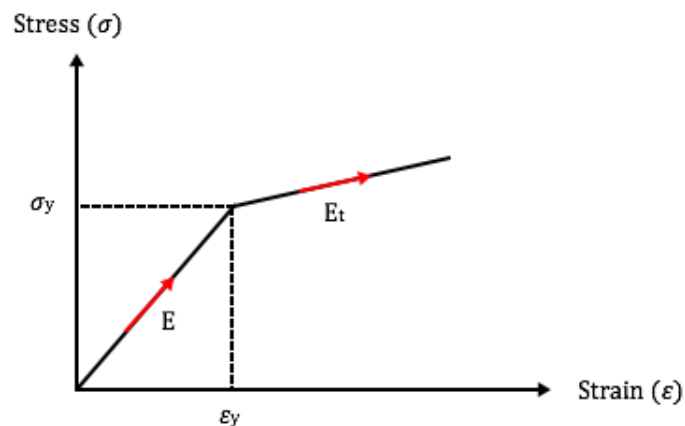


Figure 8.1: Illustration of a non-linear stress-strain relationship.

The effects of material non-linearities in concrete structures are really not that present. The material experiences a brittle behavior when approaching the ultimate strength, as seen in Section 2.1 as Figure 2.1. This means that a linear material model, as described by the concrete modulus

of elasticity E_c , may be sufficient. As the primary focus within this thesis is cracking in the SLS, the use of a linear material model is further supported.

In terms of deformations, linearity suggests that these remains small. Within a finite element formulation, this assumption states equal stiffness properties although the structure deforms. The equilibrium equations are then established at the initial configuration. In a physical manner, this really means that the different internal load components maintain their initial direction throughout the deformation.

For a concrete tank exposed to a hydrostatic pressure, there will be some geometric non-linearities present. As the panel deforms, the equilibrium equations for the initial configuration no longer holds. For a certain deformation amplitude, the panels activate membrane forces which will contribute to the load-carrying. As for the material non-linearities, the performance may then be described in incremental form. A linear load-displacement relation is expressed as $R = Kr$, where R is the external load vector, K is the stiffness matrix and r the displacement vector. When accounting for the geometrical non-linearities, the relation may then be described as $\Delta R = K_I \Delta r$. Here K_I denotes the incremental stiffness as the stiffness at a certain stage in the deformation. An illustration is given in Figure 8.2.

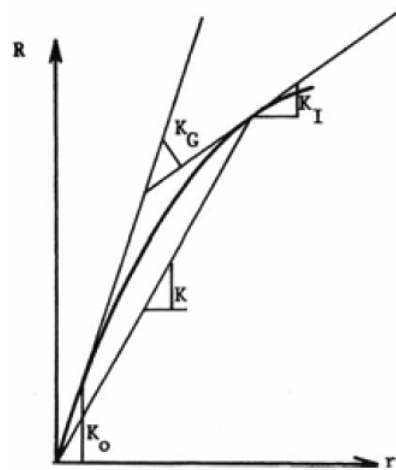


Figure 8.2: Illustration of a non-linear load-deformation relationship. Moan (2003, p. 12.9)

The incremental stiffness is decomposed into a geometrical, K_G , and linear term, K_0 . The latter relates to the stiffness within linear analysis referring to the initial configuration, while the geometric stiffness represents the additional stiffness as the panel deforms.

In this study, linear considerations have been made. Especially in terms of non-linear geometry, the activation of membrane forces may interrupt the cross-sectional characteristics. It is impor-

tant to have in mind, and may be utilized if a non-linear analysis of the concrete tank is to be performed as a further work.

8.3 Recommendations for Further Work

As the study considers design for cracking limit state, it is apparent that the design should be approved in terms of the ULS by a software supporting this issue. These design checks are presented in Section 3.4.1, covering both the shear and flexural capacity. In addition, when applying prestressed steel, the simultaneous action of moment and normal force, M-N, should be considered and checked against the corresponding capacity. This design procedure really states the necessary amount of ordinary reinforcement, which in my study is taken as the minimum quantity from the design codes.

Prior to a design for ultimate capacity, it may be interesting to do a more detailed study on the governing boundary conditions. The foundation base may then be modeled as moment springs with a stiffness close to a fixed condition. For the vertical joints, stating the type of connection between adjacent panels, the governing degrees of freedom varies with the solution strategy.

In the design, some considerations regarding the optimal distribution of the prestressing force were made. Along the vertical direction, the prestressing steel design was intended to give a uniform distribution. In the other principal direction, the use of various spaced tendons should produce a linear force distribution. The idea was then to fit the prestressing force to the corresponding hydrostatic load distribution so to control the compressive zone in an efficient way. As recognized by the moment distribution resulting from the water pressure in Figure 6.2, it is apparent that other prestressing force distributions could be proposed. A study investigating higher order distributions may become of interest to optimize the design.

Bibliography

Abaqus (2013). *Abaqus User's Guide (6.13)*.

Abetong (2015). <http://www.abetong.se/sv/Tanksystem>. [Online; accessed 22-January-2015].

AlchemyPolymers (2015). www.alchemypolymers.com. [Online; accessed 5-April-2015].

Bergin, M., Bjartnes, E., and Brønstad, J. M. (2011). Structural design of precast concrete tanks for on-shore fish farming (prefabrikkerte betongkar til landbasert fiskeoppdrett). Master's thesis, HIST.

Betongelementforeningen (2010). *Betongelementboken*, volume A,B,C. Byggnæringens Forlag AS, 4th edition.

CivileA (2015). <http://cdnpic.civilea.com/images/00889091634474826378.jpg>. [Online; accessed 9-February-2015].

ConsolisGroup (2015). <http://www.xprestank.eu>. [Online; accessed 9-February-2015].

CSi (2013). *CSi Analysis Reference Manual*. Berkeley, California, USA, eight edition.

CSi-wiki (2015). <https://wiki.csiamerica.com/display/etabs>. [Online; accessed 2-April-2015].

Holm, J. C. (2015). *Vilkår for landbasert oppdrett av laksefisk*. Fiskeridirektoratet.

Leira, B. J. (2011). *TMR4170 Marine Structures, Basic Course*. Dept. Marine Technology.

Moan, T. (2003). *Finite Element Modelling and Analysis of Marine Structures*. Dept. Marine Technology.

MooreConcrete (2015). <http://www.mooreconcrete.com>. [Online; accessed 9-February-2015].

NS-9415 (2009). *Marine fish farms - Requirements for site survey, risk analysis, design, dimensioning, production, installation and operation*, 1st edition.

NS-9416 (2013). *Landbased aquaculture farms for fish - Requirements for risk analyses, design, execution, operation, user handbook and product data sheet*, 1st edition.

NS-EN-1991-4 (2010). *Eurocode 1: Action on structures - Part 4: Silos and tanks*, 1st edition.

NS-EN-1992-1 (2008). *Eurocode 2: Design of concrete structures - Part 1: General rules and rules for buildings*, 1st edition.

NS-EN-1992-3 (2009). *Eurocode 2: Design of concrete structures - Part 3: Liquid retaining and containment structures*, 1st edition.

OverhallaBetongbygg (2015). Tekset 2015. <http://tekset.sircondesign.net/2015-2/>. [Online; accessed 6-May-2015].

Rashed, A., Elwi, A. E., and Rogowsky, D. M. (2002). Reinforced, partially prestressed concrete water tank walls. *ACI Structural Journal*, 99(3).

Solstad, I. H. (2015). Personal communication.

Sørensen, S. I. (2013). *Betongkonstruksjoner*. Akademika, 2nd edition.

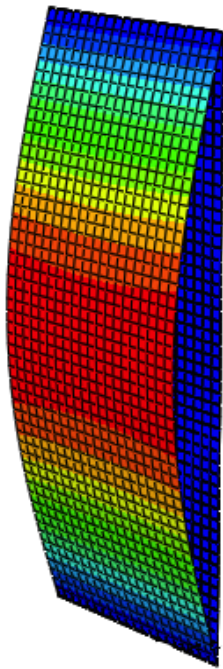
Appendices

Appendix A

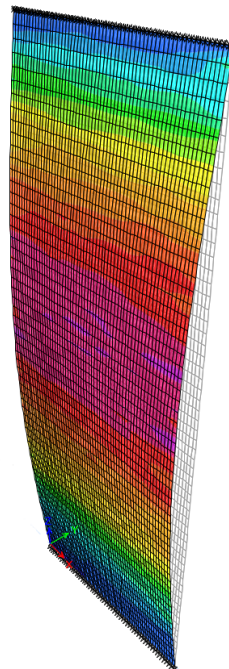
Results from buckling analysis

A.1 Concrete panel subjected to monoaxial compressive stress

Panel 2



(a) Buckling shape as visualized by Abaqus.

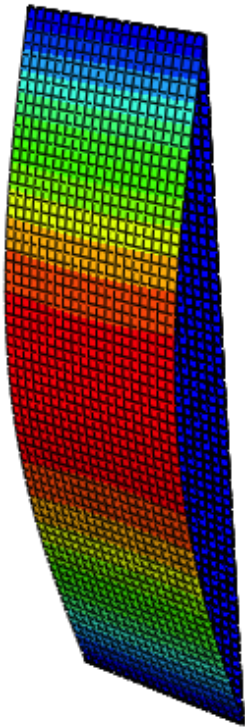


(b) Buckling shape as visualized by Etabs.

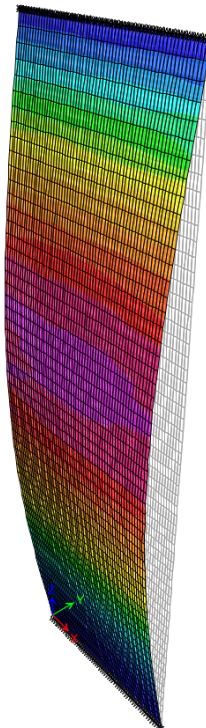
Figure A.1: Lowest eigenmode for Panel 2 within the first case study.

Panel 2	Buckling stress [Mpa]
Abaqus	18.1
Etabs	17.8

Panel 3



(a) Buckling shape as visualized by Abaqus.

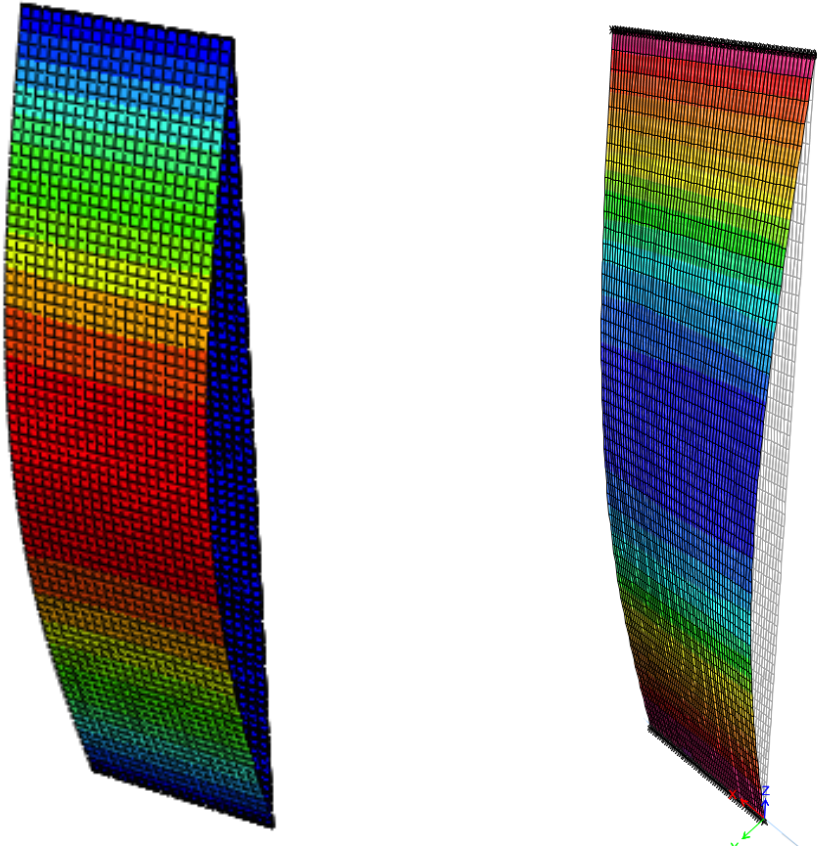


(b) Buckling shape as visualized by Etabs.

Figure A.2: Lowest eigenmode for Panel 3 within the first case study.

Panel 3	Buckling stress [Mpa]
Abaqus	11.6
Etabs	11.4

Panel 4



(a) Buckling shape as visualized by Abaqus.

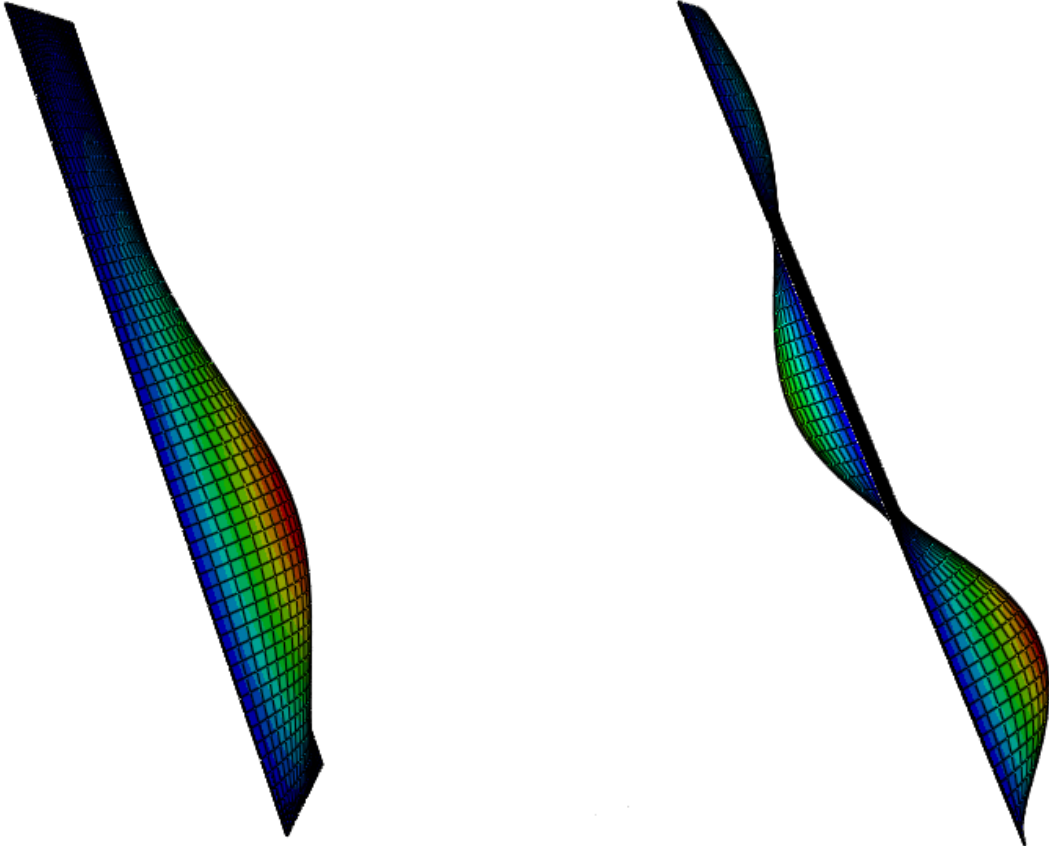
(b) Buckling shape as visualized by Etabs.

Figure A.3: Lowest eigenmode for Panel 4 within the first case study.

Panel 4	Buckling stress [Mpa]
Abaqus	8.0
Etabs	7.9

A.2 Concrete panel subjected to biaxial compressive stress

Panel 2

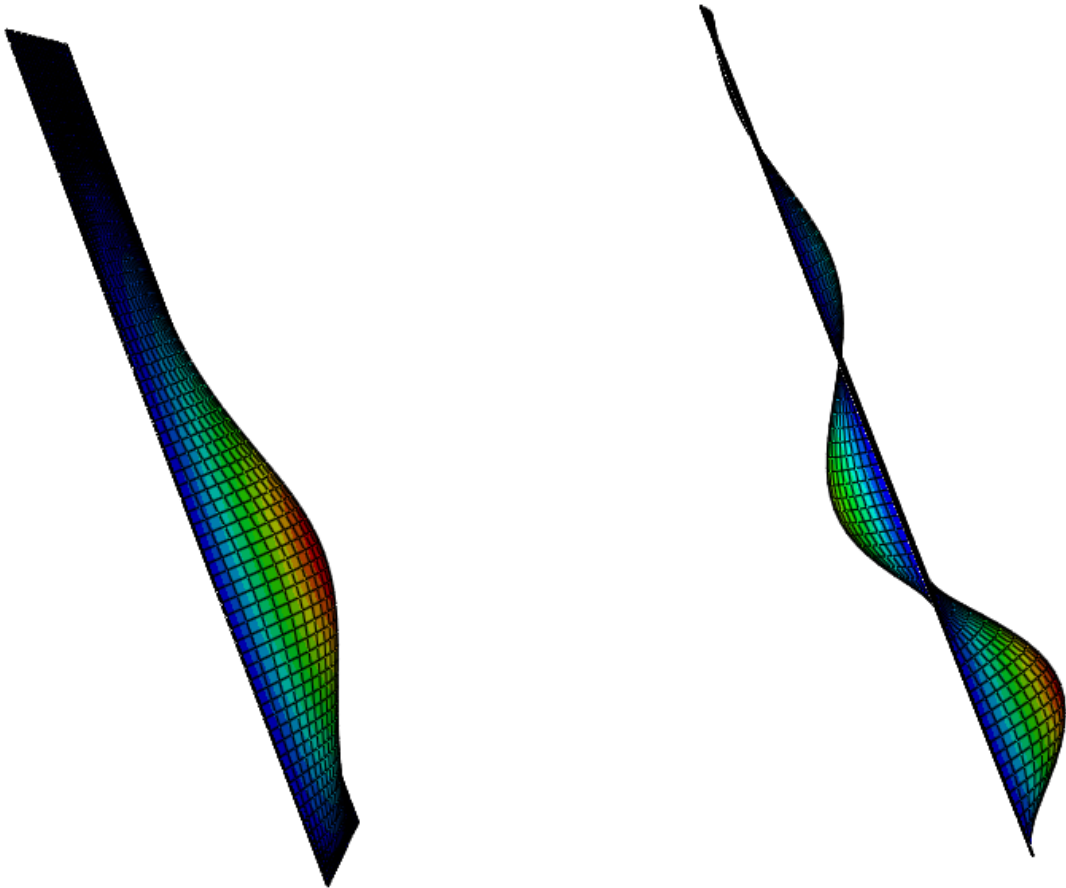


(a) Minor influence from vertical prestress.

(b) Major influence from vertical prestress.

Figure A.4: Lowest eigenmode for Panel 2 within the second case study for various degree of vertical prestress.

Panel 3

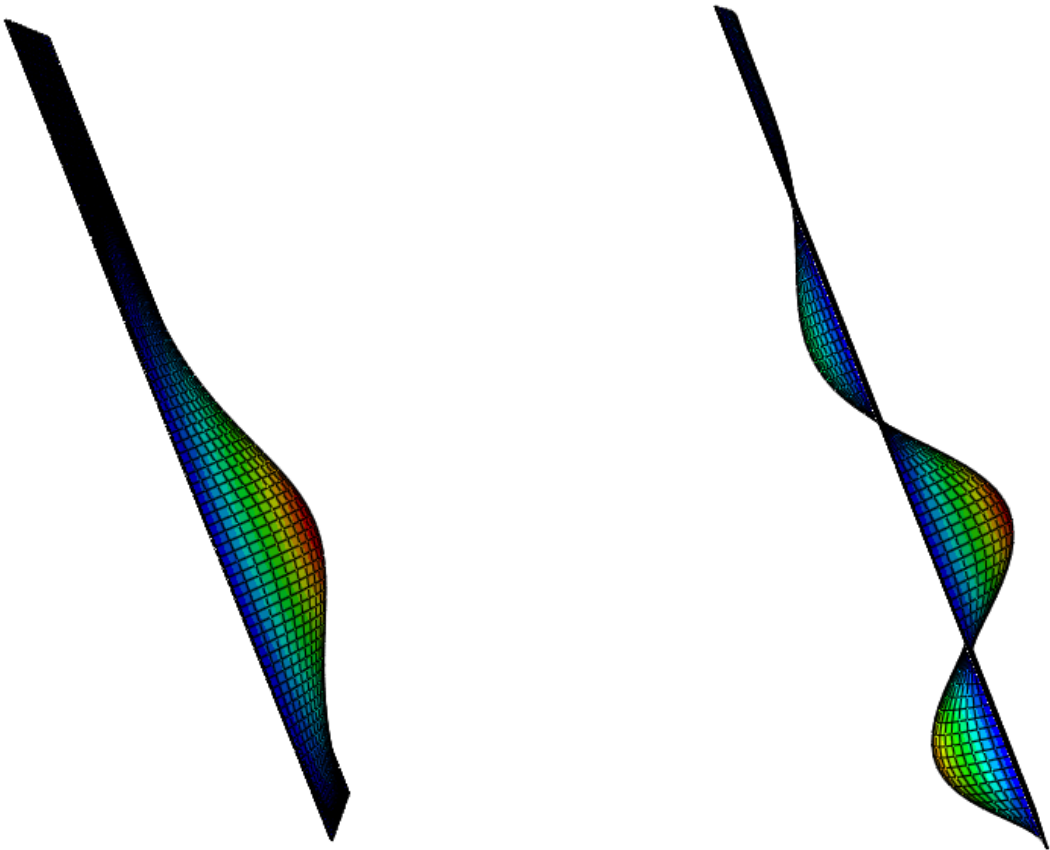


(a) Minor influence from vertical prestress.

(b) Major influence from vertical prestress.

Figure A.5: Lowest eigenmode for Panel 3 within the second case study for various degree of vertical prestress.

Panel 4



(a) Minor influence from vertical prestress.

(b) Major influence from vertical prestress.

Figure A.6: Lowest eigenmode for Panel 4 within the second case study for various degree of vertical prestress.

A.3 Biaxially loaded concrete panel subjected to a triangular lateral pressure

Panel 2

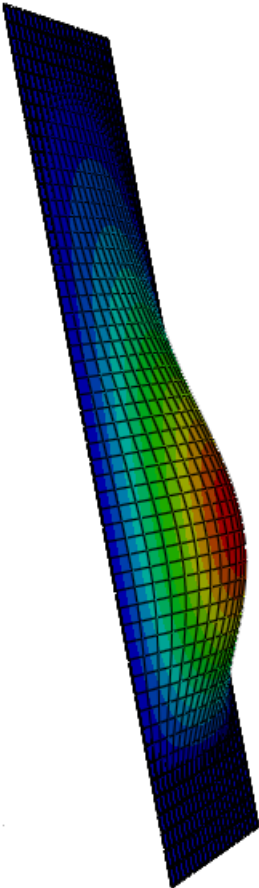


Figure A.7: Lowest buckled shape of Panel 2 within the third case study.

Panel 3

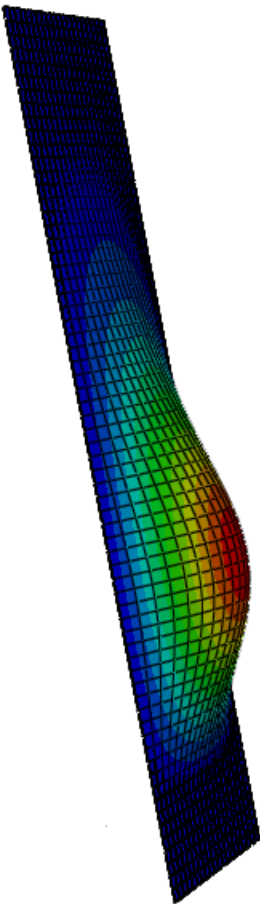


Figure A.8: Lowest buckled shape of Panel 3 within the third case study.

Panel 4

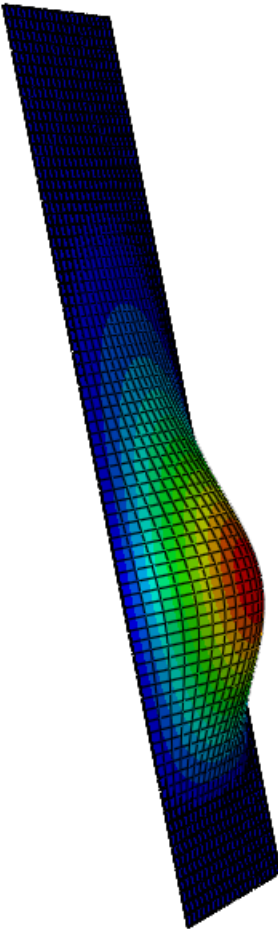


Figure A.9: Lowest buckled shape of Panel 4 within the third case study.

Appendix B

Finite element analysis of concrete panel

B.1 Response of non-prestressed panel

B.1.1 Stress

Side of panel corresponding to tensile stress at the critical location

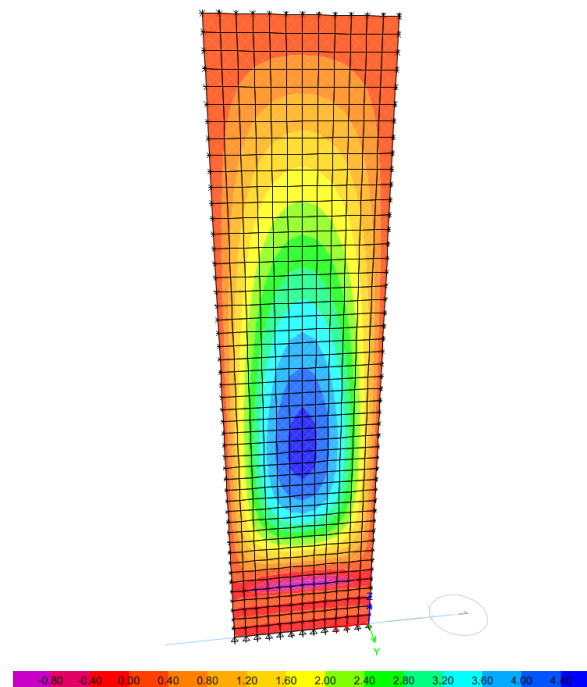


Figure B.1: Stress distribution in x-direction at the side of the non-prestressed panel experiencing tensile stress at the critical location.

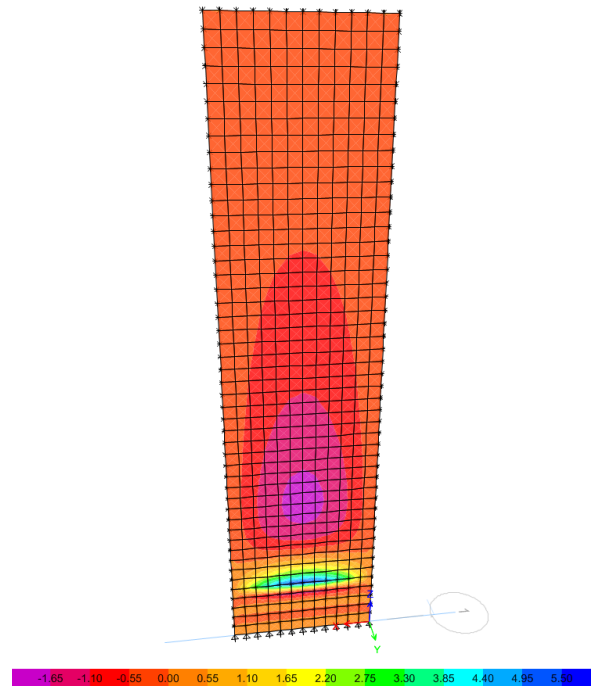


Figure B.2: Stress distribution in y-direction at the side of the non-prestressed panel experiencing tensile stress at the critical location.

Side of panel corresponding to compressive stress at the critical location

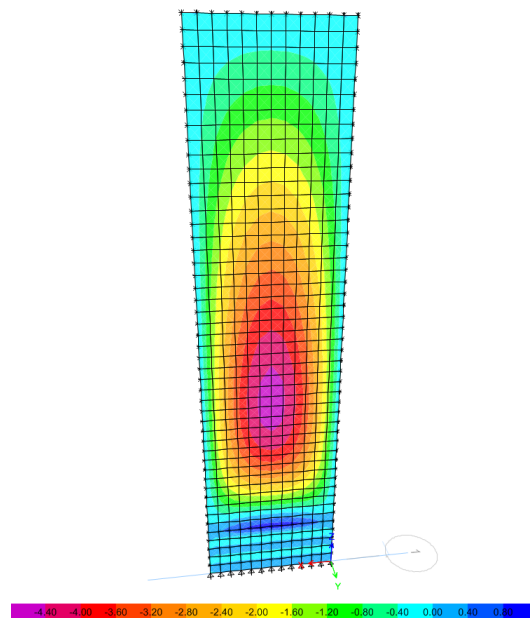


Figure B.3: Stress distribution in x-direction at the side of the non-prestressed panel experiencing compressive stress at the critical location.

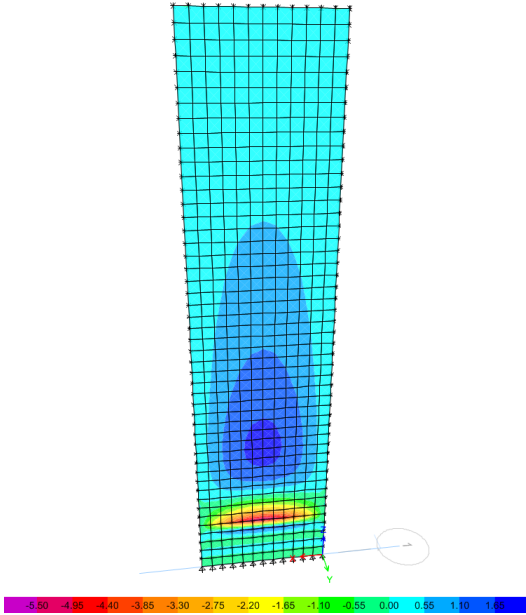


Figure B.4: Stress distribution in y-direction at the side of the non-prestressed panel experiencing compressive stress at the critical location.

B.1.2 Deflection

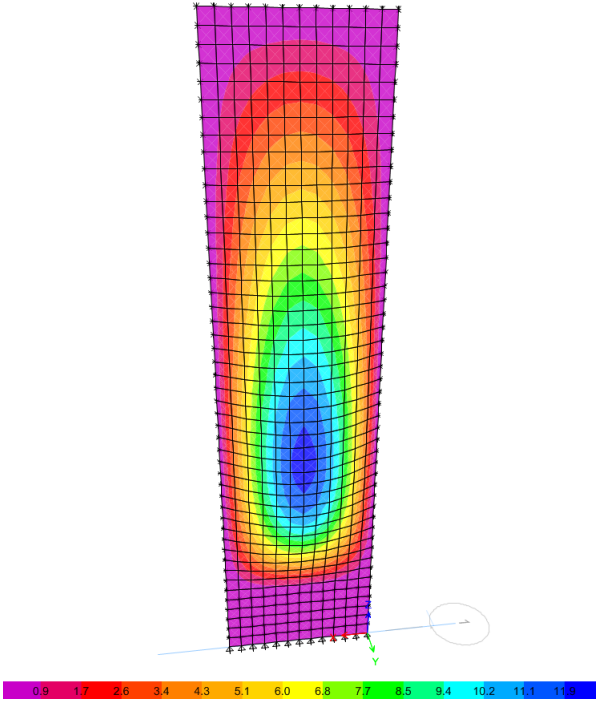


Figure B.5: Out-of-plane deflection of non-prestressed concrete panel.

B.2 Response of prestressed panel

B.2.1 Stress

Side of panel corresponding to compressive stress at the critical location

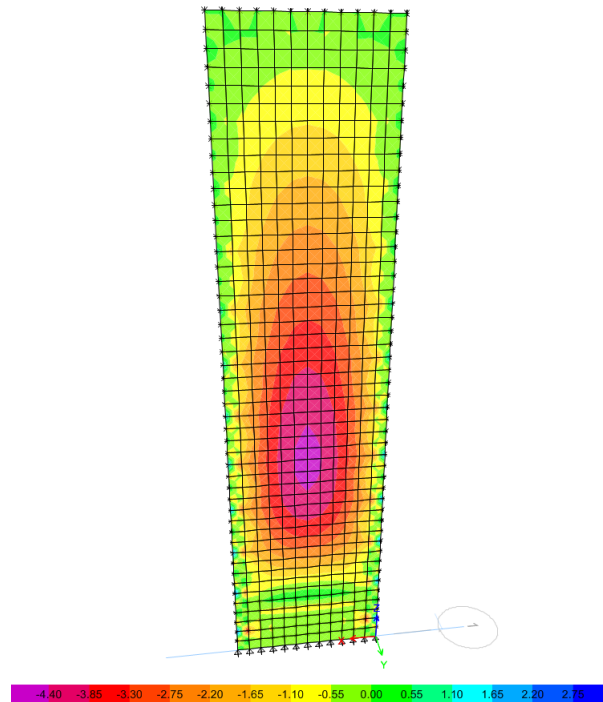


Figure B.6: Stress distribution in x-direction at the side of the prestressed panel experiencing compressive stress at the critical location.

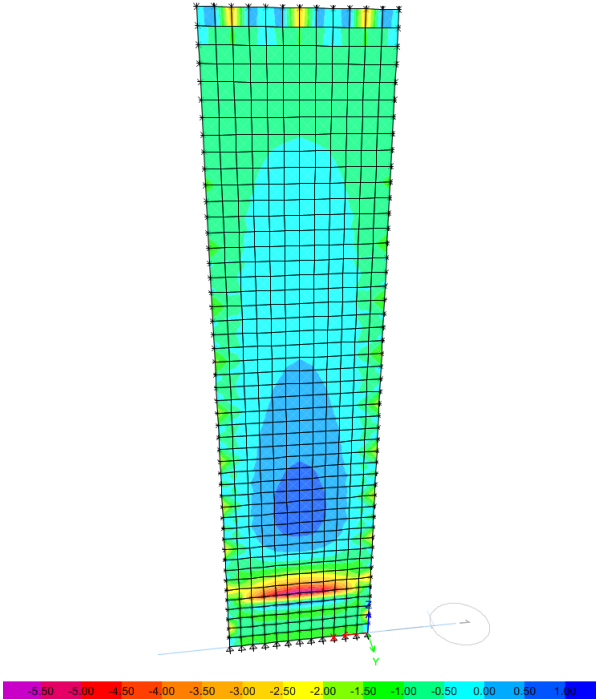


Figure B.7: Stress distribution in y-direction at the side of the prestressed panel experiencing compressive stress at the critical location.

Appendix C

Matlab scripts

C.1 Design for cracking limit state

```
1 %% Calculation of the compressive zone for strips of concrete panel %%
2
3     %% ----- DATA ----- %%
4
5     %% Lengths and dimensions %%
6
7     b=0.001;      %Unit width of concrete section$
8     l_y=12;      %Height/y-span of panel%
9     l_x=3;       %Width/x-span of panel%
10    t=0.3;       %Thickness of panel$
11    d_s=0.28;    %Distance from section surface to COG of ord. steel$
12    d_p=0.22;    %Distance from section surface to COG of pres. steel$
13    e=d_p-0.5*t; %Eccentricity relative to the COG for prestressing force%
14
15    A_p=(250*10^-6)/1000;    %Amount of prestressed reinforcement%
16    A_s=(510*10^-6)/1000;    %Amount of ordinary reinforcement%
17    A_sc=(510*10^-6)/1000;   %Amount of ordinary compressive reinforcement%
18
19
20    %% Material properties %%
21
22    E_p=195*10^9; %Modulus of elasticity prestressed reinforcement%
23    E_cm=35*10^9; %Modulus of elasticity concrete, C40%
24    E_s=200*10^9; %Modulus of elasticity ordinary reinforcement%
25
```

```

26  %-----%
27
28      %% ----- Loading ----- %%
29
30  sigma_pmax=1360*10^6;    %Maximum steel stress from jacking%
31  N=sigma_pmax*A_p;      %Corresponding total prestressing force%
32  M_yp=N*e;              %Eccentricity moment due to prestressing%
33  M_yh=90;               %Max moment adopted from Etabs%
34  a=(M_yh-M_yp)/N;      %Equivalent arm for the total force%
35
36  %-----%
37
38      %% ----- Calculation procedure ----- %%
39
40  etta1=E_p/E_cm;
41  etta2=E_s/E_cm;
42
43  i=0;
44
45  for x=0.02:0.000001:0.5 %Iteration on the compressive zone%
46
47      i=i+1;
48
49      eq1=0.5*x*b-etta1*((d_p-x)/x)*A_p-etta2*((d_s-x)/x)*A_s ...
50          +etta2*((d_s+x-t)/x)*A_sc;
51      sigma_c1(i)=N/eq1;
52
53      eq2=(1/(e+a))*(0.5*x*b*(d_p-(1/3)*x)+etta2*((d_s-x)/x)*A_s*(d_s-d_p) ...
54          +etta2*((d_s+x-t)/x)*A_sc*(d_s+d_p-t));
55      sigma_c2(i)=N/eq2;
56
57      err(i)=abs(sigma_c1(i)-sigma_c2(i));
58
59          if err(i) < 0.1*10^6 %Gives the error limit for the results%
60
61              break
62
63          end
64
65  end
66
67  X
68
69  %-----%
70

```

```

71         %% ----- Post processing of results ----- %%
72
73         %% Stress-strain in steel and concrete top %%
74
75     eps_c=sigma_c1(i)/E_cm;           %Strain at concrete top%
76     eps_s=((d_s-x)/x)*eps_c;         %Strain in ordinary reinforcement%
77     eps_sc=((d_s+x-t)/x)*eps_c;     %Strain in compressive reinforcement%
78     eps_p=((d_p-x)/x)*eps_c;        %Strain in prestressed reinforcement%
79
80     sigma_s=(eps_s*E_s)*10^-6;      %Corresponding stress in ord. steel%
81     sigma_sc=eps_sc*E_s;            %Corresponding stress in comp. steel%
82     sigma_p=eps_p*E_p;              %Corresponding stress in pres. steel%
83
84     sigma_c=((sigma_c1(i)+sigma_c2(i))/2)/10^6; %Stress at concrete top%
85
86
87         %% Plot algoritms %%
88
89     % scatter(0:50:400,sigma_c_3,'b')
90     % hold on
91     % xlabel('Amount of prestressed steel per unit width, A_p [mm^2/m]')
92     % ylabel('Stress [Mpa]')
93
94     % scatter(A_p*10^9,x*1000,'r')
95     % hold on
96     % xlabel('Amount of prestressed steel per unit width, A_p [mm^2/m]')
97     % ylabel('Height of compressive zone, x [mm]')

```